A RAMAN STUDY OF ORDER IN SOME COMPLEX POLYESTERS

A thesis submitted to the
UNIVERSITY OF SOUTHAMPTON
in support of candidature for
the degree of

Doctor of Philosophy

by

Jonathan Kofi Akroma Agbenyega

Department of Chemistry

October 1992

"..... and so there ain't nothing more to write about, and I am rotten glad of it, because if I'd "a" knowed what a trouble it was to make a book I wouldn't "a" tackled it, and ain't a-going to no more."

Mark Twain, *Huckleberry Finn*

to my family

UNIVERSITY OF SOUTHAMPTON

ABSTRACT

FACULTY OF SCIENCE
CHEMISTRY

Doctor of Philosophy

A RAMAN STUDY OF ORDER IN SOME COMPLEX POLYESTERS

by Jonathan Kofi Akroma Agbenyega

The development of the Fourier Transform Raman spectrometer in the polymer field has substantially eliminated many of the difficulties previously encountered when using the conventional technique. Their sensitivity is such that the Raman spectra of a wide range of polymers, in the as-received form may be obtained in a few minutes, and with-out prior time consuming optimization of sample placement in the spectrometer. Furthermore the use of the 1.064μ line from a Nd^{3+}:YAG laser as the excitation source has largely eliminated the fluorescence problem. This thesis describes the application of the technique to three very different polyester systems.

In **Chapter 3** of the thesis the technique has been used successfully to monitor the autoxidative curing process of a commercially based Alkyd resin and its model compounds. FT-Raman showed the configurational changes occurring for the C=C bond (*cis/trans* isomerism, and conjugation) during autoxidation.

In **Chapter 4** a range of novel liquid crystalline polyesters have been analyzed by FTIR, FT-Raman spectroscopy, Differential scanning calorimetry, X-ray diffraction, and Thermo-optical analysis. Results have been compared and contrasted between the techniques, with an emphasis placed on the effects of lateral substituents and flexible spacer lengths.

Chapter 5 investigates the FT-vibrational spectra of amorphous vs crystalline polybutylene terephthalate and polybutylene terephthalate blended with an epoxy resin (synthesised from epichlorohydrin and diphenyl propane) over a range of cure times and temperatures. Phase separation under certain conditions has been reported.

ACKNOWLEDGEMENTS

The author would like to thank the following people who have been a great support throughout my years at Southampton.

Dr. P. J. Hendra, for his endless enthusiasm, energy, his excellent supervision and guidance, and for always reminding me of my Mancunian accent.... Ta Pat!!

To the past members of the Hendra group, in particular **Dr. Cathy Passingham**, and her help and encouragement over the past 3 years. **Anne Rowlands** and our many "chats". **Drs. C. Jones, C. Petty** and **G. Warnes,**

and to the present members of the Hendra group, keep-up the good work!

Dr. M. Claybourn of ICI Paints Division, and his enthusiastic collaboration in chapter 3, and our many working lunches. **Dr. E. Neilds**, and **Dr. Riaz Choudhery**, in their support of chapter 5.

To my Spanish friends, **Prof. J. Fatou**, and **Dr. Carlos Marcos** of the Institute of Science and Technology of Polymers, Madrid, for their help and advice during my stay in Madrid. To **Javier del Pino** without whom chapter 4 would not have been possible. Again to Javier and **Dr. Juan Lorente** for many interesting discussions and supplying 2 of the polymers mentioned herein. Last but by no means least to **Dr. Gary Ellis** and **Alicia Huidobro** for making my stay in Madrid memorable and enjoyable. Muchas gracias!

(Financial assistance for this work was provided by The Science and Education Research Council, and ICI Paints, Slough.)

CONTENTS

CHAPTER 1: Introduction

1. Background and aims of thesis

Commercial Fourier transform Raman instruments are based on Fourier Transform infra-red (FTIR) optical benches with the Raman as an add-on module. This type of system gives a very flexible and powerful tool for performing molecular vibrational analysis. Since both FTIR and FT-Raman spectra can be acquired on the same instrument, this new breed of instrument is relatively inexpensive and certainly accessible to most analytical laboratories. The devices are safe, and easy to use with little or no sample handling, no instrument alignment, and minor sample alignment. The result is that Raman spectra can now be routinely and rapidly measured by technical staff without the need for extensive training. FT-Raman spectroscopy provides unique information and as a complementary technique to FTIR, previously intractable problems can be approached.

This thesis has been written, to prove FT-Raman spectroscopy has potential, as an analytical tool, to study a broad range of polymer applications.

One of the key factors behind FT-Ramans early success is the time and money saved per sample, compared with the conventional technique. If a sample can be persuaded to give a spectrum the operator will know this within a few seconds. If, however, the sample is a poor Raman scatterer, and perhaps fluorescent, or an absorber for whatever reason, very little can be done to improve the spectrum. Using the conventional technique sometimes requires several hours to align the instrument and sample, only to find that the sample fluoresces! Using the FT-technique valuable time and effort in industrial laboratories can be saved, thus keeping the cost per spectrum down [1].

Perhaps the most convincing piece of evidence for the interest and early success in near infra-red (nir) FT-Raman spectroscopy is that all the major optical instrument manufacturers have produced commercial instruments. There has been a flurry of short courses on the subject and many excellent papers are

appearing in the literature on applications. Pergamon Press now publishes a special annual edition of *Spectrochimica Acta* devoted to the applications of nir FT-Raman spectroscopy. There is definitely a growing market of interest in the technique: HENDRA, JONES, and WARNES wrote a book [2] to inform the new wave of Raman analysts of these advances. It is clear that many applications of FT-Raman spectroscopy will lie in the polymer area, and as such a gap in the market still persists, ie. no collection of polymer Raman spectra exists.

The book in which I co-author with P. Hendra attempts to "plug this gap". "The Raman Spectra of Polymers", published by John Wiley & Sons Ltd. has been written and designed to be of interest to analysts, both in academia and industry. Its format will be a readily up-dateable ring binder, thus, when new polymer spectra become available or existing spectra are improved, they may be simply slotted into the existing atlas of spectra. It is proposed to produce annual packs of new and up-dated material. The up-dating theme also applies to the text sections in the book which provides a sufficient level of theory covering molecular vibrations and instrumentation to satisfy the requirements of the analyst. The final chapter provides a review of the work performed using nir FT-Raman spectroscopy in the polymer industry, references to original material and the atlas of polymer spectra are given throughout the chapter.

In the next few pages the reader will find a flavour of the diversity of the technique in the polymer field, before moving onto detailed studies in chapters 3,4 and 5 in the field of paints, liquid crystal polymers, and crystallisable coatings respectively.

1.1 Literature survey

Historically Raman spectroscopy, unlike its infra-red counterpart has not been a widely used technique in polymer science. As recently as 1964 NIELSON [3] in a comprehensive review of the Raman spectra of polymers was forced to conclude that the method, although applicable to a few polymers was of little or

no routine significance due to the difficulty in recording the spectra. The primary problem at that time was fluorescence, and sample turbidity.

With the advent of reliable continuous wave (CW) gas lasers; He-Ne, then Ar^+, followed by Kr^+, (which offer stable and intense light sources) and subsequent improvements in instrumentation the situation seemed set to change. Thus in the early 70's when KOENIG wrote a definitive review [4] he cited spectra of over 20 different polymers, illustrating the information that can be obtained from such data. This sparked great interest in the potential of Raman spectroscopy in the polymer field, several excellent review articles, from PETICOLAS, 1972 [5], HENDRA 1974 [6], FRUSHER and KOENIG 1975 [7], and WILLIS 1979 [8] then appeared, and by 1986 when GERRARD and MADDAMS published their review [9], 250 references were required just to highlight the major topics.

Despite the improvements made by the laser, and multiple monochromators in Raman spectroscopy, the technique was still inferior to infra-red spectroscopy, particularly in the industrial laboratory for the characterization and analysis of polymers. There are several reasons for the lack of appeal of Raman spectroscopy to the industrial chemist. The major reason being financial, and the problems caused by sample fluorescence.

Until recently it had always been far more economical to purchase an infra-red instrument in terms of capital outlay and level of skill and time required to obtain useful results.

By their very nature, polymers are impure, they often contain traces of catalysts, monomers or other impurities, and in some applications are compounded with anti-oxidants and fillers which tend to exacerbate the fluorescence problem. The efficiency in terms of photon yield of the fluorescence process is far greater than that of the Raman effect, so the presence of even the smallest levels of fluorescence can totally obscure the weak Raman scatter. Several techniques have been devised to attempt to try and overcome the fluorescence problem [1],

such as solvent extraction, and recrystallization. The most successful of these methods has been the process of "burning out the fluorescence" [1]. Here the user leaves the sample for a period of time, (ranging from a matter of minutes, in the more favourable situations to a number of days) in the focused laser beam, during which time it is hoped that the fluorescent centres are "burnt out". These techniques even though sometimes quite successful are both time comsuming and uneconomical to the industrial chemist. Infra-red absorption spectroscopy therefore remained the preferred technique for industrial polymer analysis, even though in many applications of the technique one was required to melt or dissolve the sample to obtain a thin film. This was a highly undesirable process if the thermal history of the polymer was important.

An increasing number of polymers are now compounded. With for example fillers, such as glass fibres, or in coatings, with pigments. These additives tend to strongly interfere with the IR spectra of the polymers due to their own characteristic absorptions, and/or the scatter of the incident radiation that they cause. Although FT procedures and unconventional sampling methods have improved the situation, examination of this type of sample is frequently far from satisfactory. Pigments (apart from carbon black) and glass are poor Raman scatterers, so in principle the Raman spectrum should be obtainable from these samples without removal of the fillers or adverse sample preparation.

The development of the near infra-red Fourier transform Raman spectrometer [10] has led to the re-evaluation of the Raman technique for the routine analysis of polymeric systems. Commercial dual-purpose infra-red/Raman spectrometers are now available from all the major instrument manufacturers at prices very similar to that of high specification FTIR instruments. With the advent of Near Infrared (nir) FT-Raman spectroscopy which uses the 1.064μm line from the Nd^{3+}:YAG laser as the excitation source, 90% of all polymers hitherto impossible to analyze have become accessible. The Fourier transform spectrometer allows rapid acquisition of data, thus a wide range of polymers in the "as-received" form can be examined in a matter of minutes.

Near infra-red Fourier transform Raman spectroscopy has already proved to be an invaluable tool in the study of many different polymers, copolymers and blends [1]. It has been proved useful in the identification of materials, end-group analysis, morphological studies, kinetic measurements, the investigation of mechanical changes, and following degradations when the polymer is exposed to the atmosphere. We will now review these applications, and commence with general qualitative and quantitative analysis, including kinetic studies.

1.1.1 Routine Analysis

Raman spectroscopy is an ideal tool for the study of the changes occurring in the C=C moiety of polymers. This non-polar bond happens to provide only a weak and undescernable group frequency correlation in the infra-red but is dominant in the Raman spectrum. Because the intensity of Raman bands are a direct indication of the concentration of a particular species and the Raman shift is dependent on the chemical environment within the system [11], kinetic studies as well as characterizations can be carried out easily.

In 1968 CORNELL et al [12] reported one of the first Raman spectroscopic studies of polybutadienes where the various conformations were determined qualitatively from the ν(C=C) Raman bands of vinyl, *cis* and *trans* moieties. Bands due to the *cis,trans,* and vinyl groups near 1650cm^{-1} can be characterized and hence their composition within the rubber can be determined quite simply. In fact results obtained using FT-Raman spectroscopy tend to be far more reliable than the classical method involving NMR spectroscopy [13] and are applicable more widely. It should also be noted that vulcanized systems can be studied with ease using nir FT-Raman spectroscopy, and data can be obtained in a matter of minutes. NMR, applied in this case is dogged by experimental problems and tend to out-way the normal advantages associated with the technique [13].

KOENIG [14] used Raman spectroscopy to follow the polymerization mechanism of butadiene. The polymerization conditions determine the amount of 1,2 and 1,4 products present in the final mixture. It is important to monitor these values as each plays an important part in determining the properties of the polybutadiene produced. The νC=C band is weak in the infra-red spectrum but strong in the Raman, (in actual fact characteristics of the 1,4 *trans* structure are so weak in the IR that they cannot be seen). The degree of unsaturation and conformation can therefore be readily determined using the Raman technique in general and specifically with ease using the FT method.

A similar example demonstrating the quantitative value in a polymerization reaction was presented by GULARI et al [15]. They monitored the decrease in intensity of the exocyclic stretching band in the polymerization of styrene. They were able to quantify their results by capitalising on the fact that the CW lasers when run in the "light control mode" give very stable outputs for several hours. Thus keeping all other variables constant, the change in the intensity of the C=C moiety was a direct indication of the course of reaction. This is one of the major advantages of FT-Raman spectroscopy to the industrialists, its capability of monitoring reactions in-situ.

Work carried out at Southampton University in 1991 by a third year undergraduate project student demonstrates the versatility of the technique; nir FT-Raman spectroscopy was used to study a nitration reaction in the attempt to gain vital kinetic data for an industrial sponsor. A specially designed kinetic cell was used for the analysis. An external microprocessor connected to a heating unit controls the temperature of the oil bath, the sample tube simply slots into the kinetic cell opening, followed by alignment in the instrument, which is fairly straight forward. The relatively fast speed of the FT technique [16] allowed data to be acquired every few seconds. Reaction temperatures of up to 80°C were reached without any problems from background emission. WILLIAMS and MASON [17] have studied the thermal emissions that occur from materials when heated above ambient temperature. Only at temperatures above 180°C did they

perceive any serious problems occurring from the thermal background encroaching on the weak Raman signal.

WILLIAMS et al [17] made a quantitative study of the polyurea/polyurethane content of commercial foams. Until their study, these systems had only been characterizable by other spectroscopic methods, and then not very satisfactoraly, each requiring rigorous sample pre-treatment. The non-destructive nature of the Raman technique and the use of optical fibres provides an ideal method of analysis.

Further examples of copolymer analysis using Raman spectroscopy can be found in the work of AGBENYEGA et al [18], who describe the analysis of tetrafluoroethylene/hexafluoropropylene systems. These systems were of interest, because the copolymer spectra containing up-to 10% hexafluoropropylene showed only slight differences from the spectrum of the homopolymer. Data subtraction provided a viable method for analyzing these copolymer systems. MEEKS and KOENIG used Raman spectroscopy to study quantitatively the copolymers of vinyl chloride/vinylidene chloride [19]. BOERIO and YUANN [20] performed a compositional analysis of styrene glycidal methacrylate and methyl glycidalmethacrylate copolymers. SLOAN and BRAMSTON-COOK studied a three component system, comprising of styrene, butadiene and methyl methacrylate [21]. All of these classical studies could be repeated much more easily on FT-Raman devices, and would not be problematic if the specimen were degraded or oxidized.

1.1.2 Crystallinity in Polymers

The vibrational spectra of crystalline polymers are characterized by a high degree of definition, since it is only the in-phase modes of the species characteristic of the crystalline phase that gives the more prominent observed spectral bands. As the crystallinity falls in a set of samples for whatever reason, distinct changes can be noticed in the spectra; the bandwidth increases

significantly and often new characteristics appear in the spectrum due to rotameric species present in the disordered phases [22].

A detailed description of the method used to determine the degree of crystallinity from Raman data has been made by STROBL and HAGEDORN [23]. They use a three phase model for partially crystalline polyethylene consisting of an orthorhombic crystalline phase, a melt-like amorphous one and a disordered anisotropic phase[1]. The method is therefore geared to estimate the degree of crystallinity as well as the amount of interfacial material in the sample. The integrated intensity of the band at 1416cm^{-1} (A_g -CH_2 bending vibration) reflects the amount of orthorhombic crystalline material present in the sample whilst bands at 1301 and 1080cm^{-1} are used to estimate the amorphous content.

When the crystal habit is altered via changes in temperature or pressure, corresponding changes in the vibrational spectrum occur, because modes of a chain within a unit cell are influenced by others within it. A classic example is polyethylene, which contains two chains per unit cell. Each mode of each chain in polyethylene can be in-phase or out-of-phase with its partner, giving rise to sets of doublets in the Raman spectrum. The effect has been observed in several other polymers [24]. Changing the crystalline habit obviously effects this so called "correlation splitting". Some linear paraffins can occur in modifications with one and two chains per unit cell and the Raman spectrum alters significantly between them. In the case of the straight chain paraffins, analysis of the band near 1450cm^{-1} can be used to identify the local configuration of $(CH_2)_n$ sequences in polymers and has been used by one of the authors [25,26] over the years.

Conventional Raman spectroscopy can be used to study the Longitudinal Acoustic Modes (LAM) of polymers, thus the lamellar thickness of polymer crystals are determined. The chains within a lamellar unit vibrate along their

[1] These phases are associated with the lamellar cores, the intercore layers, and the transitional layer between them respectively

length in an accordion-like motion, the frequency of which depends on the length of the vibration, and since the chains lie at characteristic angles to the surface of the lamella, the frequencies of the LAMs lie in the frequency range $\Delta\nu$ 5-30cm^{-1}. These frequency shifts are not accessible with current FT instruments, and it is very unlikely that the manufacturers will be able to close the range to this value without developing a completely new approach to filtering the scattered radiation.

Cooling the sample is a technique often used in the analysis of polymers, it has the effect of narrowing the bandwidth. Conversely, if the sample absorbs a significant amount of the exciting radiation then it will heat-up, with the effect of broadening the bandwidth. This point is born-out in polytetrafluoroethylene (PTFE). PTFE undergoes a phase transition at 19°C due to a change in the helical degree from 13/6 to 15/7. The bands near 500cm^{-1} change quite dramatically. These changes are known to be due to this phase change [27].

It should also be noted that the sample is hotter than the temperature actually measured due to absorption of the near infrared laser, this heating effect is relatively modest, if low laser powers are used.

Before moving onto the project areas, it is necessary to explain the experimental techniques, that were used in the course of the research.

References

1. J.R. Nielsen, *J. Polm. Sci.* Part C7 **19**, (1964)

2. J.L. Koenig, *Appl. Spectrosc. Rev.* **4**, 233, (1971)

3. W.l. Peticolas, *Adv. Polym. Sci.* **9**, 285, (1972)

4. P.J. Hendra, in "Polymer Spectroscopy", D.O. Hummels, ed. Verlag Chemie, Weinheim/Bergstr., (1974)

5. B.G. Frushour and J.L. Koenig, in "Advances in Infra-red and Raman Spectroscopy", **1**, R.J.H. Clark, and R. Hester, eds., Heyden, London, (1975)

6. H.A Willis, Proc. 5th Eur. Symp. Polym. Spectrosc., Hummel, Weinheim, (1979)

7. D.L. Gerrard, and W.F. Maddams, *Appl. Spectrosc. Rev.* **22**, 251, (1986)

8. T.R. Gilson and P.J. Hendra, "Laser Raman Spectroscopy", Wiley, London, (1970)

9. D.B. Chase, *Analyt. Chem.,* **59**, 881A, (1987)

10. P.J. Hendra, and H.M. Mould, *Int. Laboratory,* **18**, 34, (1988)

11. S.W. Cornell, and J.L. Koenig, *Macromol.* **2**, 540, (1969)

12. B.P. Straughan, S. Walker, "Spectroscopy", Chapman and Hall (1976)

13. T.R. Crompton, "Analysis of Polymers, an Introduction". Pergamon, (1989)

14. J.L. Koenig, *Chem. Technol.* **2**, 411, (1972)

15. E. Gulare, K. McKeique, and K.Y.S. Ng, *Macromol.* **17**, 1822, (1984)

16. D.P. Strommen, and K. Nakamoto, "Laboratory Raman Spectroscopy", J. Wiley and Sons. (1985)

17. K.P.J. Williams and S.M. Mason, *Spectrochimica Acta* **46A**, No. 2 (1990)

18. J.K. Agbenyega, G. Ellis, P.J. Hendra, W.F. Maddams, C. Passingham, H.A. Willis and J. Chalmers, *Spectrochimica Acta* **46A**, No. 2 (1990)

19. M. Meeks, and J.L. Koenig, *J. Polym. Sci. Polym. Phys. Ed.* **9**, 717, (1971)

20. F.J. Boerio, and J. Yuann, *J. Polym. Sci. Polym. Phys. ed.* **11**, 1848, (1973)

21. H. Sloan and R. Bramston-Cook, *Appl. Spectrosc.* **27**, 217, (1973)

22. G.V. Fraser, P.J. Hendra, J.M. Chalmers, M.E.A. Cudby, and H.A. Willis, *Makromol. Chem.* **173**, 195, (1973)

23. G.R. Strobl and W. Hagedorn, *J. Polym. Sci., Polym. Phys. ed.* **16**, 1181, (1978)

24. P.J. Hendra, D.S. Watson, M.E.A. Cudby, H.A. Willis, and P. Holliday, *Chem. Commun.* 1084, (1970)

25. D.J. Cutler, P.J. Hendra, and G. Fraser, "Developments in Polymer Characterization", **2**, Applied Science. (1980)

26. G.V. Fraser, P.J. Hendra, J.H. Walder, M.E.A. Cudby, and H.A. Willis, *Makromol. chem.* **173**, 205, (1973)

27. N.J. Everall, J. Lumsdon, and J.M. Chalmers, *Spectrochimica Acta,* **47A**, No 9/10 1305-1311, (1991)

Chapter 2: Experimental Techniques

2.1 A Brief Introduction to Molecular Vibrations

Raman spectroscopy (like infra-red) can give information on molecular rotations, vibrations and in rare cases electronic transitions, but as far as the polymer scientist is concerned interest is confined exclusively to vibrations.

Molecules vibrate perpetually. Consider a homonuclear diatomic molecule such as chlorine, the potential energy vs interatomic separation has a minimum hence the molecule will cycle periodically around this minimum and further, quantum mechanics require that it will do so continuously. The form of the potential energy function approximates to that of Morse, beloved of all first year undergraduates, and is shown in figure 2.1. The Morse potential energy curve fits reasonably closely to a parabola near the bottom of the well implying that the molecule at small displacements will vibrate with something approaching simple harmonic motion. At the other extreme, large displacements lead to a poor approximation to the parabolic function, i.e. the true potential strays further and further from the parabola, until dissociation occurs and a separated pair of chlorine atoms are produced.

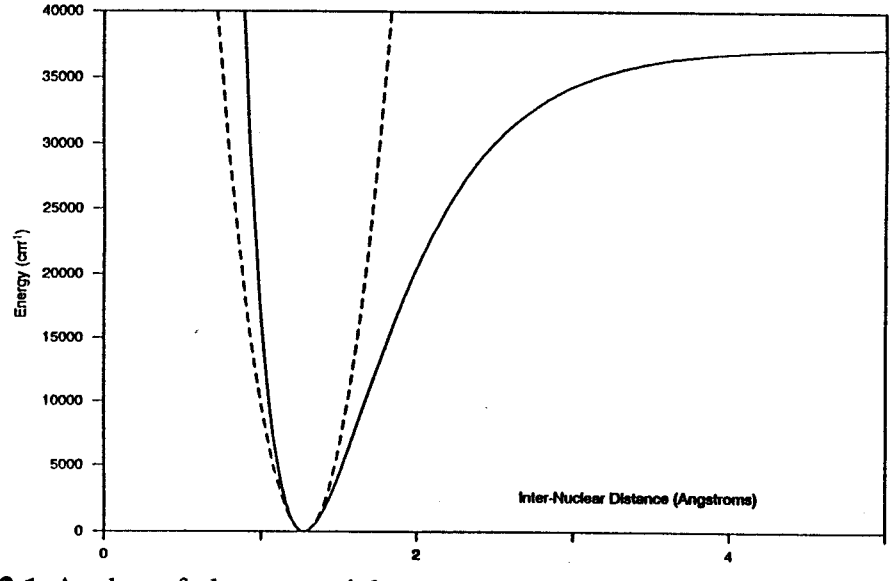

Figure 2.1 A plot of the potential energy versus interatomic separation for a diatomic molecule

Although strictly unjustified, let us assume that the potential function is indeed

$$\upsilon_{vib} = \frac{1}{2\pi}\sqrt{\left(\frac{k}{\mu}\right)} \quad Hertz \qquad 1$$

parabolic. This means the system will vibrate at a frequency given by equation 1. Where k is the Force constant and μ the reduced mass, (see equation 2)

$$\mu = \frac{m_1 m_2}{m_1 + m_2} \quad Kg \qquad 2$$

The force constant is identical to the Young's modulus and hence is an indication of the molecular *stiffness*; not, it must be emphasised, its bond strength. In a classical vibrator removal of all the vibrational energy will result in the molecule resting at the minimum of the potential function i.e. at the equilibrium interatomic separation. If one then injects energy into the system, vibration will recommence and gradually increase in amplitude as the energy is absorbed. As with all forms of molecular energy, vibrational energy is quantized, i.e. it is present at strictly defined levels. If one investigates the quantum mechanical requirements for vibration one would find that the permitted energy levels lie (for the simple harmonic oscillator) at;

$$E_{vib} = \left(V + \frac{1}{2}\right) h\upsilon_{vib} \quad Joules \qquad 3$$

Where;

h = Plank's constant (joules Seconds)

ν_{vib} = Vibrational frequency (Hertz)

V = Vibrational quantum number

If one now draws these permitted levels onto the parabolic energy function figure 2.2 is the result.

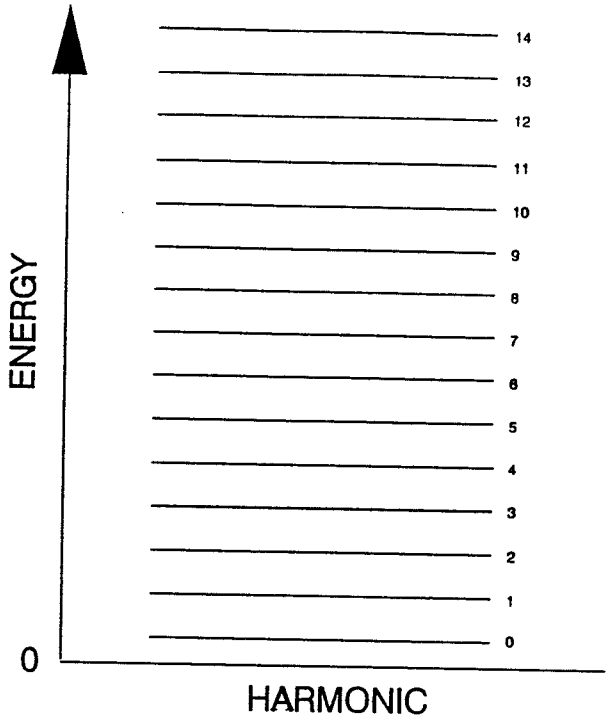

Figure 2.2 Energy level ladder for the harmonic oscillator

As already mentioned the potential function is **not** parabolic, and as a result the motion is not simple harmonic, but **anharmonic**, however the difference between the two at small displacements is very little. The anharmonic behaviour lowers the energy of each vibrational level below that of the (theoretical) harmonic behaviour and the discrepancy gets larger as the displacement increases. All of this is shown in figure 2.3.

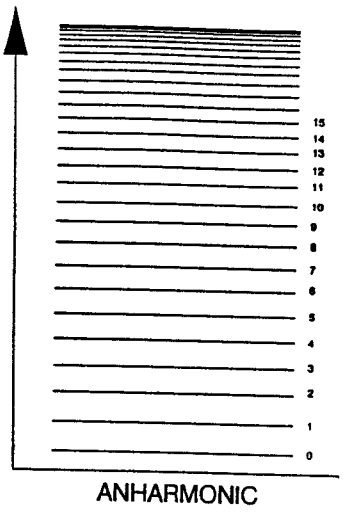

Figure 2.3 Energy level ladder for the anharmonic oscillator

Now consider a more complex molecule viz carbon dioxide.

2.1.1 Fundamental Modes

One can define the position of the molecule as a whole by locating its centre of mass, i.e. one needs three of the 3n coordinates to fix the position of the molecule. Similarly, 3 coordinates will define the molecular orientation. This leaves 3n-6 coordinates which in-effect define the molecular shape and size. Thus, it is obvious that the maximum number of fundamental modes of vibration must be limited to 3n-6. In a linear molecule like carbon dioxide rotation about the molecular axis does not occur. Therefore only two coordinates will define the orientation. Thus, a non-linear molecule can possess up to 3n-6 fundamental modes of vibration, whilst a linear molecule is limited to 3n-5.

Carbon dioxide undergoes a very complicated vibrational motion which is the arithmetic sum of a set of four fundamental modes of vibration. It turns out that the meaningful figure is three, rather than the maximum of four. The discrepancy arises because one pair of modes $\nu_{3,4}$ are a degenerate pair, i.e. they are experimentally indistinguishable. See figure 2.4.

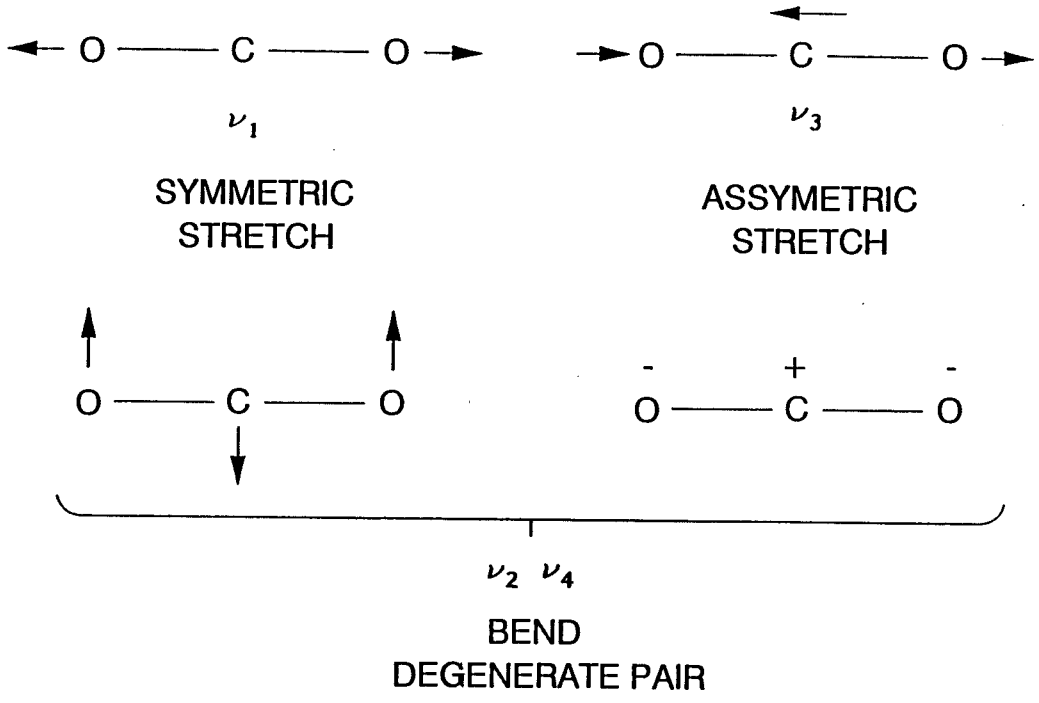

Figure 2.4 The fundamental vibrational modes of carbon dioxide

What happens when one increases the complexity of the molecule still further? Needless to say, the analysis becomes more and more complex. Fortunately several simplifications are available. Of these by far the most valuable is symmetry.

2.1.2 Vibrations of polyatomic molecules

KRIMM [1], amongst many others, has analyzed the symmetry operations of several polymeric systems using Group Theory [2], in order to classify the number and activity of the normal modes of vibration. The symmetry elements of a particular molecule, or the repeating unit in a polymer, can be categorized into *point groups*, and fundamental vibrational modes (see section 2.2) can be labelled according to these symmetry elements by using *character tables*, found in standard texts [3,4]. Once the symmetry of a normal mode has been determined, its spectral activity can be established by referring to these character tables.

Clearly, very complex molecules and particularly those of ill defined or unknown structure are not amenable to symmetry analysis. However, infrared spectroscopists since the early days have adopted an alternative, that absorption in particular narrow frequency ranges are typical of specific chemical groups. A similar set of correlations has developed for Raman spectroscopy and has been known for many years [3]. The group frequency approach does not replace the fundamental mode analysis. Rather it is a trivial but none the less valuable simplification of the true situation. As early as the 1890's it had been noted that all hydroxy containing species absorbed infra-red radiation at roughly the same wavelength, near ν = 3500cm^{-1} and again at approximately 1650cm^{-1}. These bands have been assigned to -OH stretching and bending vibrations, the motions of which have been depicted in figure 2.5.

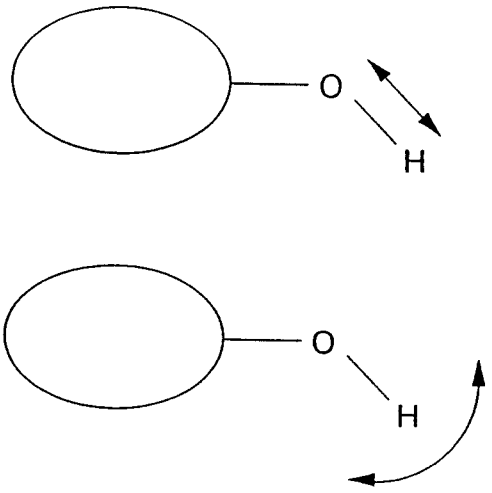

Figure 2.5 The -OH bending and stretching vibrations in a large molecule X

The frequency of the vibration of -OH functionalities in ROH is almost exclusively dependent on the magnitude of the force constant, k_{OH}, which is directly related to the electronic structure of the bond which may be slightly perturbed, depending on the R group. Another example; all molecules containing the carbonyl functionality have a characteristic frequency in the range 1600-1800cm^{-1}. The exact frequency depends on whether the side groups R_1 and R_2 are electronegative species, for example chlorine, or electropositive units such as methyl groups. Thus if R_1 is an electronegative chlorine atom and R_2 is a methyl group, the chlorine will draw electrons towards itself and increase the π character of the bond, thus increasing the bond order. Methyl groups are weakly electron donating and hence when both R_1 and R_2 are methyl groups the bond order is lower than in the previous case. Hence we expect $k_{c=o}$ to be larger, and the band frequency to be higher in ethanoyl chloride CH_3COCl than in acetone CH_3COCH_3. The band frequencies are 1805cm^{-1} and 1712cm^{-1} respectively demonstrating this point. As in the ν_{OH} case the carbonyl correlation is predominantly an infrared one. Stretching of the C=C group is, however, a

feature of much greater value in the Raman spectra. This point is demonstrated in figure 2.6 which shows the spectra of predominantly *cis, trans,* and vinyl polybutadienes. Raman bands near 1660cm^{-1} of high and reliable intensity are found in all unsaturated compounds, the frequency order being *trans* > *cis* > vinyl. As is so commonly the case the strong Raman, weak infrared rule applies here demonstrating the complimentary nature of the two techniques.

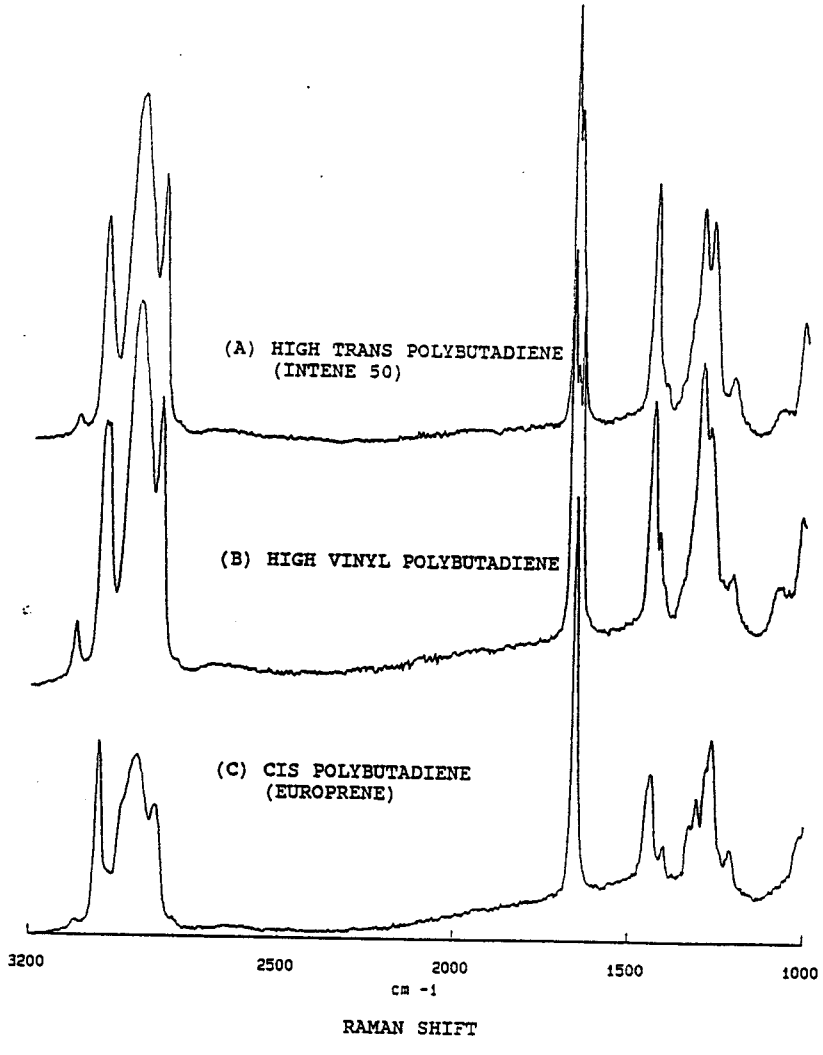

Figure 2.6 The Raman spectrum of *cis, trans* and vinyl polybutadiene. (Courtesy of C. Jones).

2.2 The measurement of vibrational frequencies

2.2.1 Infra-red activity

As molecules vibrate they generate changes in the magnitude of the dipole associated with the molecule and/or changes in the polarizability. These changes give rise to the spectroscopic effects (Infra-red absorption in the first case and Raman scattering in the second) which enable the analyst to measure the vibrational frequencies. It is said that for a given technique the vibrational mode must satisfy a "selection rule". Infra-red and Raman activity can be pictured by plotting the dipole (μ) and polarizability (α) against the progress through the vibration (q). Infra-red spectroscopy only observes vibrations which have finite values of $(\delta\mu/\delta q)_0$, whilst for Raman activity $(\delta\alpha/\delta q)_0$ must have non-zero values.

Consider first infra-red absorption in carbon dioxide. The values of μ against q for the fundamental vibrational modes of CO_2 are drawn in figure 2.7. Where it is clear that $\nu_{2,3\ \&\ 4}$ satisfy the criterium,

$$\left(\frac{\delta\mu}{\delta q}\right)\neq 0 \qquad 4$$

i.e. the dipole is changing as the molecule distorts close to the equilibrium configuration.

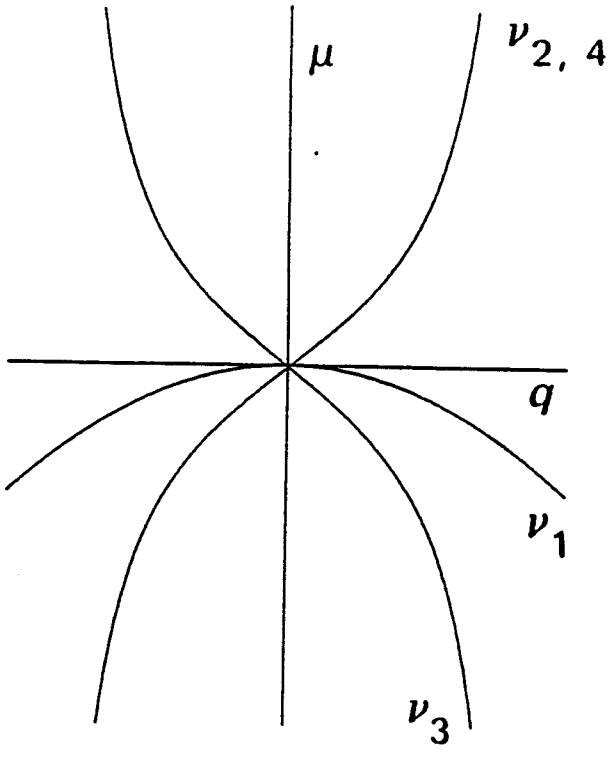

Figure 2.7 Plots of dipole moment against normal coordinates for carbon dioxide

Thus if a sample of CO_2 is illuminated with polychromatic infra-red radiation, absorption will occur at the frequency of ν_2 and also $\nu_{3,4}$ and the absorbed energy will increase the amplitude of the relevant vibrations.

2.2.2 Polarizability and the classical description of the origin of the Raman effect

All materials possess a "polarizability", i.e. if they are placed in an electric field of magnitude E (volts/metre) a dipole will be induced, the proportionality constant being termed the polarizability i.e.

$$P = \alpha E \qquad 5$$

The polarizability, i.e. the ease with which the electron "cloud" can be distorted by the applied potential field, is not confined to the bulk material, it originates in the properties of the molecule. At the molecular level the polarizability will of course vary with respect to the orientation of the field relative to the molecular axis i.e. the polarizability is not a vector quantity but rather a tensor quantity hence it has magnitude in all directions, and not just one. The standard representation of molecular polarizability in three dimensions is the "polarizability ellipsoid". The ellipsoid is constructed by placing the molecule at the origin of a three dimensional cartesian system, and then plotting a three dimensional locus of $1/\alpha_i$, where α_i is the polarizability along the line between the point i and the origin. See figure 2.8.

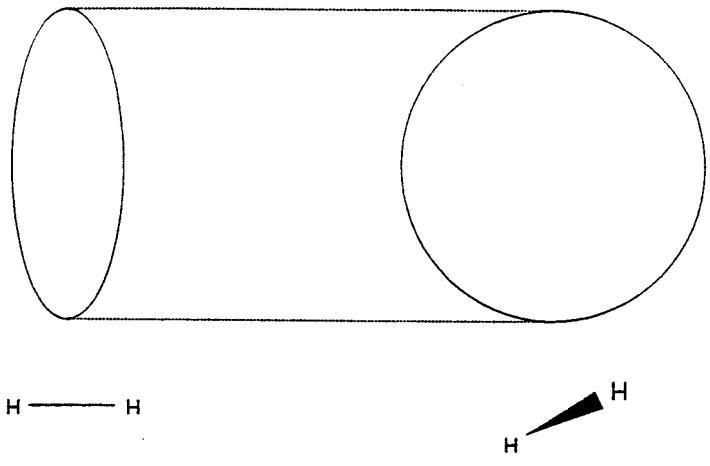

Figure 2.8 The polarizability ellipsoid of an H_2 molecule seen from two directions at right angles

Consider the carbon dioxide molecule once more. As the molecule expands and contracts the interaction of the nuclei and the electrons will vary hence the polarizability sweeps up and down and follows the plot of α versus q given in figure 2.9.

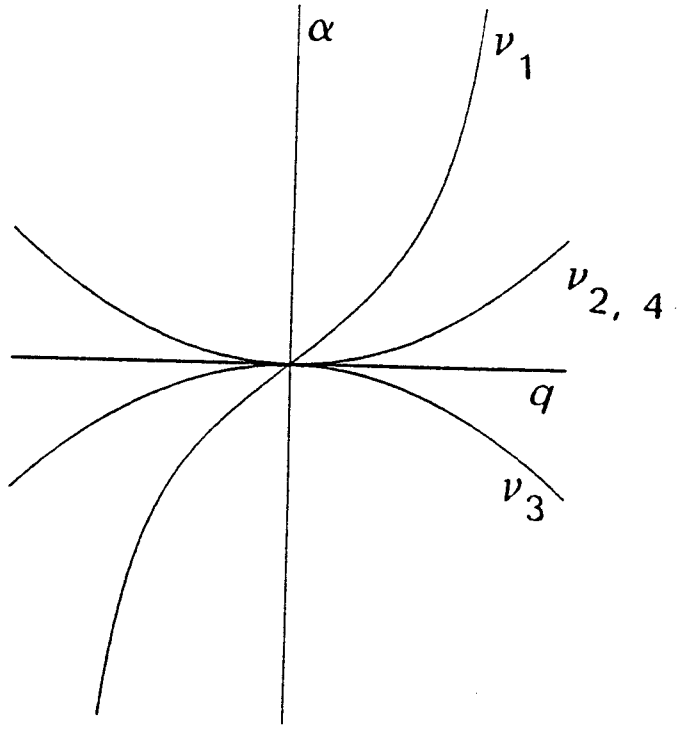

Figure 2.9 Graphs of polarizability α for the vibrational modes of carbon dioxide as a function of phase angle.

ν_3 will follow a very different graph because the molecule is chemically identical at the two extremes of the vibration, i.e. the molecule at $\pi/2$ and $3\pi/2$ are mirror images of one another. The same applies to $\nu_{2\&4}$. Thus to summarise, ν_1 has a finite value of $(\delta\alpha/\delta q)_0$ the others do not. As we shall see in a moment this feature will lead to Raman activity, hence we have the entries in table 2.10,

Carbon dioxide	Frequency (cm^{-1})	IR activity	Raman activity
symmetric stretch (ν_1)	1388	NO	YES
asymmetric stretch (ν_3)	2349	YES	NO
O-C-O bending pair ($\nu_{3,4}$)	667	YES	NO

Figure 2.10 Infra-red and Raman activity of carbon dioxide

Let us now return to the origin of the Raman effect. Let us start by considering a light wave of frequency ν_0 in an electric field (E).
The electric field may be represented in time (t) by,

$$E = E_0 \cos 2\pi \nu_0 t \qquad 6$$

Where E_0 is the maximum amplitude of the electric field. (volts/metre)
From equation (5) it can be seen that such an oscillating field would produce an oscillating dipole described by,

$$P = \alpha E_0 \cos(2\pi \nu_0 t) \qquad 7$$

Now let us assume that the molecule is vibrating with a frequency ν_{vib}, the nuclear distortion from its equilibrium position q will be given by,

$$q = q_0 \cos(2\pi \nu_{vib} t) \qquad 8$$

where q_0 is the maximum vibrational amplitude and ν_{vib} is the vibrational frequency (hertz).
If there is a change in the polarizability with the nuclear displacement, we assume the variation will be linear, and the amplitude of the vibration small, the polarizability of the periodically distorting molecule will become,

$$\alpha = \alpha_0 + \left(\frac{\delta \alpha}{\delta q}\right)_0 q \qquad 9$$

where α_0 is the polarizability at the equilibrium position, and the rate of change of α and q are evaluated around the equilibrium position. Hence the variation in polarizability during the vibration will be,

$$\alpha = \alpha_0 + \left(\frac{\delta \alpha}{\delta q}\right)_0 q_0 \cos(2\pi \nu_{vib} t) \qquad 10$$

By substituting α from equation (10) into equation (7) we obtain,

$$P = \alpha_0 E_0 \cos(2\pi \nu_0 t) + \left(\frac{\delta \alpha}{\delta q}\right)_0 q_0 \cos(2\pi \nu_{vib} t)\cos(2\pi \nu_0 t) \qquad 11$$

using the trigonometric identity,

$$\cos A \cos B = \frac{1}{2}(\cos(A + B) + \cos(A - B)) \qquad 12$$

We can rearrange equation (11) to give,

$$P = \alpha_0 E_0 \cos(2\pi \nu_0 t) \qquad (13)$$
$$+ \frac{1}{2}\left(\frac{\delta \alpha}{\delta q}\right)_0 q_0 (\cos(2\pi[\nu_0 + \nu_{vib}]t) + \cos(2\pi[\nu_0 - \nu_{vib}]t))$$

Now as already mentioned the induction followed by the relaxation of a dipole results in absorption and the scattering of radiation (because the radiation is the source of the field causing the "electron cloud" to distort). The first part of equation 13 predicts that a dipole will be induced (and hence scattering will occur) at the same frequency as the source of radiation ν_0. The second part of the equation indicates that this scattering is accompanied by radiation at **shifted frequencies** $\nu_0 + \nu_{vib}$ and $\nu_0 - \nu_{vib}$. It is this **inelastic** scatter that is named after Sir C.V. Raman. In figure 2.11 the experiment is defined.

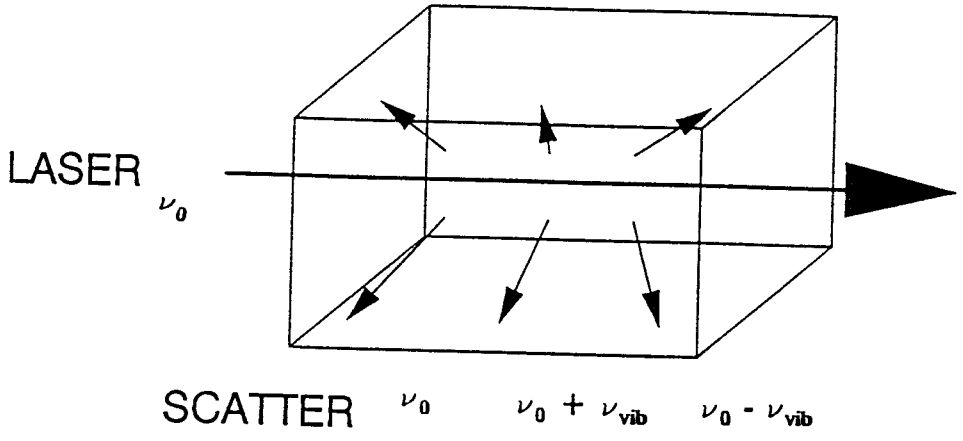

Figure 2.11 A schematic diagram showing the Raman experiment

The **elastic** scatter is known as Rayleigh scatter named after Lord Rayleigh who extensively studied the phenomenon in the 19th century. The inelastic light scatter with a frequency ($\nu_0 + \nu_{vib}$) is colloquially known as anti-Stokes Raman scatter, and scatter at a frequency ($\nu_0 - \nu_{vib}$) is known as Stokes Raman scatter. Since the vibration of chlorine is at 505cm^{-1}, the analysis (equation 13) then predicts that excitation with light at frequency ν_0 would produce a three line spectrum as in figure 2.12.

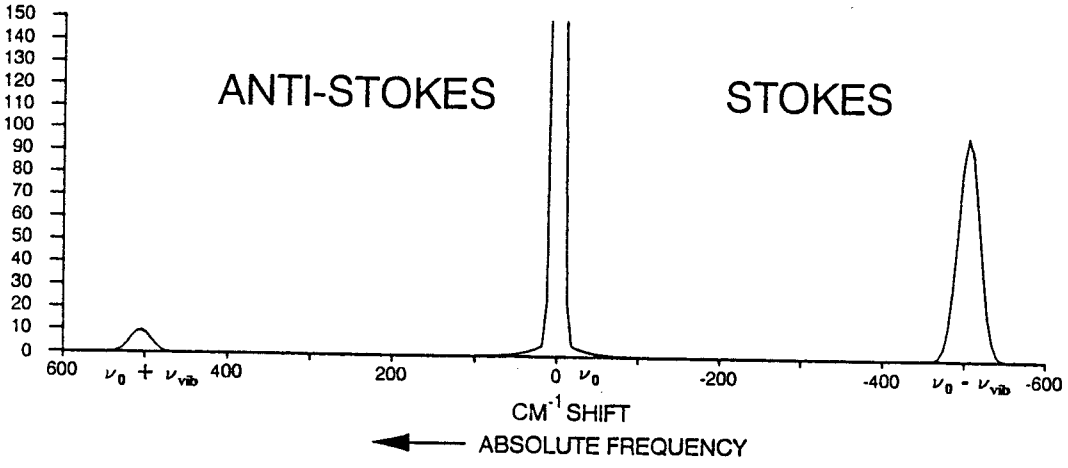

Figure 2.12 Raman spectrum of chlorine gas

Several points are clear; the source radiation is not classically absorbed[2] (if it were, no scattering would occur) but rather, slightly attenuated. The Rayleigh scatter is weak, the Raman much weaker. The intensity of the Stokes is invariably greater than the anti-Stokes equivalent bands, see section 2.2.3. If an argon ion laser had been used as a source and the line at 488nm selected for the purpose the Stokes line would be at 18931cm^{-1} and the anti-Stokes at 19941cm^{-1} i.e. the whole scattering spectrum would lie in the blue part of the visible. If a near infra-red laser eg. Nd^{3+}:YAG (ν_0 = 9398cm^{-1}) was used, the whole spectrum would lie at 8893, 9398 and 9903cm^{-1} all in the near infra-red part of the spectrum. Thus the useful plot for displaying Raman data is to plot the intensity of scatter versus **frequency shift**. In this mode the spectra can then be directly compared with its infra-red counterpart. An example displaying this point is shown in figure 2.13.

[2] Strictly this is nonsense, because if no absorption occurs then their is no scatter!

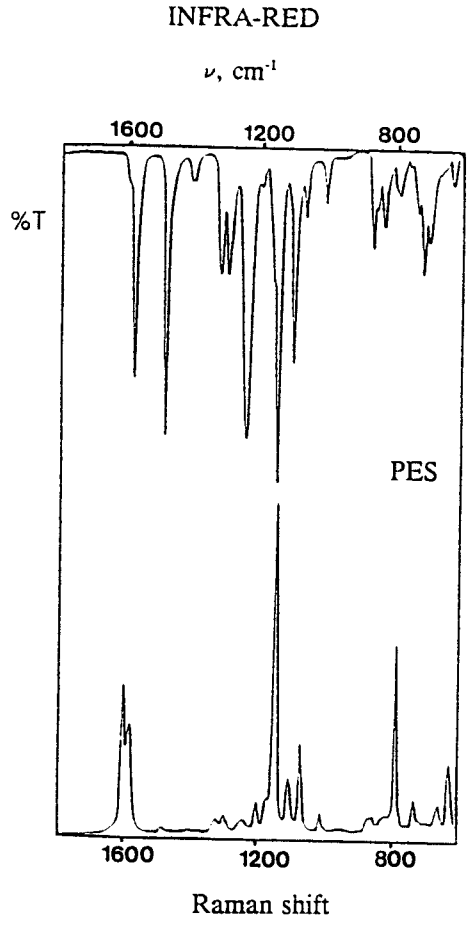

Figure 2.13 The infra-red and Raman spectrum of poly(ether sulphone). (Courtesy of G. Ellis).

Further, classical analysis yields the rather unexpected result that the intensity of Rayleigh and Raman scatter is proportional to the frequency of the scattered radiation raised to the fourth power.

2.2.3 The quantum mechanical definition of the Raman effect

Viewed quantum mechanically, the polarization process instantaneously elevates the energy of the molecule, and scatter allows it to return to either the state from which it came **or** another vibrational energy level. The process is drawn in figure 2.14.

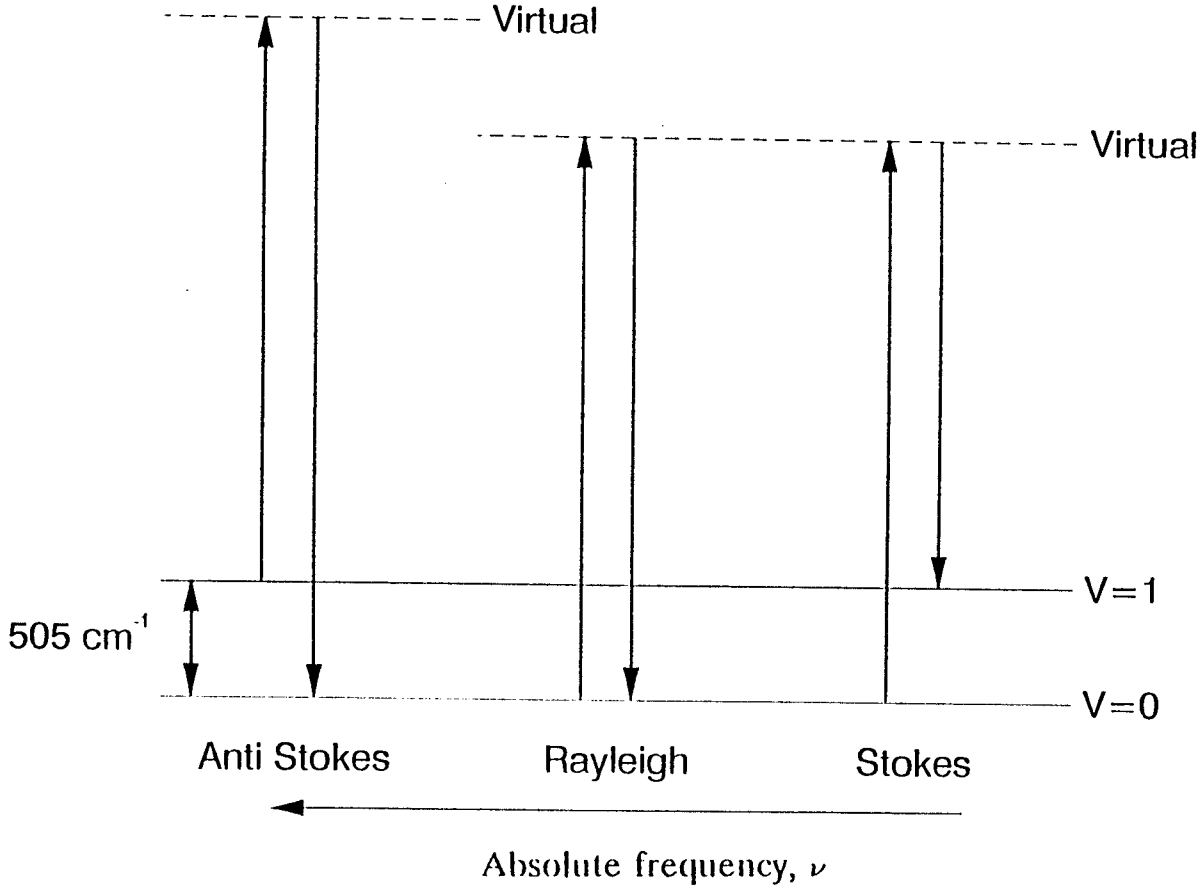

Figure 2.14 Diagram showing the Raman effect

Looking back at figure 2.12, the red shifted Stokes spectra of chlorine clearly consists of one relatively intense line. Clearly the blue shifted line is weaker than its equivalent red shifted partner, why is this so? The intensity of the Raman

scatter is related to the population of the initial state of the molecule. For Stokes scatter the intensity is normally related to the population of the ground state, V=0, and for anti-Stokes to that of the first excited vibrational level, V=1. These populations are given by the Boltzmann distribution,

$$\frac{n'}{n} = \frac{g'}{g}\exp\left(\frac{-\Delta E}{kT}\right) \qquad 14$$

Where n is the population, g is the degeneracy of the levels, ΔE the energy difference between the levels ($Jmol^{-1}$), k is the Boltzmann constant, and T the absolute temperature, $'$ denotes the upper level. Hence the population of the V=0 level will be greater than that of the excited levels, so the Stokes scatter at normal temperatures will be more intense than the equivalent anti-Stokes scatter. To summarise, assuming that the same specimen can be examined by both Raman and infra-red techniques, (and this can pose a sampling problem) two studies can be made of the vibrational behaviour of the molecule, one absorption over the frequency domain of the electromagnetic radiation range typical of the vibration (200 - 4000cm^{-1}) and the other by inelastic light scattering, the spectra being acquired in the green or near infrared. If presented as absorption vs frequency and scattering intensity vs frequency shift the two spectra are directly comparable, see figure 2.13.

Although we have seen an analysis of the activity in IR and/or Raman spectroscopy for carbon dioxide, we obviously need to know which fundamental modes are expected to appear in each spectrum. Several rules of thumb need emphasis before we proceed.

(a) If a molecule is centrosymmetric (e.g. polyethylene) **no mode occurs in both spectra.** Modes give rise to bands in IR or Raman or neither.

(b) Modes characterized by having large polarizability changes associated with them almost invariably give rise to weak infrared absorption and vice versa. i.e. Even where mutual exclusion arises, as in centrosymmetric molecules, strong

Raman bands are rarely intense in the IR and vice versa. Poly(ether sulphone) exhibits this effect nicely, the appearance of the two spectra in figure 2.13 are very different.

(c) Vibrations involving heavy elements frequently give rise to intense Raman bands, similarly π electrons are more polarizable than σ ones, hence strong spectra occur where vibrations involve large vectors on π bonded species.

2.3 Raman spectrometers

The two dominant problems in Raman spectroscopy are the incredibly low intensity of Raman light and the relatively high intensity of the light collected at the laser wavelength. To solve these dual problems we need a highly sensitive spectrometric system combined with very high discrimination i.e. the ability to see one feature and ignore another close to it in wavelength. The classical method of recording spectra has been to use a laser source, an efficient system for collecting the scattered light and a scanning multiple monochromator monitored by a high performance photomultiplier. More recently, the use of spectrographs and position sensitive detectors [5-7] (rather than scanning multiple monochromators [8] and photomultipliers) have become popular, because they provide higher quality spectra more rapidly than using the old methods. Very recently a new method has appeared; the so called Fourier Transform technique. In this instance the laser operates in the near infrared, the scattered light is collected and passed through a modified FT-infrared instrument, the interferogram so generated being transformed into the spectrogram.

2.3.1 Laser

The Nd^{3+}:YAG lasers are solid state devices relying on a crystal of yttrium aluminium garnet doped with about 3% Nd^{+++} ions. The driving source is either broadband (a high pressure xenon arc lamp or a powerful tungsten quartz iodine lamp) or, more efficiently, near infrared power sources (provided by a set of optically coupled gallium arsenide injection lasers)

The broadband powered Nd^{3+}:YAG lasers tend to be more powerful and more economical to purchase but are very inefficient. As a result, very high powers are fed into an optically reflecting cavity containing both the laser rod and the source lamp, the whole system being cooled by pure water. The solid state laser powered devices can approach 50% in overall efficiency, hence they have no cooling problems. The solid state lasers are of a relatively low power output but are rapidly improving and must in time replace the lamp powered devices.

Nd^{3+}:YAG lasers emit at 1.0645μ (9398cm^{-1}) with a line-width of about 0.6cm^{-1} at powers up to several watts. Stabilised devices are available, hence making them an ideal laser for Raman studies. The Nd^{3+}:YAG can be made to generate radiation at 1.3μ and this will quite probably prove to be of use as a Raman source in some areas of polymer science. The tuneable lasers (dye or Ti sapphire) have been used mainly in the study of resonance Raman phenomenon but will certainly be utilized in FT and dispersive systems in the 800nm range.

2.3.2 Interferometer

In a Michelson interferometer colimated radiation is split into two beams of roughly equal intensity. These two beams are then passed through two optical paths, one of which can be varied in length, and then they are recombined. Figure 2.15 shows a block diagram of the classical design.

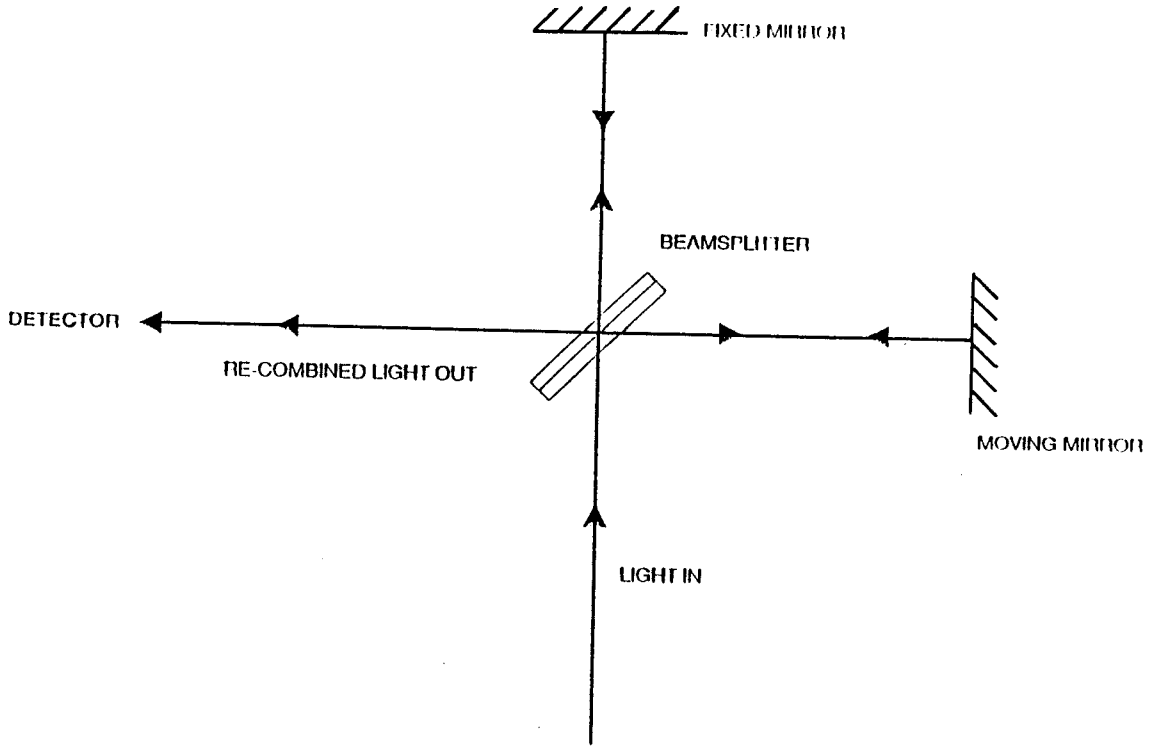

Figure 2.15 The Michelson interferometer

The device is so designed that as the length of one path is varied, it sweeps through a position where the two paths are optically identical. At this point, constructive interference between the beams occurs and efficient transmission results. At other optical delays, namely at $n\lambda/2$ where n is an integer and λ the wavelength, destructive interference occurs. As a result, the transmission characteristics of an interferometer for a white source have a centre burst and a falling complex waveform to each side of it to produce the so-called interferogram, shown in figure 2.16. It is this, that is Fourier transformed to produce the familiar spectrogram.

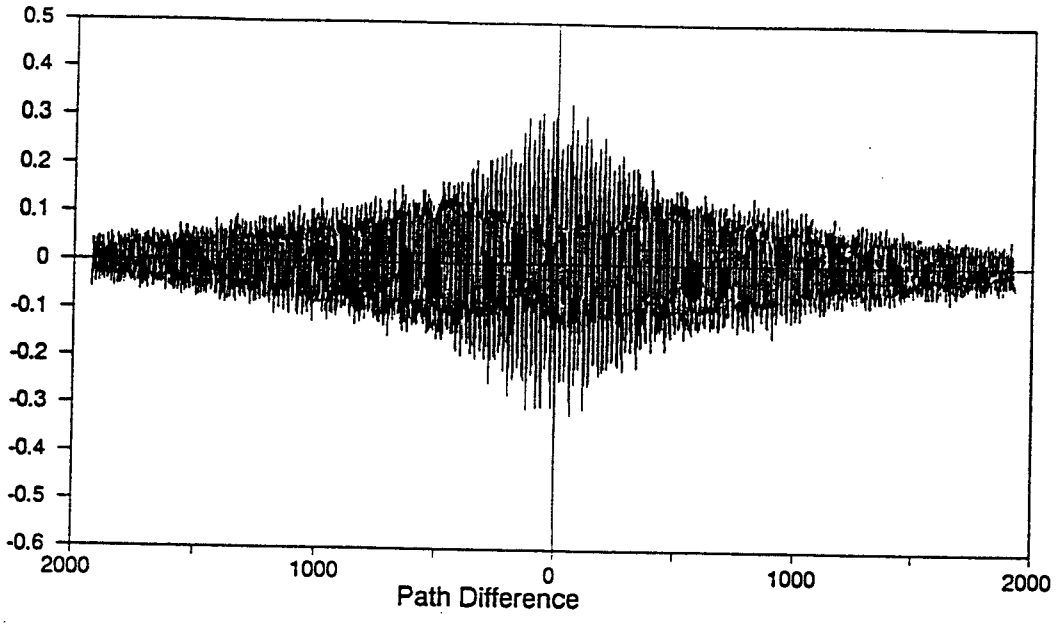

Figure 2.16 A Raman interferogram

2.3.3 Detectors

Since photomultipliers are insensitive beyond 1μ, solid state detectors are invariably used in near infra-red experiments. Several are popular, but the battle seems to be drawn between those who prefer the InGaAs detectors and others the extended germanium devices. The former performs adequately at room temperature, the latter requires cooling to liquid nitrogen temperatures.

Both devices are solid state systems and are relatively "noisy". Of course the noise can be accommodated using interferometers, although it does limit their performance.

2.4 Thermal analysis

Thermal-analytical methods embrace a broad group of measurements of great importance to the polymer industry, since not only are the thermal properties of polymers important to the users, but their technological properties depend to a great extent on their thermal history.

2.4.1 Differential Scanning Calorimetry (DSC)

Essentially, the DSC instrument permits the measurement of the amount of heat taken up from, or emitted to the surroundings, per unit time, under isothermal conditions, or during heating or cooling. In this manner, heat capacities, melting and crystallization enthalpies, transition temperatures, specific heats, etc.. can be measured, and from this, data about phase transitions, crystallization processes can be obtained, and kinetic processes, such as melting, recrystallization, isothermal polymerization, etc.. can be followed.

Figure 2.17 shows a schematic diagram of a DSC instrument. In essence the instrument consists of two platinum alloy cups mounted in an aluminium block. The sample is placed in one cup (enclosed in an aluminium pan) whilst the other cup containing an empty aluminium pan, acts as a reference. The instrument operates on the principle of maintaining the sample temperature equal to that of the reference, as the temperature is scanned. The melting of a sample is an endothermic process, which would make the temperature of the sample pan colder than the reference pan. However, the temperatures are controlled by means of small heating coils placed under the cups. The difference in electrical power required to maintain the two cups at the same temperature is output to the chart recorder and gives a trace of the endotherm as the temperature is scanned.

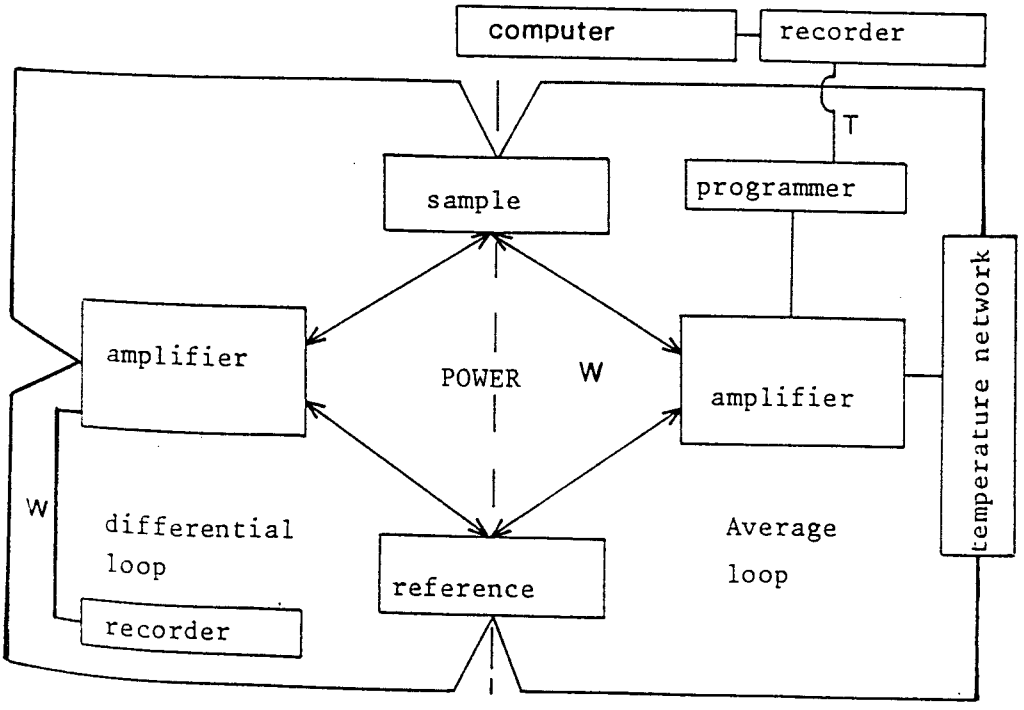

Figure 2.17 Schematic diagram of a differential scanning calorimeter

The conventions used in DSC are shown in figure 2.18. The area under the peaks indicate the total energy transfer to or from the sample compared with the reference material.

The melting point is usually taken as the "position" of the endotherm peak maximum, but the peak shape and position is dependent on the heating rate and size of sample. These complications are related to a thermal time-lag effect caused by the poor heat conduction through the polymer sample. The effects can be minimised by a slow heating rate and small sample size, but these conditions cause additional problems with sample annealing.

The heat of fusion data can be used to determine the crystallinity, χ, using the following expression,

$$\chi = \frac{\Delta H_s}{\Delta H_c} \times 100\% \qquad 15$$

Where the subscripts s and c refer to the sample and the 100% crystalline material respectively.

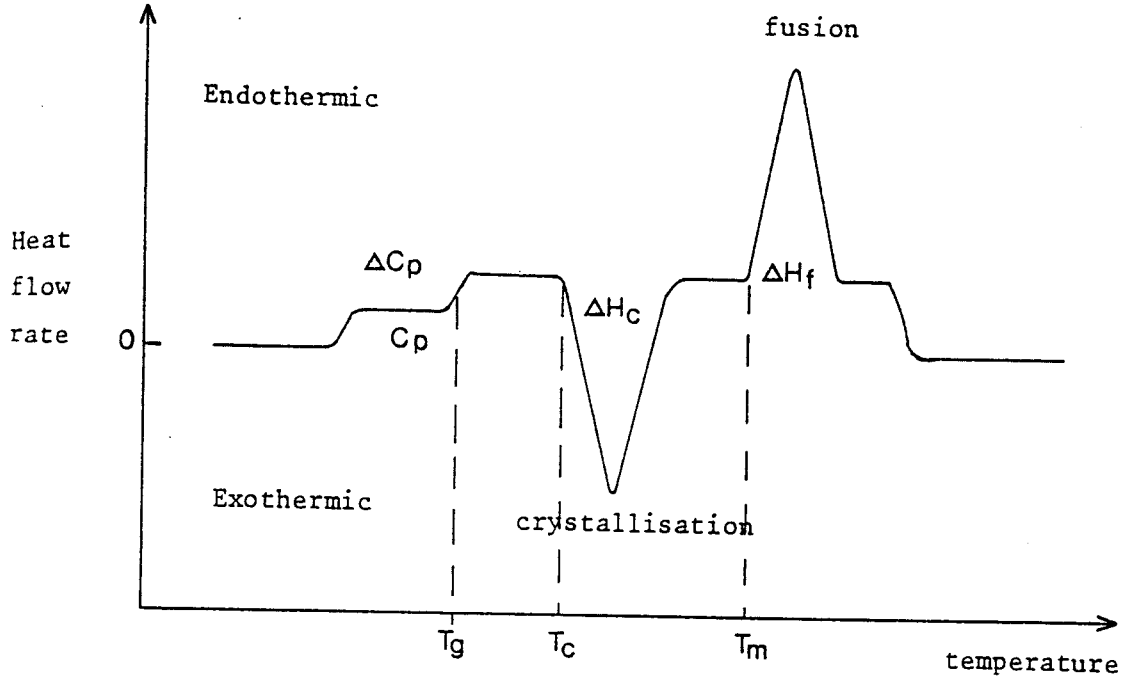

Figure 2.18 Conventions used for thermal analysis (C_p = specific heat, T_g = glass transition temperature, T_m = melting transition temperature, T_c = crystallization temperature

2.4.2 Thermogravimetric analysis (TGA)

TGA measures the change in weight of a sample under isothermal conditions, or at a constant rate of heating or cooling. The balance and sample chamber can be filled with inert or reactive gas.

2.5 X-Ray diffraction

X-ray diffraction is one of the fundamental techniques for studying the order in solids, and in particular crystalline polymers [10]. Information on the polymer texture can yield parameters such as degree of crystallinity, crystalline orientation and crystallite size. Information can also be obtained on the lower degree of ordering present in amorphous polymers or melts.

2.5.1 Instrumentation

Figure 2.19 shows a typical X-ray tube.

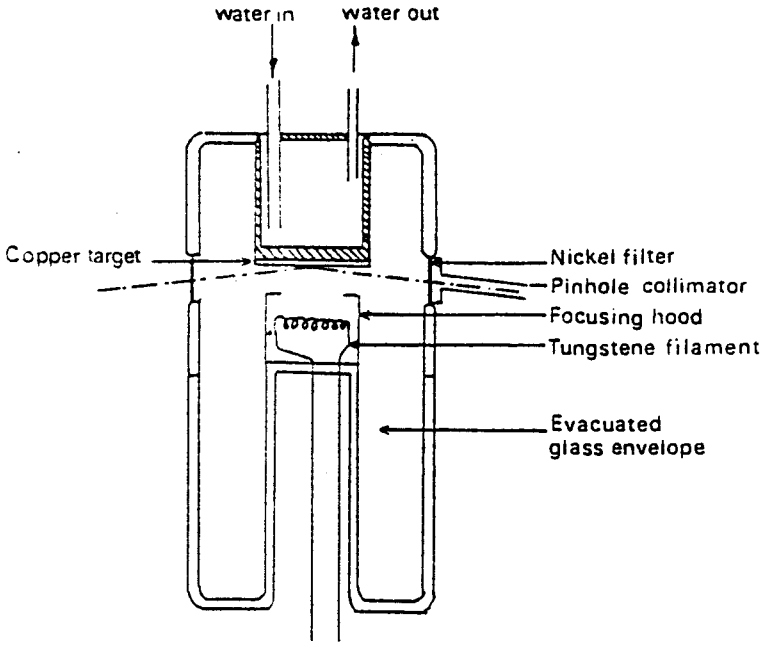

Figure 2.19 An X-ray emission tube

The tube consists of a permanently evacuated glass envelope into which is sealed a tungsten filament separated by about 1cm from the copper target. A low voltage is applied across the filament which is heated by the passage of the current. The electrons emitted are accelerated towards the anode by the application of a high voltage of about 35kV between the filament (cathode) and the copper target (anode). The high energy electron stream hits the anode, and

about 98% of the energy is converted to heat. The anode is cooled by a rapid flowing stream of water. The filament is surrounded by a focusing hood to form a line focus approximately 1cm x 0.01cm at the target. The heat dissipation of a line focus is greater than that of a spot focus, this allows a higher electron current to pass (22mA) and hence produces a greater intensity of X-rays at the sample.

X-rays are emitted from the target in all possible directions, but only a narrow beam (in the angular range of highest intensity) making an angle from 3 to 6° with the face of the target is used. This radiation passes out of the evacuated envelope through a window made of beryllium (a low absorber of X-rays).

The X-ray radiation emitted by the target is never monochromatic, it covers a considerable spectral range as can be observed from figure 2.20.

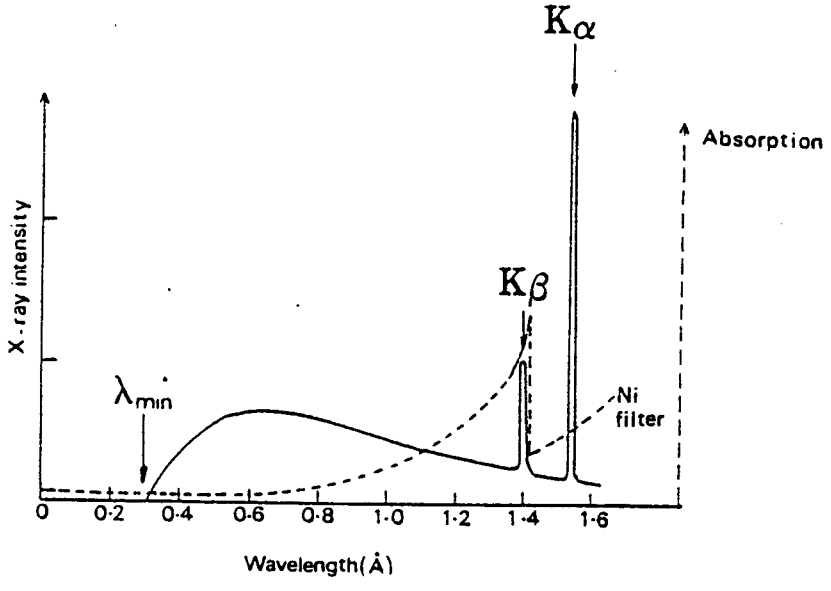

Figure 2.20 The emission of an X-ray tube with a copper target

X-ray tubes emit white (Bremstrahlung) radiation and characteristic radiation

(dependant on target material). White radiation is produced by electrons losing part of their energy on collision with the target, according to the equation:

$$\lambda - \frac{hc}{\Delta E} \quad 16$$

λ_{min} is where the striking electron loses all of its energy on one collision which is converted to X-radiation. This occurs when $\Delta E = eV$ where e is the charge on an electron and V is the drop in potential between the cathode and anode. The probability is that only part of the kinetic energy of an electron is lost on collision with the target. Thus X-radiation is emitted over a range of wavelengths. The white radiation depends on the operating voltage of the tube and causes a background level in the diffraction pattern.

The characteristic radiation evident in figure 2.20 occurs when an electron of sufficient energy strikes the target and causes the ejection of an electron from the K shell of, in this case the copper target atoms. Ejection of the K atoms is followed by the transfer of an electron from a higher energy level to fill the vacant site. The copper target is capable of producing two emission lines; K_α and K_β depending on the energy level from which the electron comes to fill the vacant K shell energy level. The K_α line has a greater intensity than the K_β line so is therefore preferred. K_β radiation is filtered out by using a nickel filter.

The emerging X-ray beam is collimated by a pin-hole collimator, thus resulting in a greater resolution of diffraction pattern.

2.5.2 Theory

Most X-ray diffraction experiments consist of a monochromatic beam of X-rays incident upon a three-dimensional lattice having a particular group of atoms at each of its lattice points. The distance between adjacent lattice points are

comparable with the wavelength of the X-rays. The X-rays interact with the electron density of each atom in the regular lattice array. Each atom in the array can be thought of as a secondary X-ray source radiating in all directions. The scattering is coherent so that interference occurs between X-rays emitted from these secondary sources. The basic laws relating the lattice geometry, X-ray wavelength and the directions of the diffracted beams are relatively simple. Consider, the planar array of dots shown in figure 2.21a.

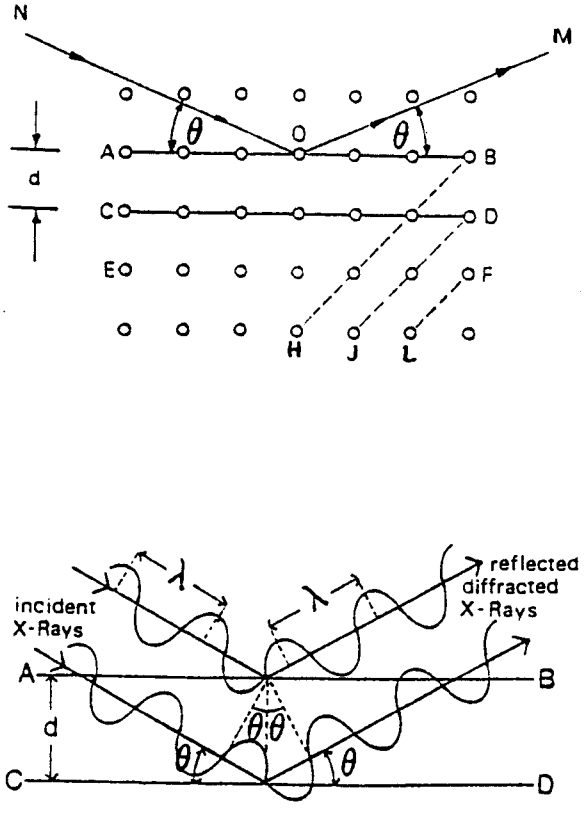

Figure 2.21 The diffraction of X-rays by a simple crystal lattice

The line AB represents the section of a particular crystallographic plane which belongs to the set of planes AB, CD, EF, ...etc. If a narrow parallel beam of monochromatic X-rays (NO) is incident upon the plane AB in isolation, then a diffracted beam (OM) will appear as if reflected by the mirror plane AB.

Similarly, if taken in isolation, the same behaviour will occur at CD, EF etc. If all planes are considered together then interference occurs, dependent on the path difference of the emerging diffracted beams. Constructive interference occurs when BRAGGS law applies, which is given by the equation:

$$n\lambda = 2dSin\theta \quad 17$$

where n is any integer, λ is the wavelength of radiation and d is the perpendicular spacing between the planes. This is illustrated in figure 2.21b.

Diffracted beams, obeying the same law, will be associated with all other sets of crystallographic planes such as HB, MD, LF, etc shown in figure 2.21a. It must be emphasised that the angles at which diffracted beams appear are dependent on the perpendicular spacing between the planes and not the type or arrangement of atoms within the plane. The latter determines the intensity of the diffracted beam.

Now consider a crystalline powder which is in effect a large number of randomly oriented small crystallites. When a parallel monochromatic beam of X-rays passes through such a sample there will inevitably be a number of small crystallites which satisfy the Bragg angle for a particular set of planes. The diffracted beam will completely cover the surface of an imaginary cone, see figure 2.22a.

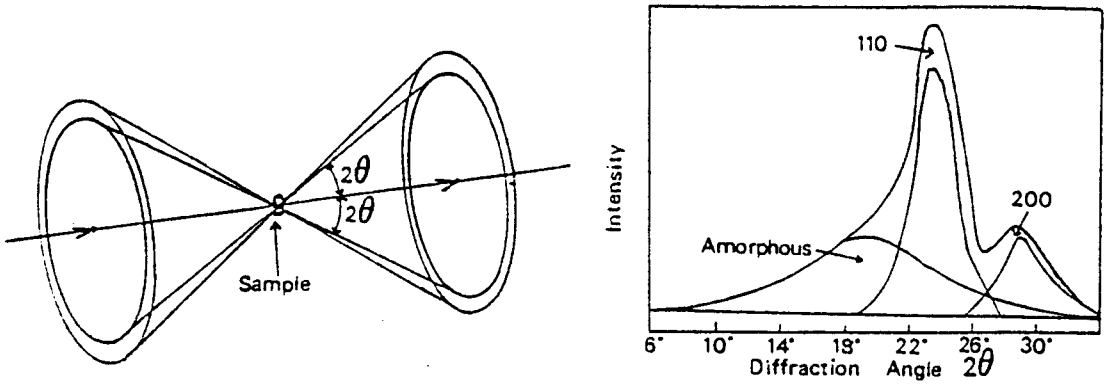

Figure 2.22 (a) The diffracted beams of a crystalline powder, (b) The X-ray scattering of polyethylene

Other sets of cones corresponding to planes with different spacings will also occur. One of the most common methods of recording the diffraction pattern is on a flat photographic film perpendicular to the incident X-ray beam., In this case, the diffraction pattern appears as a series of concentric rings, known as DEBYE-SCHERER rings, about the intersection of the "transmitted" beam and the photographic film.

Considering the type of diffraction patterns which can be recorded on a flat film when a beam of monochromatic X-rays is incident on a polymer sample. If the polymer is completely amorphous then the pattern consists of one or two broad diffuse rings concentric with the transmitted beam. The outer ring or halo (corresponding to a Bragg spacing of 4-5Å) is the most intense, and occurs for all amorphous polymers, and is more or less independent of the chemical structure of the polymer. This ring is associated with the average separation of two molecular chains. The inner halo is less frequently observed and appears

only in polymers which have side groups, and depends on their nature and number, corresponding to polymer chains separated by a single side group.

The diffraction pattern of a semi-crystalline polymer is best described as a super position of amorphous and powder diffraction patterns. Figure 2.22b shows the typical scattering envelope of a polyethylene sample resolved into the contributions from two crystalline peaks, and a broad amorphous peak. The degree of crystallinity can be estimated from the areas under the peaks. In oriented samples the diffraction rings become incomplete arcs due to the absence of crystallites at particular angles or orientation with respect to the incident beam. The measurement of the variation in band intensity around the circumference of a diffraction ring gives an indication of the degree and direction of the orientation for a particular crystal plane.

In the following chapters readers will find the analysis of a series of polyester systems (all of significant commercial interest), in order to assess the potential of FT-Raman for routine analysis, as already mentioned several other techniques will be encountered whilst reading this thesis, these have been included as supporting evidence for results supplied by Raman spectroscopy.

Chapters 3 and 5 of the thesis were in collaboration with my industrial sponsors, ICI Paints, Slough, and I would like to take this opportunity to acknowledge their support.

References

1. S. Krimm, *J. Chem. Phys.*, **25**, 549 (1956)

2. A. Vincent, "Molecular Symmetry and Group Theory", J. Wiley and Sons, Chichester, (1977)

3. N.B. Colthup, L.H. Daley, S.E. Wiberley, "Introduction to Infra-red and Raman Spectroscopy", Academic Press, New York, (1975)

4. A. Fadini, F.-M. Scnepel, "Vibrational Spectroscopy: Methods and Applications", Ellis Horwood, Chichester, (1989)

5. D.N. Batchelder, *European Spectroscopy News*, 80, 28, (1988)

6. H.O. Hamaguchi, *Appl. Spectrosc. Rev.*, 24, 137, (1988)

7. M. Bridoux and M. Delhaye, "Advances in Infra-red and Raman Spectroscopy, 2, R.J.H. Clark and R.E. Hester, eds,. Heyden, London, (1976)

8. D.P. Strommen and K. Nakamoto, "Laboratory Raman Spectroscopy", J. Wiley and Sons, New York, (1984)

9. F.W. Billmeyer Jr., "Textbook of polymer science", 3rd edn. J. Wiley and Sons, (1984)

10. H. Tadokoro, "The Structure of Crystalline Polymers", J. Wiley and Sons, New York, (1979)

CHAPTER 3: THE APPLICATION OF FOURIER TRANSFORM RAMAN SPECTROSCOPY TO THE STUDY OF ALKYD RESINS

3.1 Introduction

Unlike infra-red spectroscopy, there has been little interest by the Paint and Coating industry in the possible use of conventional Raman spectroscopy in the analysis of surface coatings. There are four basic reasons for this lack of interest in the conventional Raman technique;

(a) The cost of instrumentation generally exceeds the budget of most industrial analytical laboratories.,

(b) If the sample under investigation absorbs strongly at the excitation and/or Raman wavelengths, then the Raman scatter will be to weak to be detectable.,

(c) FLUORESCENCE- Which may be inherent to a material or due to impurities, may obscure the weaker Raman scattered radiation.,

(d) Only a relatively small number of industrial samples will give interpretable Raman spectra, and do so only after considerable time and effort, skilled operators are a prerequisite, and the cost per sample is therefore very high [1].

Although there are clear problems with conventional Raman spectroscopy, in the Paints and Coatings field, the technique can provide unique information and there are potential advantages for the investigation of a broad range of analytical problems. For example, highly polarizable functional groups give a strong Raman scattering intensity, while groups with high polarity tend to give intense resonant absorptions in the infra-red. Hence, structural and chemical properties of a material not easily characterized by infra-red alone may-be approached by Raman methods. Raman spectroscopy has a high sensitivity for the symmetrical bonds, such as C-C, N-N, S-S, O-O, and also those showing greater π character; C=C, etc, which as we shall see later has important implications for chemical processes, such as conformational and configurational modifications.

Ideally, investigators would like to examine the chemical changes while they are taking place in a film and in-situ. Infra-red spectroscopy, and to a lesser extent Raman spectroscopy fulfil this desire. Infra-red spectroscopy has thus been used for a considerable number of years [2,3] to examine resin curing. Despite its

popularity infra-red spectroscopy tends to be insensitive to the subtle changes associated with the cure of these resins. For these reasons many studies have been limited to the later stages of drying [4,5]

Despite the fact that Raman spectroscopy is sensitive to the subtle changes occurring during autoxidation, there are only a few examples to be found in the literature where conventional Raman spectroscopy has been used in the investigation of paint systems. These include monitoring the cure of alkyd resins [4], and accelerated weathering of alkyd paints [6]. The spectral data recorded was poor due to the problems of sample fluorescence and high background response, which becomes increasingly significant as the paint cures.

With the advent of the Near infra-red (nir) FT-Raman technique, many of the problems related with sample fluorescence and the correspondingly high backgrounds encountered in conventional Raman spectroscopy have been alleviated, although fluorescence can still be encountered in some samples.

3.1.1 Advantages of FT-Raman spectroscopy for studying paint materials

Several advantages exist;

(1) Little or no sample preparation is required so samples in the, "as received" form can be examined, thus aiding rapid routine analytical analysis.

(2) Pigmented films are easily analyzed (see later).

(3) Waterborne systems can be studied, since water is a weak Raman scatterer. Water does however absorb in the (nir) so the Raman radiation from the sample can be absorbed.

(4) Symmetrical bonds tend to be strong Raman scatterers (eg. C-C, N=N, and S-S, etc.), this fact is capitalized upon in following appropriate chemical

processes, such as emulsion polymerizations, crosslinking reactions, and polymer network growth.

(5) C=C configurations (ie. *trans, cis,* vinyl vinylidene, etc.) can be distinguished.

(6) FTIR reflectance measurements on films tend to suffer from spurious optical effects that can make direct interpretation difficult, [7,8] whereas films can be easily characterized using nir FT-Raman spectroscopy[3].

(7) Since the laser beam can be focused down to about 100μm, small samples and defects in coatings can be studied without the use of microscopic techniques.

(8) There is little or no interference from atmospheric carbon dioxide. However atmospheric water will weakly absorb some of the Raman radiation but this is a negligible effect particularly for purged optical benches.

3.1.2 Aims

Preliminary feasibility studies, for the application of the FT-Raman technique (corresponding to sections 3.4-3.4.3) have been made. The project was sponsored in-part by ICI Paints Research Centre, Slough, and at this stage I would like to thank Dr. M. Claybourn for numorous and humorous discussions, and for supplying materials during the course of the research.

3.2 Background

Conventional paint technology based on oil modified alkyd resins still forms a significant proportion of currently marketed paint systems.

Oils used in the synthesis of alkyd resins are the glycerol esters of saturated and unsaturated fatty acids, (see figure 3.1) and the properties of the individual oil depend upon the type and proportion of the constituent acids making up the oil.

---

[3]Film thickness ideally should be greater than 200μm, any lower than this and wave-guide techniques need to be considered

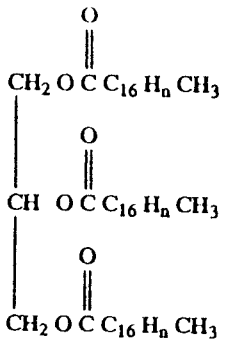

Figure 3.1 The structure of a typical glycerol ester

The oils used are divided into three quite distinct types, they are discribed as either drying, semi-drying or non-drying. This property is related to wether on its own the oil is able to oxidize and crosslink to produce a dry film. This behaviour is directly related to the concentration of the various fatty acids contained in the structure. Most of the acids contain eighteen carbon acids, which in turn have one, two, or three double bonds along their length. It is this degree of unsaturation which governs the drying properties. (see later)
Table 1 shows the formulae of the commonly used fatty acids.

Lauric acid	$CH_3(CH_2)_{10}COOH$
Stearic acid	$CH_3(CH_2)_{16}COOH$
Linoleic acid	$CH_3(CH_2)_4CH=CHCH_2CH=CH(CH_2)_7COOH$
Linolenic acid	$CH_3CH_2CH=CHCH_2CH=CHCH_2CH=CH(CH_2)_7COOH$
Eleostearic acid	$CH_3(CH_2)_3CH=CHCH=CHCH=CH(CH_2)_7COOH$

Table 1 The formulae of the commonly encountered fatty acid used in paint manufacture

Table 2 shows the composition of the fatty acids in the corresponding oils.

	saturated acid	Oleic acid	Linoleic acid	Lino-lenic	Conjug. acid
Tung	6	7	4	3	80
Linseed	10	20-24	14-19	48-54	0
Soya-bean	14	22-28	52-55	5-9	0
Castor oil	2-4	90-92	3-6	0	0
Tall	3	30-35	35-40	2-5	10-15
Coconut	89-94	6-8	0-2	0	0

Table 2 The composition of some natural oils

The fatty acid portion of the molecule comprises roughly 95% of the total molecular weight, so obviously the characteristics of the triglycerides differ widely according to the nature of the fatty acid.

3.2.1 Synthesis of an oil modified alkyd resin

In the first stage, called the "Monoglyceride Preparation", glycerol (or another polyol, for example pentaerythritol) and the oil in the molar ratio of 2:1 are reacted at elevated temperature (240°C) in the presence of a basic catalyst (NaOH), to form a monoglyceride. See figure 3.2.

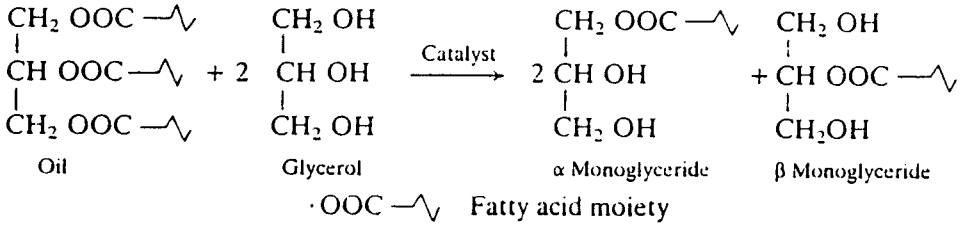

Figure 3.2 The synthesis of α and β monoglycerides

The diglyceride is also a product of the reaction, but is present at a much lower concentration. Preparation of the final resin is carried out by the addition of a dibasic acid such as phthalic anhydride which leads in turn to a partially crosslinked gel-like product, which can have the general formula shown in figure 3.3.

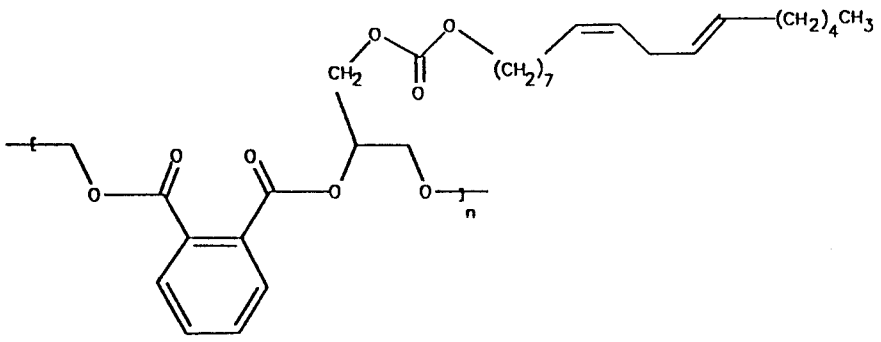

Figure 3.3 The general formula of an alkyd resin

3.2.2 The curing of alkyd resins

Autoxidation of fatty materials was first studied over a hundred years ago by DE SAUSSUERE [9]; however, the first observation of autoxidation of a C=C bond appeared 20 years later from SCHÖNBEIN [10] in 1858. Modern theories of autoxidation now date from around the early 1960's with the work from KHAN [11] and others [12-16]. They propose that as the cure proceeds oxygen is absorbed by the film, and a free-radical initiation stage promotes the formation of hydroperoxides [17], these in turn attack the α- carbon atom of a *cis* double bond in the fatty acid [11]. FTIR evidence points towards isomerism from *cis* to *trans* and conjugated hydroperoxides [17,18,19]; bands ascribed to hydroperoxide species have been observed [18,19]. Little is understood about the subsequent decomposition of the hydroperoxide, of the consumption of the C=C double bonds and its role in the formation of crosslinks. An increase in the relative intensity of bands associated with ether (C-O-C) linkages has been observed by infra-red spectroscopy [18,19,20], and recent ^{13}C NMR data has suggested that C-C crosslinks do not form and only ether and peroxy (C-O-O-C) crosslinks are observed [20].

The following mechanism provides a likely explanation based on the evidence available, but it is by no means a complete picture.

3.2.2.1 Drying mechanism of a conjugated system

Oxygen attacks the double bonds directly to form free radicals, and rearrangement of the remaining double bonds takes place to give radical sites in the -1,4 and -1,6 positions (see scheme 1).

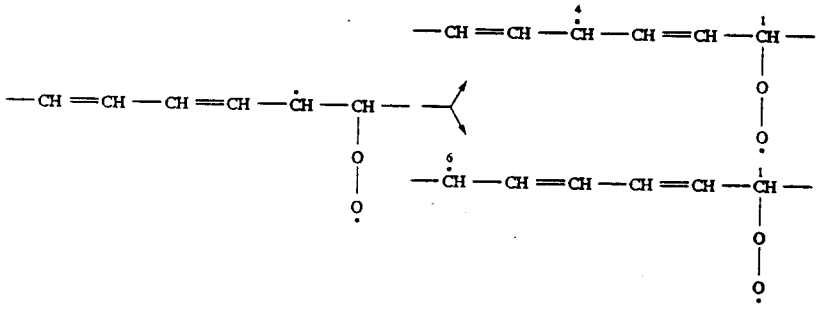

Scheme 1

Oxygen then reacts with these radicals to form peroxy radicals. Cross-linking occurs when the peroxy radicals attack double bonds in adjacent fatty acid units. The peroxy radicals produce polyperoxides, which are relatively stable but sometimes decompose under the influence of heat or light to form alkoxy radicals (RC-O•), which will in turn form ether cross-links (RC-O-CR), see scheme 2.

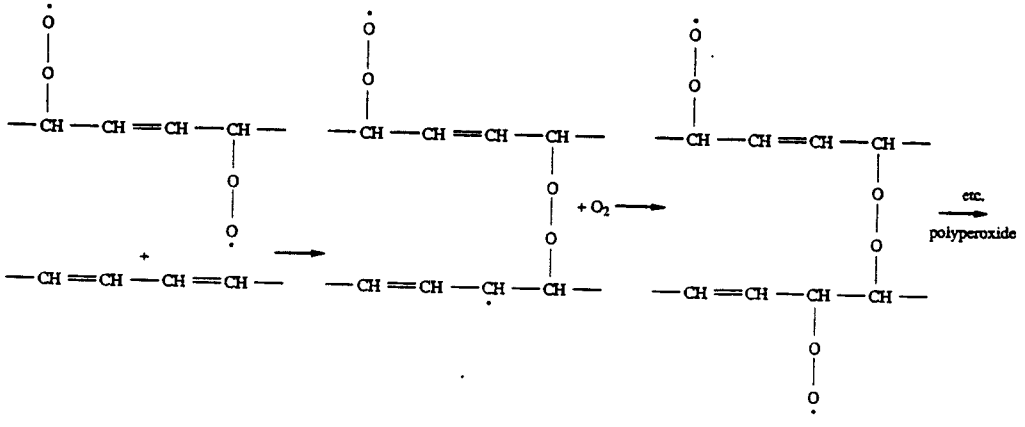

Scheme 2

3.2.2.2 Drying mechanism for non-conjugated oils

The essential difference in the non-conjugated case is that reaction occurs without the loss of unsaturation. Oxygen attacks the double bond with the formation of a hydroperoxide and a simultaneous rearrangement of the double bond system occurs to form a conjugated structure. It is believed that the hydroperoxides formed then decompose under the influence of promoters [21] to form either ether or peroxy cross-links, see scheme 3.

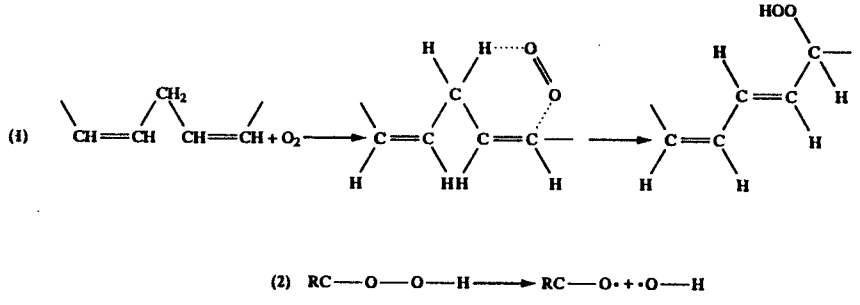

Scheme 3

A disadvantage of the air-drying-modified alkyds is the unpleasant "after odour" which persists, usually many weeks after application and exposure to the atmosphere. The odour is thought to be due to a bond scission reaction (in the fatty acid portion) leading to the formation and evolution of volatile by-products, i.e. for methyl linoleate a mixture of saturated and unsaturated aldehydes, ketones and alcohols. An in-depth study of these chain scission reactions can be found in Ref. [21].

3.2.3 Autoxidation of model compounds

Curing of alkyd resins is usually too chemically complex to permit us to draw far-reaching generalisations concerning the mechanism involved in the autoxidation process. Therefore it is necessary to study component systems such as the methyl

esters of oleic, linoleic and other similar fatty acids that model the process. In addition, these compounds can be easily obtained in a their pure form. Earlier work in this field [22] dealing with the analysis of bands in the C=C stretching region was hampered by the contribution of bands due to other components. Problems also arose from the incomplete resolution of the C=C Raman bands. Therefore it was found necessary to make a study of a range of Fatty Acid Methyl Esters (FAMEs) that are important components of the alkyd resin. Previous studies of these model compounds has helped in elucidating some of the complex processes occurring during the autoxidation, such as a study of the volatile by-products of the reaction [21]. A study of the curing processes of methyl esters of oleic, linoleic and linolenic acid have been made using FT-Raman and FTIR spectroscopy.

3.3 Experimental

A commercial soya oil based *O*-phthalate resin, supplied by Dr. M. Claybourn of ICI Paints Research Centre, Slough, Berkshire, and with the following composition was studied.

		Wt%
Pigment	titanium dioxide (optional)	27
Resin	65% soya bean oil/pentaerythritol	70
Driers	cobalt octanoate (10% Co) (surface drier)	0.2
	Zirconium complex (6% Zr) (through drier)	0.5
	Calcium octanoate (5% Ca) (auxiliary drier)	1.7
Solvent	White spirit (origin unknown)	10.6

Samples of the FAMEs were obtained from Aldrich with catalogue numbers 31,111-1, 10,335-7, and 23,526-1 corresponding to methyl oleate, methyl linoleate and methyl linolenate (all with 99% purity rating) respectively.

For the FT-Raman study of the FAMEs and alkyds, films were spread onto a 100x200mm glass plate at a constant rate of 0.065ms^{-1} using a film spreader, which produced a uniform thickness of 200 ($\pm$5)μm. The coated plates were then purged in nitrogen for 2 hours to drive off excess volatile solvents without initiating the cure. The cure started when the glass plate was removed from the nitrogen purge and placed in a well ventilated position in the open laboratory. Small samples were taken from the film at regular intervals and examined in the Raman solid cell [23]. Reproducibility tests were carried out by studying new samples of FAMEs, the results of which agree with the findings herein.

3.4 Results and Discussion

Paint films are not always ideal for study by FT-Raman spectroscopy because they are thin (typically 10-200μm) and hence, the signal-to-noise ratio in the spectra tends to be low. To optimise the measurement, when dealing with films, prolonging the signal averaging and increasing the power of the incident laser beam are utilised so that spectra can easily be obtained.

One of the major problems with FTIR in the analysis of inorganic materials is that it gives very broad absorption features, and generally make any identification of unknown inorganic materials difficult. The Raman bands from inorganic materials tend to be much sharper and details from lower frequencies become accessible. Information such as pigment-to-binder ratios can be obtained from Raman measurements with appropriate calibration data. The S/N ratio of Raman spectra from paint films can easily be improved by scraping material from the film for examination. There is a clear improvement in the S/N ratio if this is done by a factor of about 3. This improvement in the spectra is very much sample dependent since the penetration depth of the laser and the escape depth of the Raman scattered radiation will vary depending upon the components in the paint.

Generally, metallic paints give very poor Raman spectra. The reason it is thought, being the metallic flakes, which have a "cornflake" like shape, which scatter and attenuate the Raman radiation. In addition, many metallic paints contain organic pigments which tend to fluoresce, and also tinters containing carbon black. This material absorbs the laser radiation and causes sample heating and ultimately destruction of the sample. These problems combine to lead to the spectra showing very weak Raman characteristics and prominent backgrounds. Figure 3.4 shows Raman spectra taken from a metallic paint; the spectrum is of very poor quality, with few clearly definable bands.

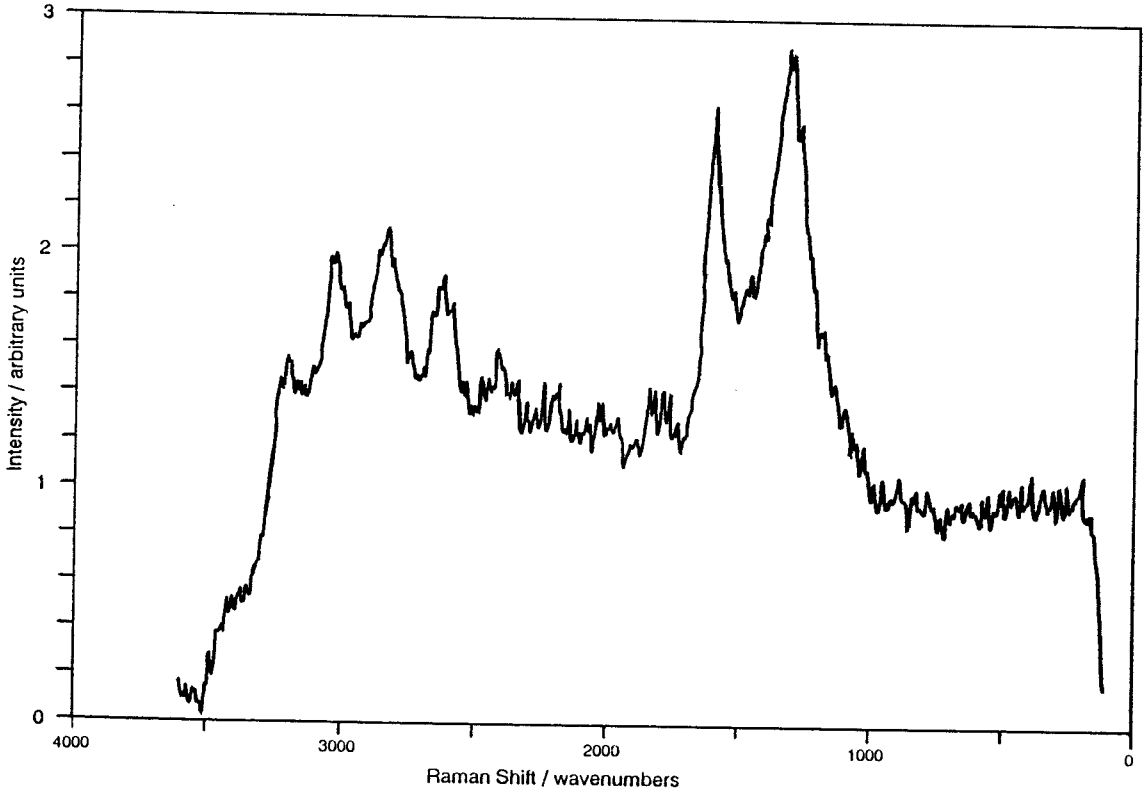

Figure 3.4 The Raman spectrum of a metallic paint

However, the fluorescence and heating effects can be reduced by pulsing the laser and ratioing the signal against the intensity of the incident pulses

(correction for pulse-to-pulse variation). The advantages of this approach have been described [24]. For this measurement the laser was pulsed at 1kHz (matched to the instrument sampling frequency) operating at 70mW. Figure 3.5 shows the spectrum of a dried metallic paint taken in this way at a resolution of $8cm^{-1}$ and with 100 scans using an extended range Ge detector operating at 77K.

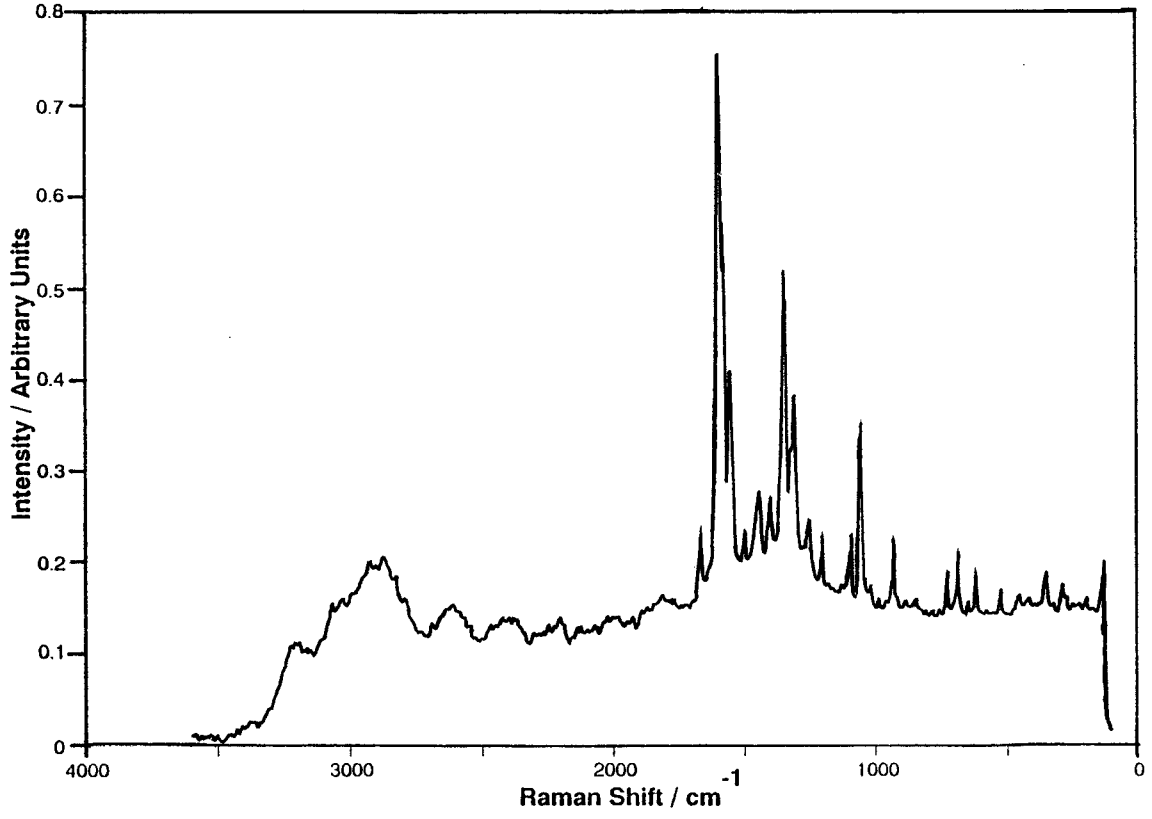

Figure 3.5 The Raman spectrum of a dried metallic paint

The instrument used in this case was a prototype based on a modified Perkin Elmer 1720 FTIR. The resulting spectrum is greatly improved with a much reduced background response.

As mentioned earlier carbon black, at low levels, is a common tinter/pigment in

paint films. Although spectra can be obtained from carbon containing materials, the presence of carbon black in paints at levels as low as 1% w/w dry film, destroys any spectral features. The reason behind this problem is two-fold. The carbon induces absorption which severely attenuates the Raman spectrum produced. Unfortunately, absorption of the laser radiation also causes the sample to heat and in the worst cases to burn. The heating effects can be reduced by spinning the sample. Conventional methods for reducing the heating effect include dilution of the sample with KBr powder which then acts as a heat sink; defocusing the laser beam so that localised heating is reduced; and reducing the laser power.

3.4.1 Un-pigmented Alkyd

Figure 3.6 shows the FTIR and FT-Raman spectra of the soya bean oil-modified alkyd resin, recorded shortly after the films were spread. Band positions have been identified for both spectra, see table 3.

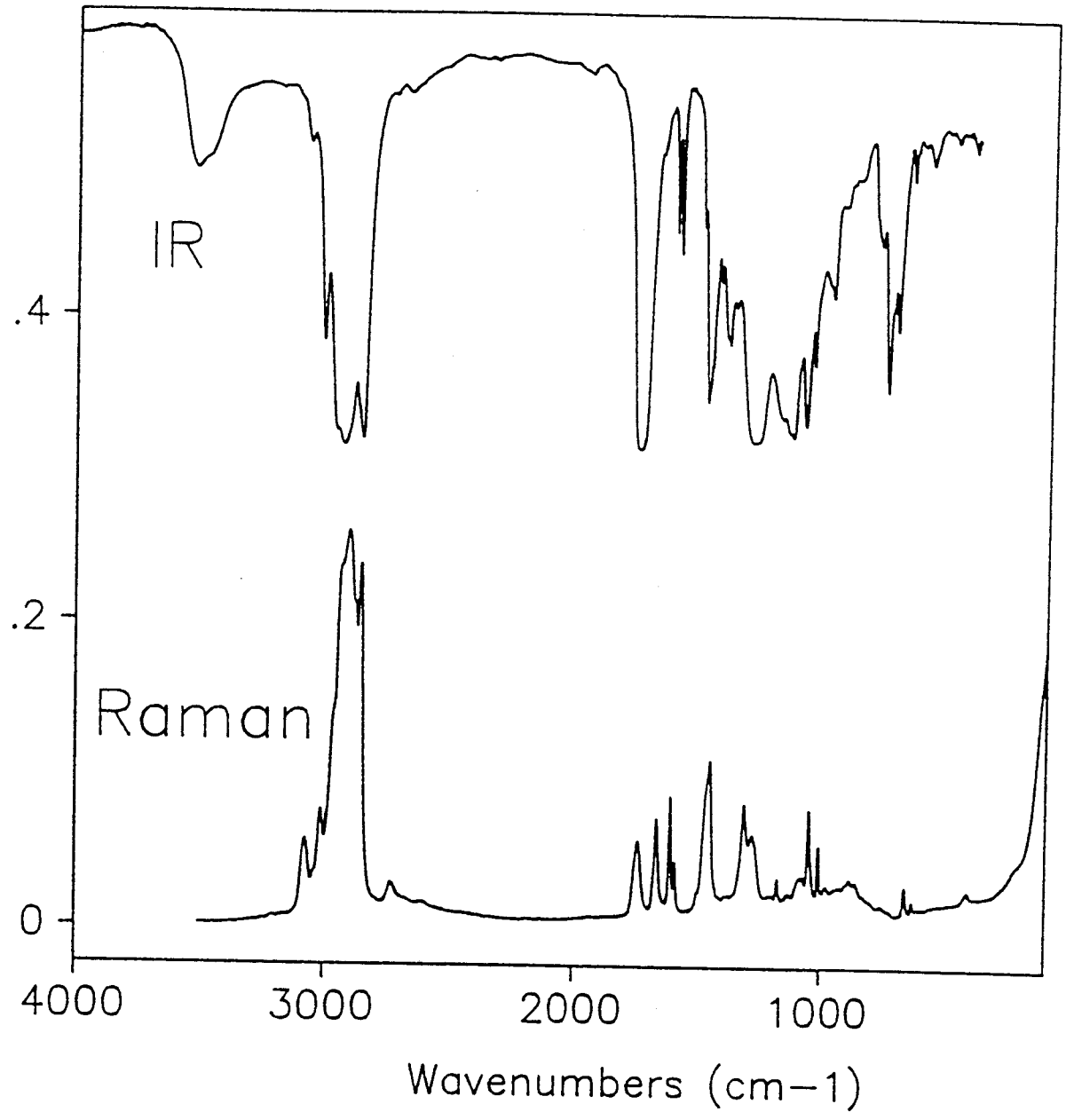

Figure 3.6 The FTIR and FT-Raman spectra of soya bean oil-modified alkyd resin

Infrared	Raman	
3522 w	-	O-H stretch (free)
3470 w	-	O-H stretch (bonded)
3066 vw	3072 m	C-H stretch (aromatic)
3008 w	3008 m	C-H stretch (aliphatic)
2955 sh	2960 sh	C-H str. (-CH_3 asym.)
2926 vs	2930 sh,vs	C-H str. (-CH_2- asym.)
-	2892 vs	C-H str. (-CH_3 sym)
2873 sh	2873 sh,s	C-H str. (-CH_3)
2855 s	2851 vs	C-H str. (-CH_2- sym.)
2732	2723 w	C-H (aliphatic CHO)
2675		
1740 vs	1745 sh	C=O stretch (ester)
-	1728 s	C=O stretch
1656 vw	1654 vs	C=C stretch (aliphatic)
1599 w	1599 s	C=C stretch (aromatic)
1581 w	1579 m	C=C stretch (aromatic)
1489 vw	-	C=C stretch (aromatic)
1465 m	1469 sh	CH_3/CH_2 deformation
-	1457 s	CH_3/CH_2 deformation
1447 sh	-	CH_3/CH_2 deformation
1437 sh,vw	1439 vs	CH_2 deformation
1380 w		
1356 vs		
-	1332 sh	C-O stretch
-	1320 sh	
-	1300 vs	CH_2 twist/rock
1270 vs	1273 sh	C-O stretch (ester)
-	1262 sh	
-	1241 sh	
1164 m	1164 w	C-O stretch (alcohol)
1137 m	-	
1120 s	-	C-O stretch (ester)
1073 m	1070 w	C-O str. (O-CH_2-)
1040 w	1040 vs	ring breathing (*O*-phthalate)
986 vs	-	
970 vw	971 w	CH_2 wag *trans*-unsat.
917 vw	920 w	C-O-C str., sym. (aliphatic ether)
867 vw	868 m	
773 w	-	
741 m	-	C-H out-of-plane bend (aromatic)
705 w	-	ring bending (aromatic)
652 vw	650 m	C=O wag
-	621 w	CH_2 wag
576 vw	-	
-	483 w	
-	410 w	
-	360 w	

vs = very strong, s = strong, m = medium, w = weak, vw = very weak, sh = shoulder.

Table 3 Infra-red and Raman bands in alkyd resins

The strongest component in the FTIR spectrum arises from the carbonyl stretching vibration, which is centred as a broad band at 1737cm^{-1}. In the FT-Raman spectrum this band is only of medium intensity. Conversely bands due to aliphatic C=C stretching vibrations are very weak in the infra-red, whilst in the Raman they are very strong, and occur at about 1655cm^{-1}. They can be clearly destinguished from the carbonyl band at 1729cm^{-1} and the characteristic doublet due to the aromatic C=C stretches at 1599 and 1581cm^{-1}. The phenyl breathing mode characteristic of an *O*-phthalate appears at 1040cm^{-1} [6,25]. Figure 3.7 shows FT-Raman spectra taken over the period of the experiment.

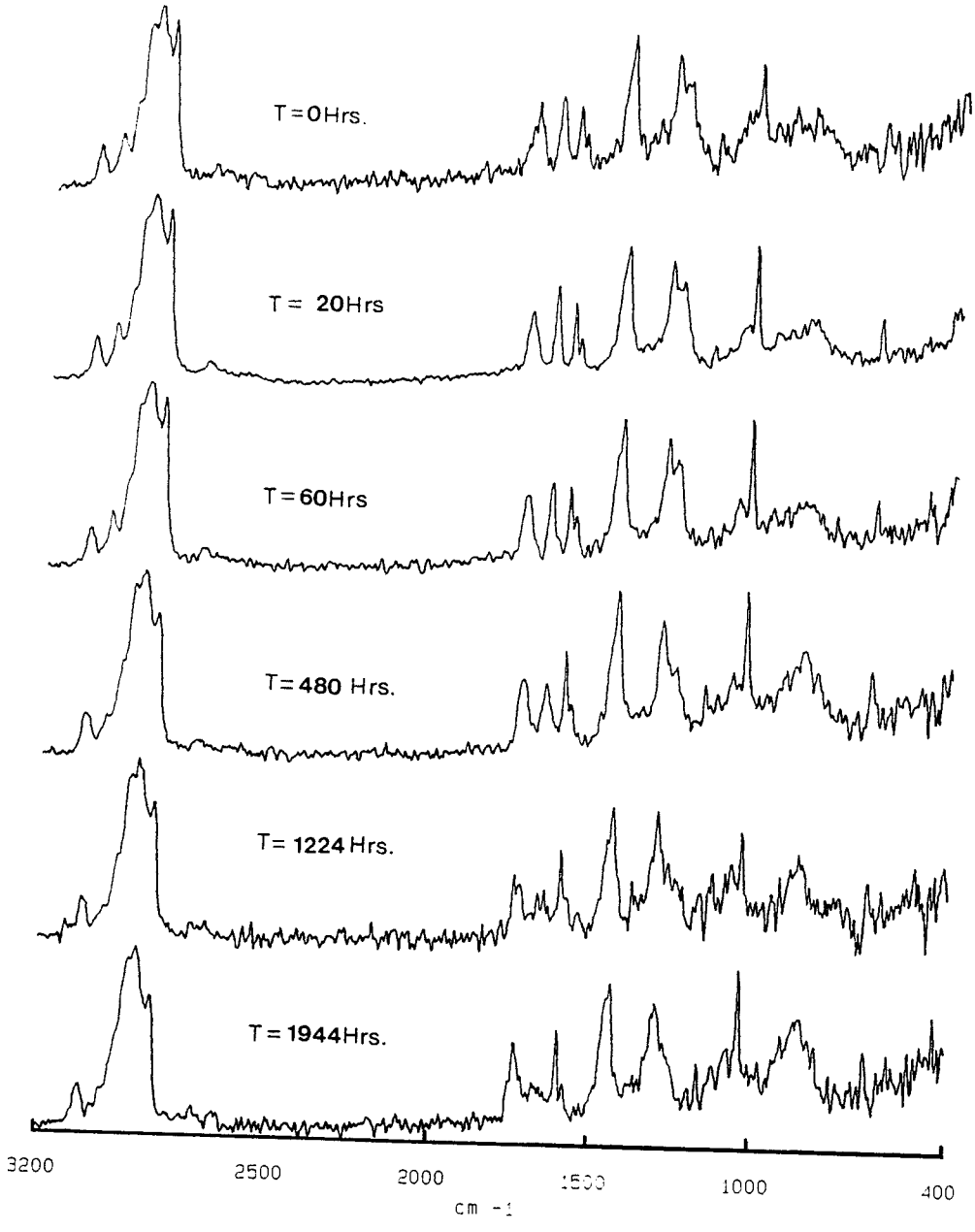

Figure 3.7 Alkyd cure by FT-Raman spectroscopy

The intensity behaviour of the C=C moiety is shown in figure 3.8;

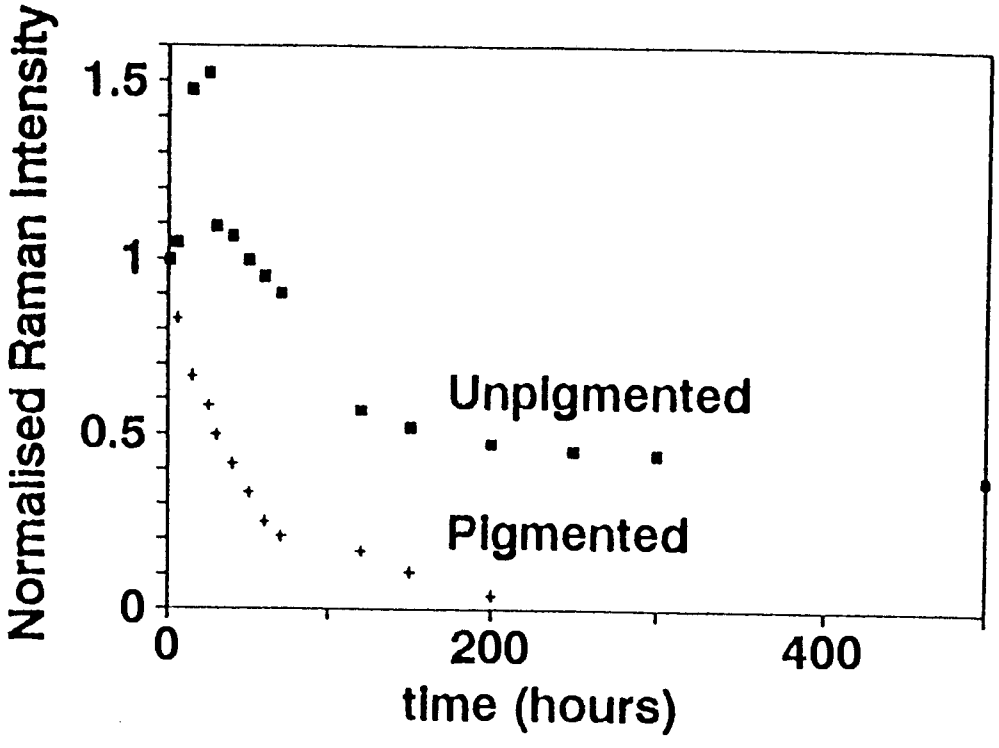

Figure 3.8 Plot of the normalized Raman intensity for the C=C band versus time

The initial increase in unsaturation is thought to be due to the normalization of the band against the 1450cm^{-1} C-H band, and is not a real effect. Their was also some broadening of the C=C band which is associated with configurational changes taking place during the cure. However, the different C=C components could not be identified from the measurements, See later. The band at about 880cm^{-1} which increases to a maximum after approximately 30 hours is probably the O-H bending mode of the hydroperoxide. The actual nature of the crosslinking could not be elucidated from the Raman results alone. However FTIR spectra taken during the autoxidation clearly show the C-O-C crosslinks, (1100cm^{-1}), -OOH formation, (3420cm^{-1}), and C=C loss, (3010cm^{-1}). Figure 3.9 shows the results obtained from time-lapse FTIR absorption spectroscopy, the results are essentially similar to those obtained by HARTSHORN [17].

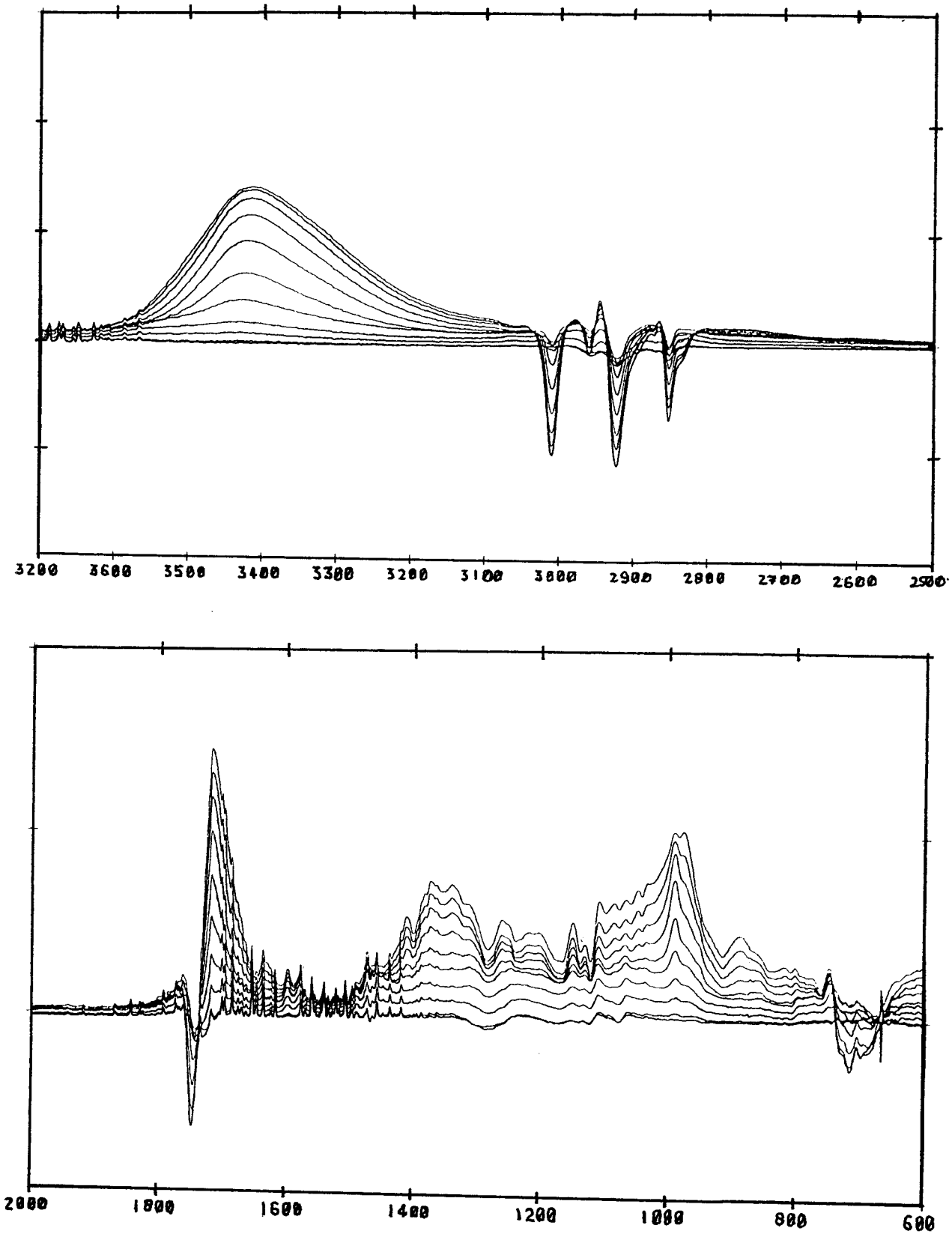

Figure 3.9 Alkyd cure by time lapse FTIR spectroscopy.

Briefly some loss of the high frequency side of the C=O band is observed ($1740cm^{-1}$) which has been associated with the loss of α,β-unsaturated aldehydes, ketones and small esters [17]. An increase in *trans-* and conjugate unsaturation is observed by the bands at 990 and $975cm^{-1}$ respectively. The band due to -OOH and -OH stretches ($3450cm^{-1}$) also shows an increase in intensity as the cure proceeds. These observations are consistent with the findings of KHAN [11] and the formation of hydroperoxides. The band which appears at $885cm^{-1}$ has been associated with the formation of hydroperoxides (-O-O- str.) [19,26]. Figure 3.10 shows the plot of the $3008cm^{-1}$ vs the 3072^{-1} band.

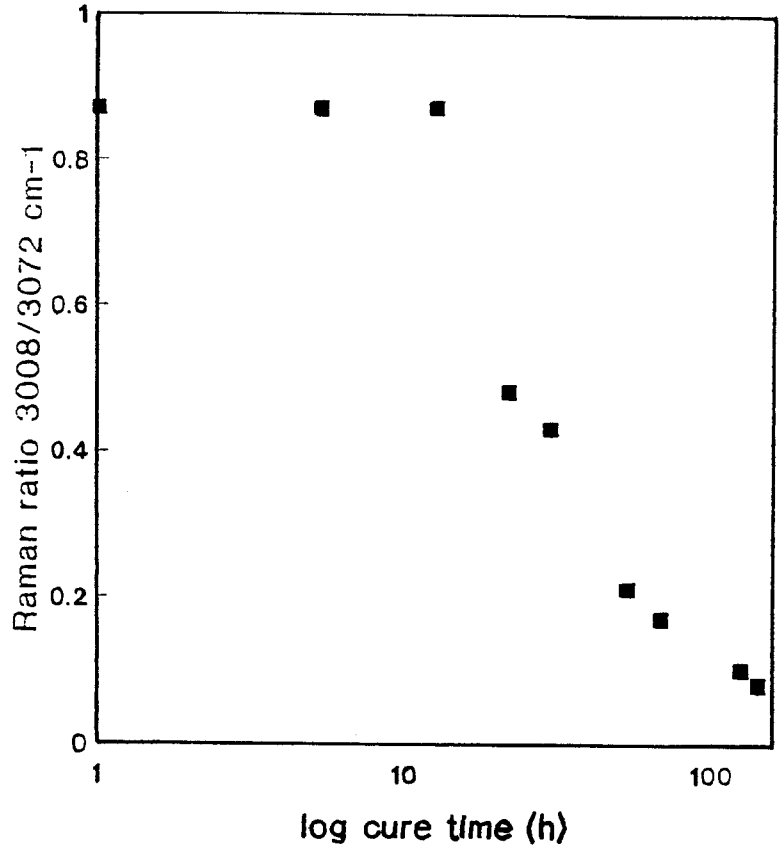

Figure 3.10 Relative intensity of $3008/3072cm^{-1}$ bands versus cure time

The intensity of the Raman band at $3008cm^{-1}$ decreases at the onset of curing. It is thought that this band is due to the stretching vibration of a C-H unit *cis* to a double bond. A similar comparison has been made for the C=C moiety. Figures 3.11 a, and b show plots of the relative intensity of the C=C band at $1655cm^{-1}$ against aromatic bands in the spectra.

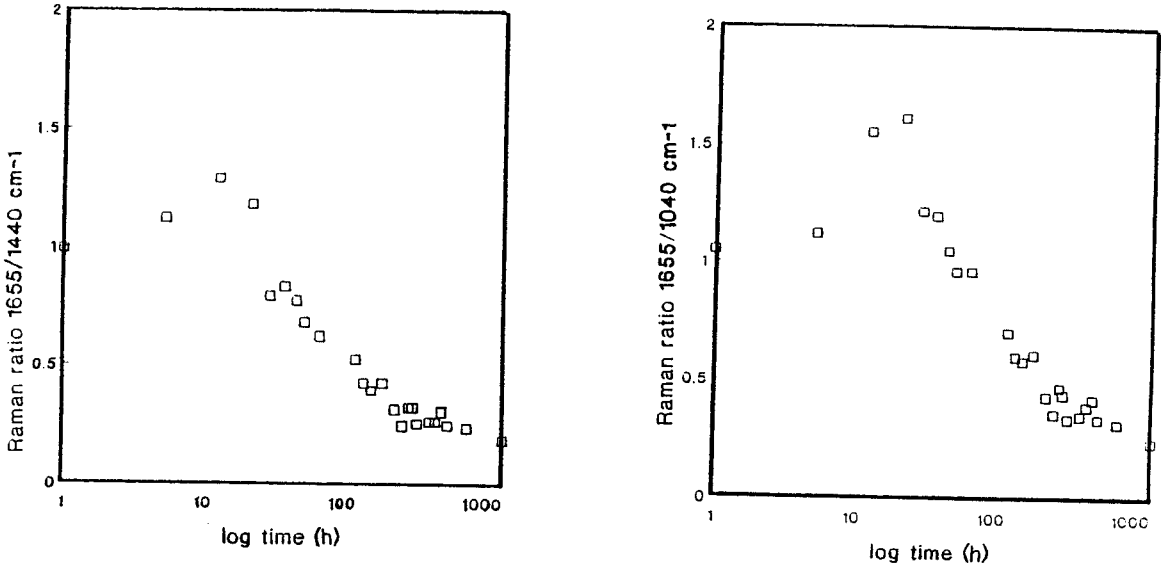

Figure 3.11 relative intensity of 1655cm^{-1} band against other bands in the spectra versus cure time

3.4.2 Pigmented alkyd resin

The same resin with 15% w/w TiO_2 was also investigated. The experiment was performed in exactly the same way as for the un-pigmented system. The first observation to note (figure 3.12) is the improvement in signal/noise (S/N), when compared to the un-pigmented equivalent.

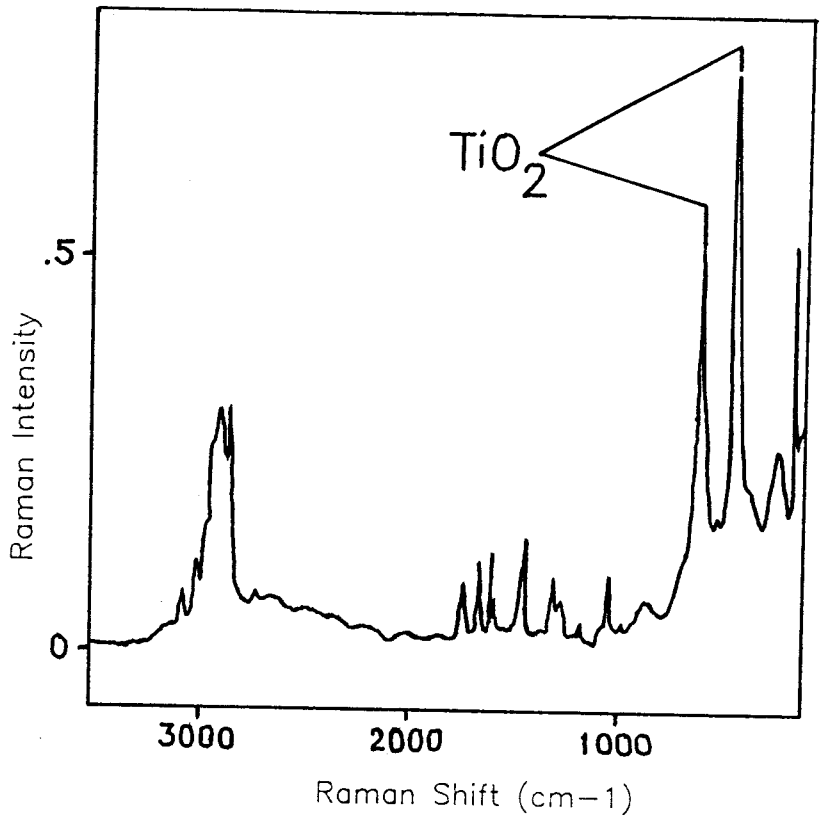

Figure 3.12 Raman spectrum of a pigmented alkyd

This is probably due to the enhanced Raman scatter by the TiO_2. This enhancement is characteristic of FT-Raman measurements: turbid samples invariably give better spectra than similar transparent ones.

As can be seen the Raman spectrum is dominated by sharp bands at 608 and 442cm^{-1} due to TiO_2.

The change in the C=C band intensity during the cure is shown in figure 3.13, and plotted in figure 3.8.

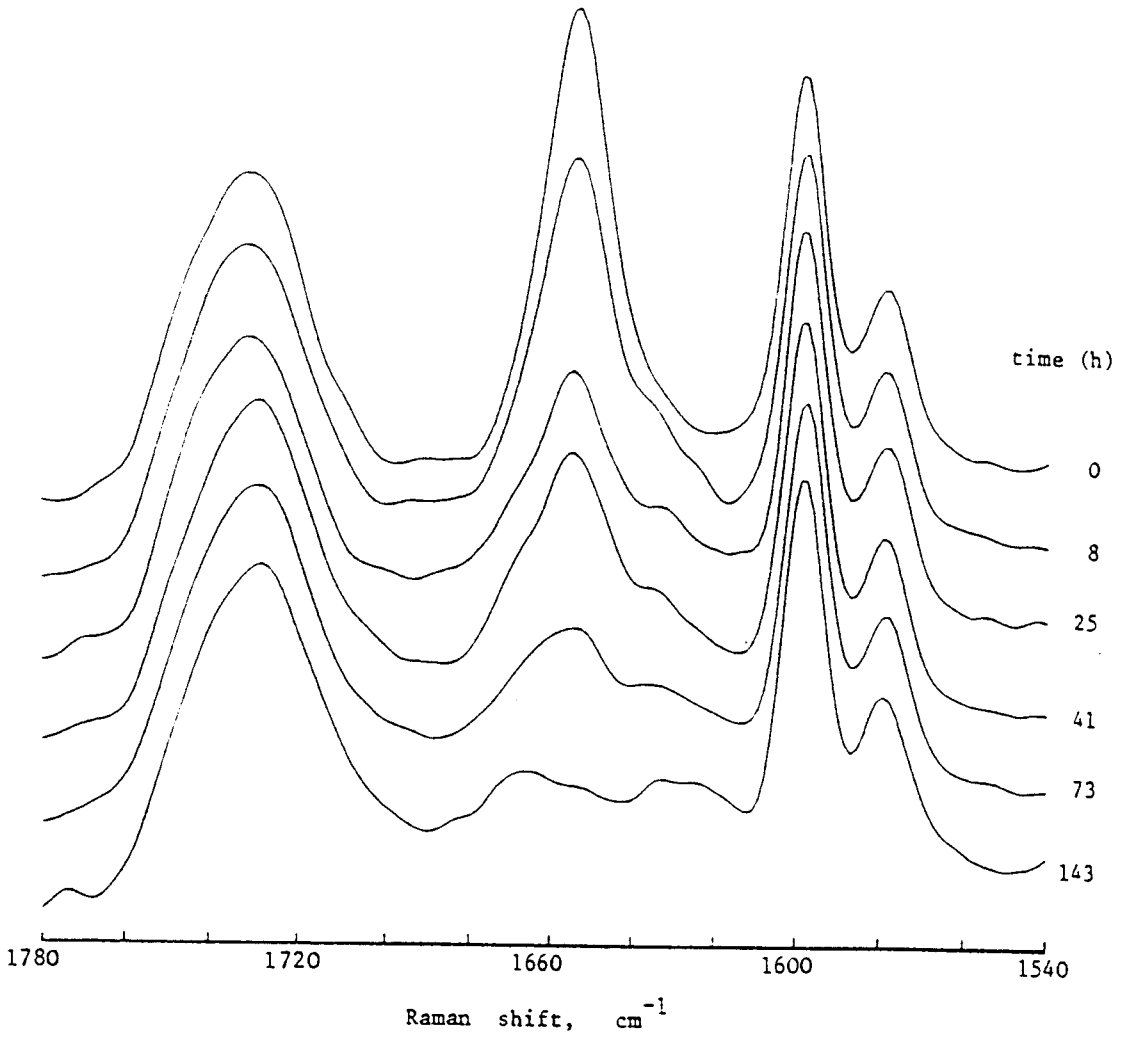

Figure 3.13 The change in the C=C band intensity during cure

Note how the onset of cure occurs much earlier, and reaches its maximum faster than in the un-pigmented resin. This enhancement in rate of autoxidation is due to the TiO_2 and its addition to the number of active sights for the process. The details of this mechanism are not clearly understood.

3.4.3 Curing of the model compounds

3.4.3.1 Introduction

As mentioned at the beginning of this chapter a study was also made of the autoxidation of methyl oleate, methyl linoleate, and methyl linolenate, as model substances of the commercially based oil-modified alkyd resin. Table 1 shows the formula of the fatty acids used in this study.

Table 4 shows the band assignments in the Fatty Acid Methyl Esters.

Infrared	Raman	
3650w	-	O-H stretch (free)
3400w	-	O-H stretch (bonded)
3010w	3004m	C-H stretch (aliphatic)
2955sh	2960sh	C-H stretch (-CH_3 asym.)
2926vs	2923sh,vs	C-H stretch (-CH_2-asym.)
-	2893vs	C-H stretch (-CH_3 sym.)
2873sh	2872sh,s	C-H stretch (-CH_3)
2855s	2855vs	C-H stretch (-CH_2-sym.)
2731	2720w	C-H stretch (aliphatic CHO)
1700vs	1743sh	C=O stretch (ester)
1656vw	1656vs	C=C stretch (aliphatic)
1465m	1469sh	CH_3/CH_2 def.
-	1457s	CH_3/CH_2 def.
1447sh	-	CH_3/CH_2 def.
1439sh,vw	1441vs	CH_2 def.
-	1302	CH_2 twist/rock
1270m	1273sh	C=O stretch (ester)
-	1262sh	
-	1244sh	
1122s	-	C-O stretch (ester)
1100m	1098w	C-O-C stretch (aliphatic ether)
970vw	971w	CH_2 wag *trans*-unsat.
867vw	850m	

vs=very strong, s=strong, m=medium, w=weak, vw=very weak, sh=shoulder.

Table 4 Infra-red and Raman bands in the fatty acid methyl esters

3.4.3.2 The cure of methyl oleate

Figure 3.14 shows the FT-Raman spectrum of methyl oleate as received; it can be seen that the spectrum is dominated by bands in the C-H stretching region. Many of the bands have been assigned, see table 4.

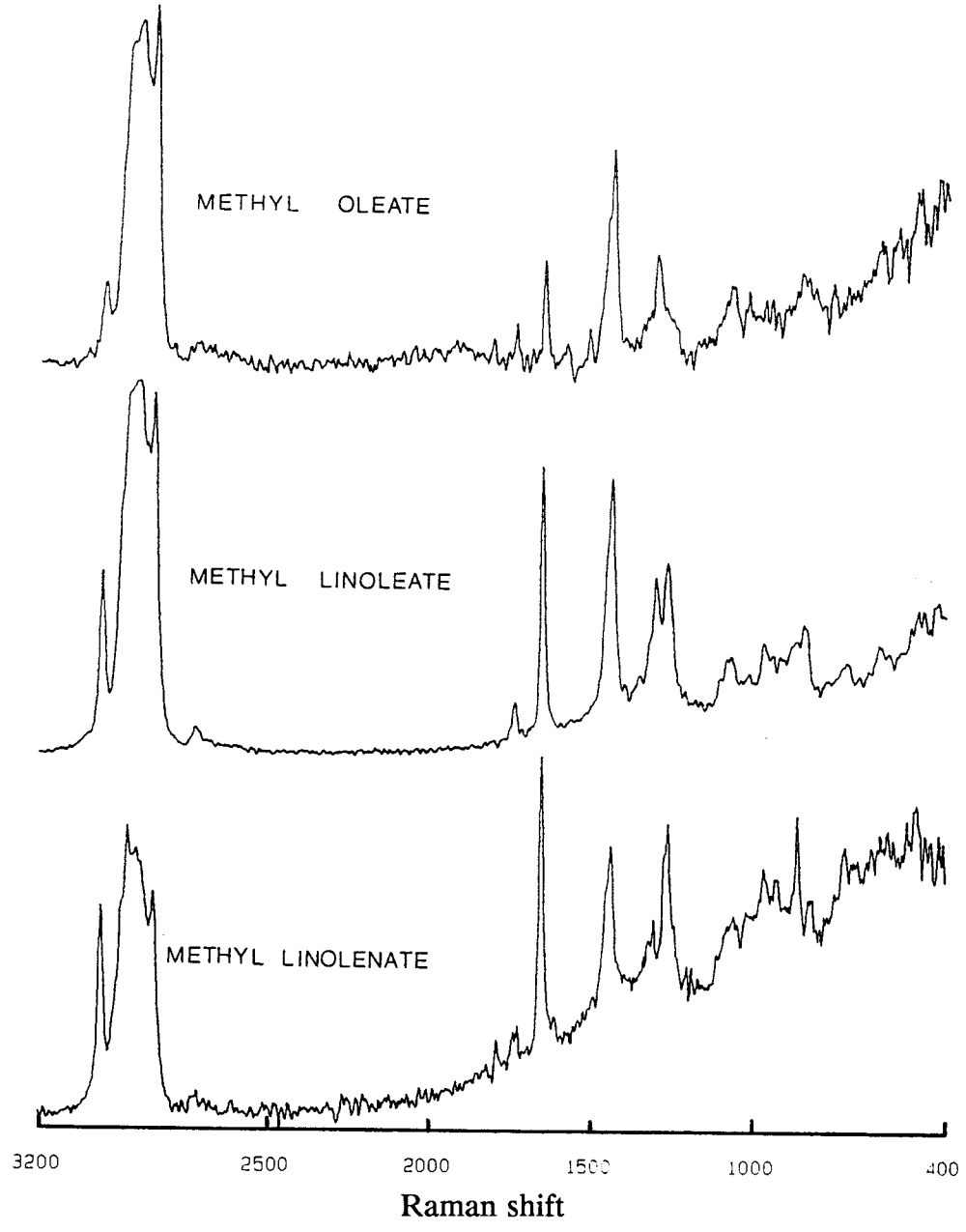

Figure 3.14 The FT-Raman spectrum of the FAMEs

Methyl oleate, having only one C=C bond does not undergo conjugation accompanying the formation of hydroperoxide during autoxidation [21]. However, some modification of the shape of the C=C band was noted although even after 72 hours there was no change in its overall intensity. Even after 4 weeks in ambient conditions there was no increase in viscosity and in fact the film remained liquid at the end of this period. Figure 3.15 shows the FTIR spectra for its behaviour during the cure process.

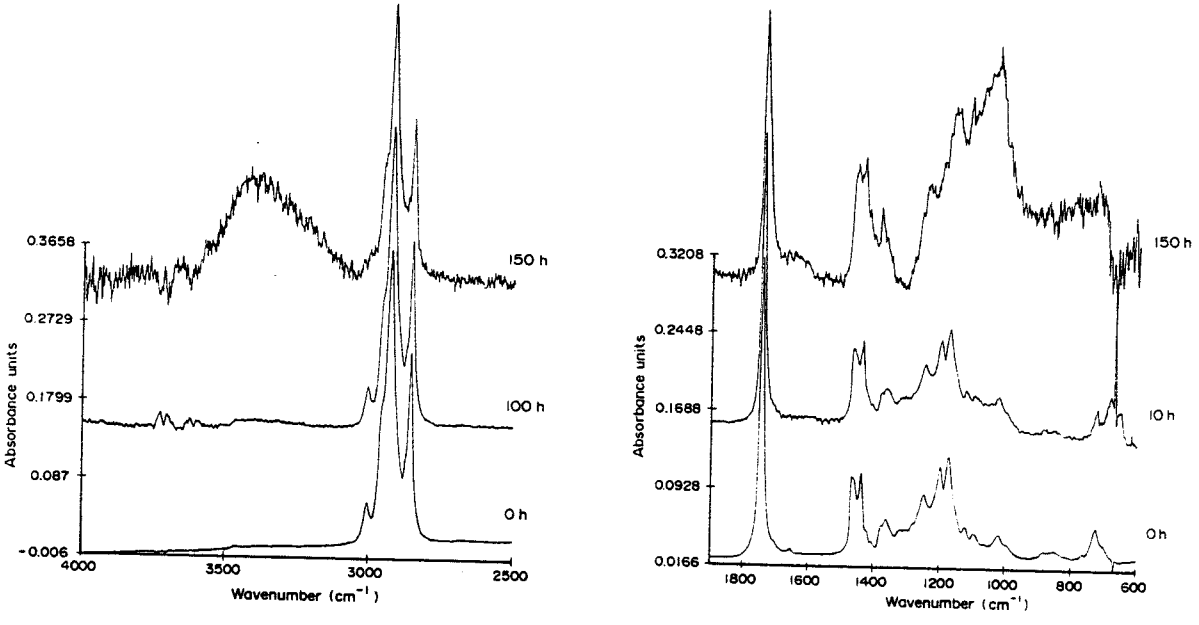

Figure 3.15 FTIR spectrum of the methyl oleate cure

There is evidence for the formation of the hydroperoxide (band at 3500cm^{-1}) and ether cross-links (1100cm^{-1}), and the degradation of the unsaturated system

($3010cm^{-1}$). The cross-link density must be very low in the case of the methyl oleate as the sample is still liquid after 4 weeks exposure to the atmosphere. The increase in noise is indicative of film thinning due to sample loss; scission reactions give rise to volatile saturated and unsaturated aldehydes ($1700cm^{-1}$) [21]. See scheme 4 below.

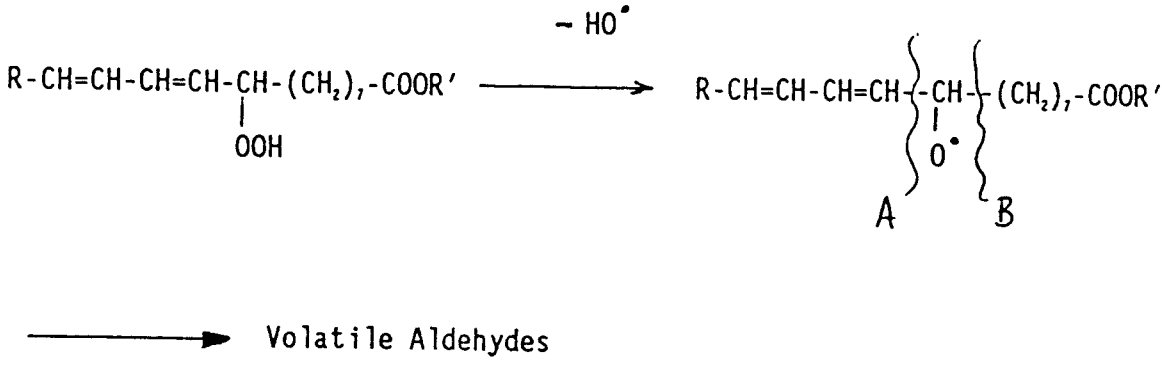

Scheme 4

Scission occurs at positions A or B and gives rise to the formation of aldehydes which give the curing paint its pungent smell.

3.4.3.3 The cure of methyl linoleate

The FT-Raman spectrum of methyl linoleate is shown in figure 3.14, whilst the band assignments are listed in table 4.

When *cis*-9-, *cis*-12-methyl linoleate autoxidises two positional isomers of conjugated methyl linoleate are formed [11], namely *cis*-9, *trans*-11- and *trans*-10,*cis*-12-methyl linoleate, the migrating double bond inverts predominantly to the *trans* form [11]. Figure 3.16 shows the effect of time on the unsaturated moiety for methyl linoleate.

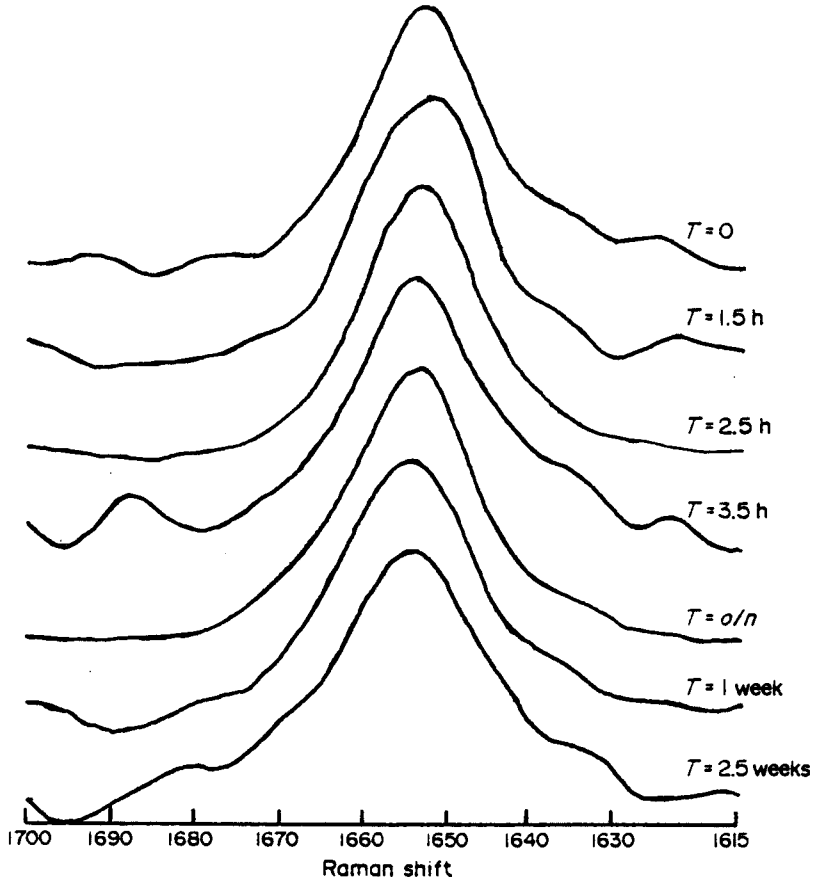

Figure 3.16 The effect of time on the C=C moiety in methyl linoleate

Cornell and Koenig in 1968 [27], reported the Raman spectroscopic studies of polybutadienes, from this and several other papers we have been able to assign the bands 1670, 1655, and 1640cm^{-1} to the *trans-*, *cis-*, and conjugated moieties respectively. As the cure proceeds changes become apparent in the microstructure which are indicative of a chain/unsaturation modification

mechanism. It should be noted however that several new features appear in the Raman spectra which have not been published before. After the first 12 hours of the cure (figure 3.17) bands appear at 3050, 1599, 1000, and 620cm^{-1} which are thought to be due to C-H stretch (conjugated cyclic structure), C=C stretch (conjugated cyclic structure), C-H bend (conjugated cyclic structure) and CH_2 wag respectively.

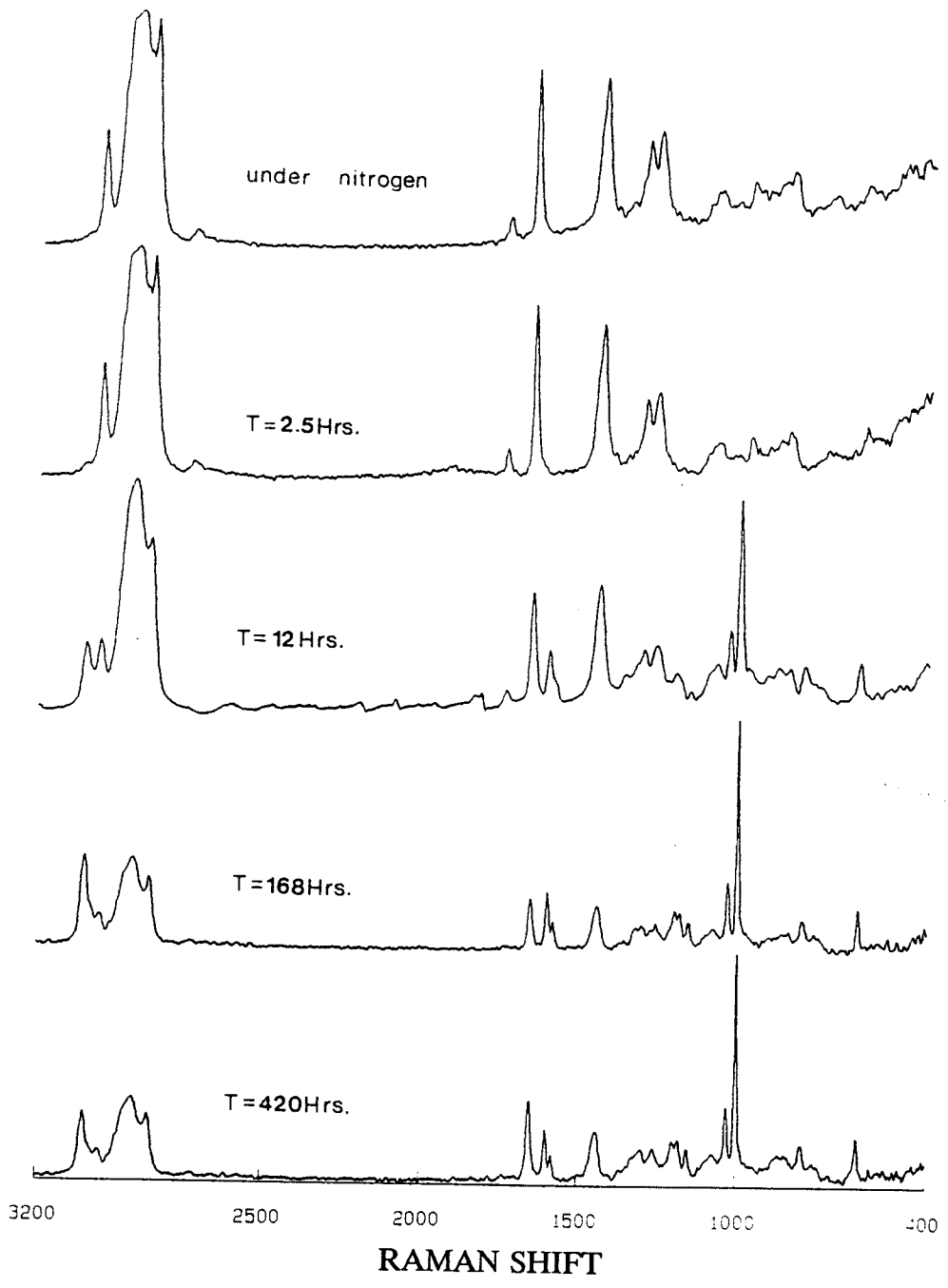

Figure 3.17 FT-Raman spectra of methyl linoleate with cure time

As the ν(C=C) moiety is not terminal or conjugated with the carbonyl group the band is very weak in the infra-red spectrum [28], it is effectively an infra-red inactive vibration. Figure 3.18 shows the FTIR spectra of methyl linoleate recorded at a series of intervals (up to 60 hours) during the drying process.

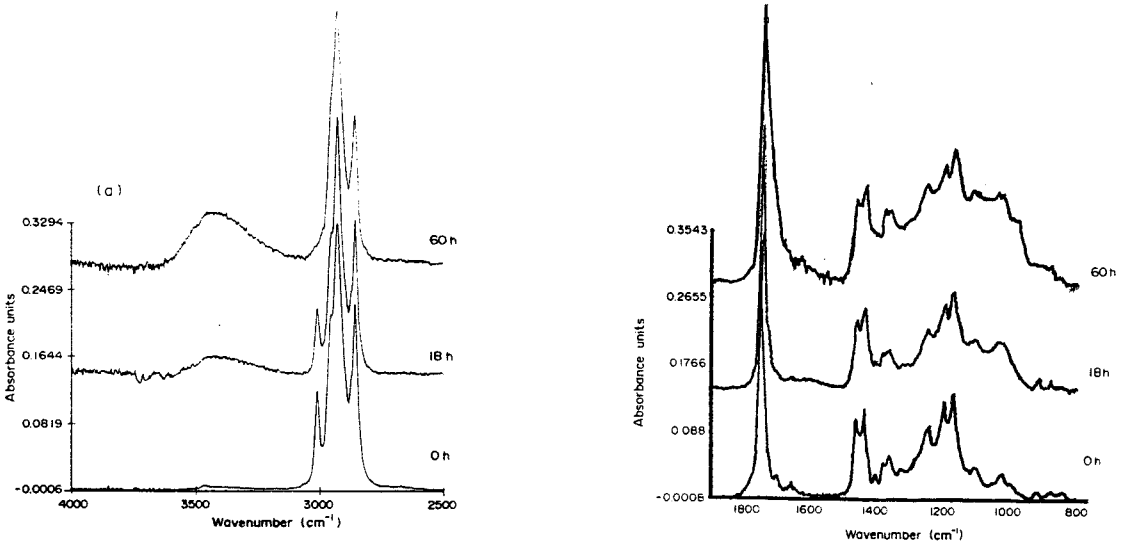

Figure 3.18 FTIR spectrum of methyl linoleate

The band near 3500cm^{-1} (due to -OOH and -OH stretches) can be seen to increase with cure time. Figure 3.19a shows a plot of the intensity of the band versus time (in hours).

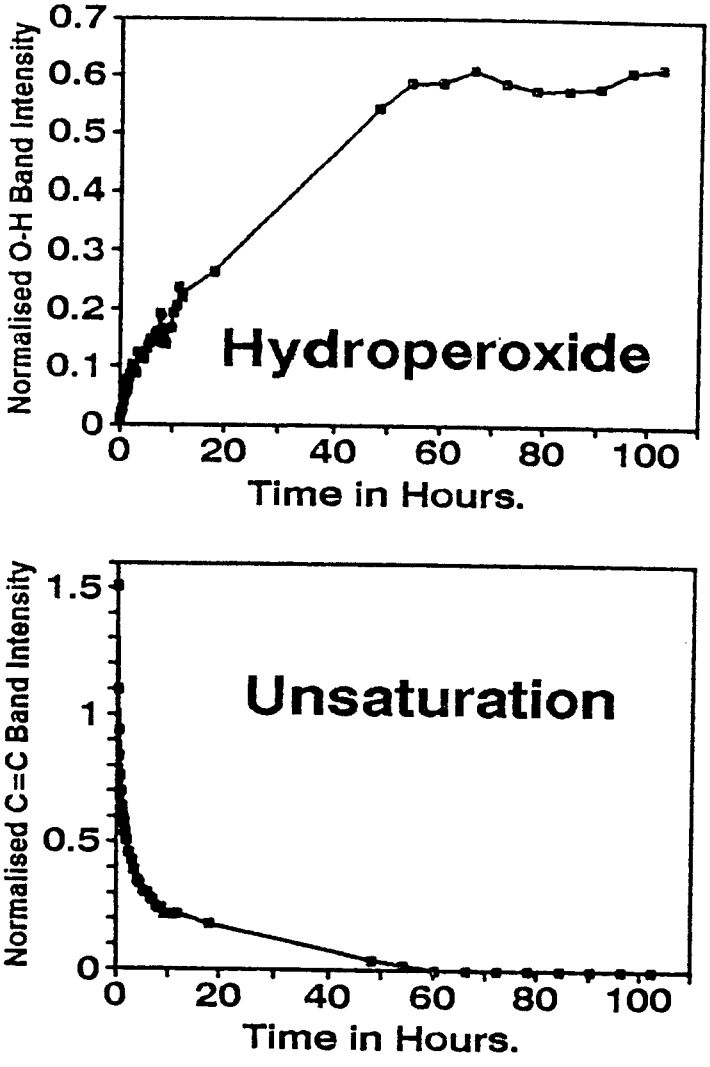

Figure 3.19 (a) Normalized O-H band intensity of methyl linoleate versus cure time. (b) Normalized C=C band intensity of methyl linoleate versus cure time

The decrease in intensity of the band at 3010cm^{-1}, which has been assigned to the C-H symmetric stretch on a C=C unit, with respect to cure time signifies the formation of crosslinks. This observation is highlighted in figure 3.19b. A broadening of the C=O band can be observed in figure 3.18 which has been associated with the formation of α, β unsaturated aldehydes, ketones and ester volatiles from the chain scission reactions [21]. The doublet centred around 1200cm^{-1} remains throughout the drying process and it has been assigned to the C-O stretch of an ester group, suggesting the ester group plays no part in the

drying process. An increase in the trans and conjugated unsaturation is observed by the appearance of a shoulder to the low frequency side of the band at around

1655cm^{-1}. These observations are consistent with the mechanism proposed earlier, ie there is an initial chain modification reaction and hydroperoxide formation, followed by the destruction of the unsaturation and the formation of crosslinks. FTIR data showed no clear evidence of the cyclization reaction observed in the Raman data.

3.4.3.4 The autoxidation of methyl linolenate

cis, cis, cis, -9,12,15-methyl linolenate (table 1, figure 3.14) autoxidises via a more involved mechanism [27]. Polymerisation results in a conjugated *trans*-10, *cis*-12, *trans*-14 isomer.

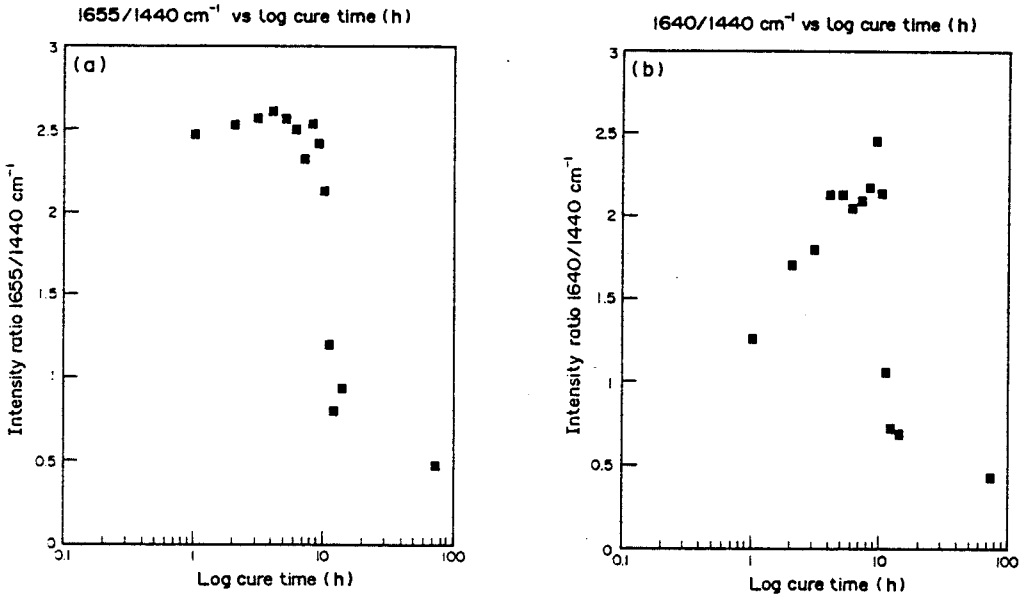

Figure 3.20 (a) Relative intensity of 1655/1440cm^{-1} bands of methyl linolenate versus cure time. (b) Relative intensity of 1640/1440cm^{-1} bands of methyl linolenate versus cure time

Figure 3.20 shows two plots a and b; figure 3.20a shows how the intensity of the unsaturated band increases to a maximum around the 10 hour mark before it starts to decrease. This confirms that after the 10 hour period the unsaturated system begins to break down, to form alkoxy radicals [20]. The apparent increase in the degree of unsaturation is probably due to the incomplete resolution of the ν(C=C) Raman bands, because they vary with intensity during the cure and therefore affect the overall band head at 1651cm^{-1}. Also because of chain scission reactions, (described earlier) we are seeing a slight decrease in the intensity of the band at 1440cm^{-1} thus resulting in the apparent increase in unsaturation. Figure 3.18b shows the behaviour of the conjugated moiety [28,29] during the cure. The increase in intensity of the conjugated band during the initial stages, probably involves hydroperoxide formation, because during the formation, there

is a rearrangement of the double bonds from a non-conjugated to a conjugated system.

Figure 3.21 shows a kinetic plot of the peaks specific for the C=C microstructures; notice how the band at 1640cm^{-1} (conjugated structure) increases significantly during the early stages of the cure before it decreases. Small changes can also be seen around 1670cm^{-1} (*trans* structure) before it becomes to weak and masked by the appearance of carbonyl by-products [21].

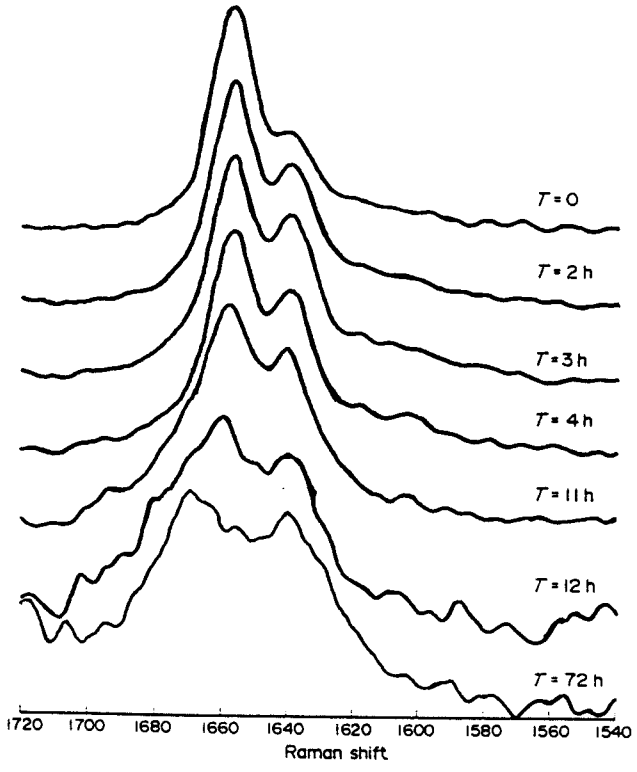

Figure 3.21 FT-Raman spectra of the C=C stretching region with cure time

Figure 3.22 shows the FTIR data recorded at a series of intervals during the cure of methyl linolenate. Bands are assigned to -OOH stretch at 3500cm^{-1}, -C-H stretch on a C=C unit at 3010cm^{-1}, CH_3/CH_2 deformations at 1440cm^{-1}, and these behave in a similar manner to the corresponding bands in the methyl linoleate. A broad band appears around 1100cm^{-1} which has been assigned to the formation of ether crosslinks. The origin of the band at 870cm^{-1} is unclear; it is possibly due to the -O-O- stretching vibration of the hydroperoxide [19].

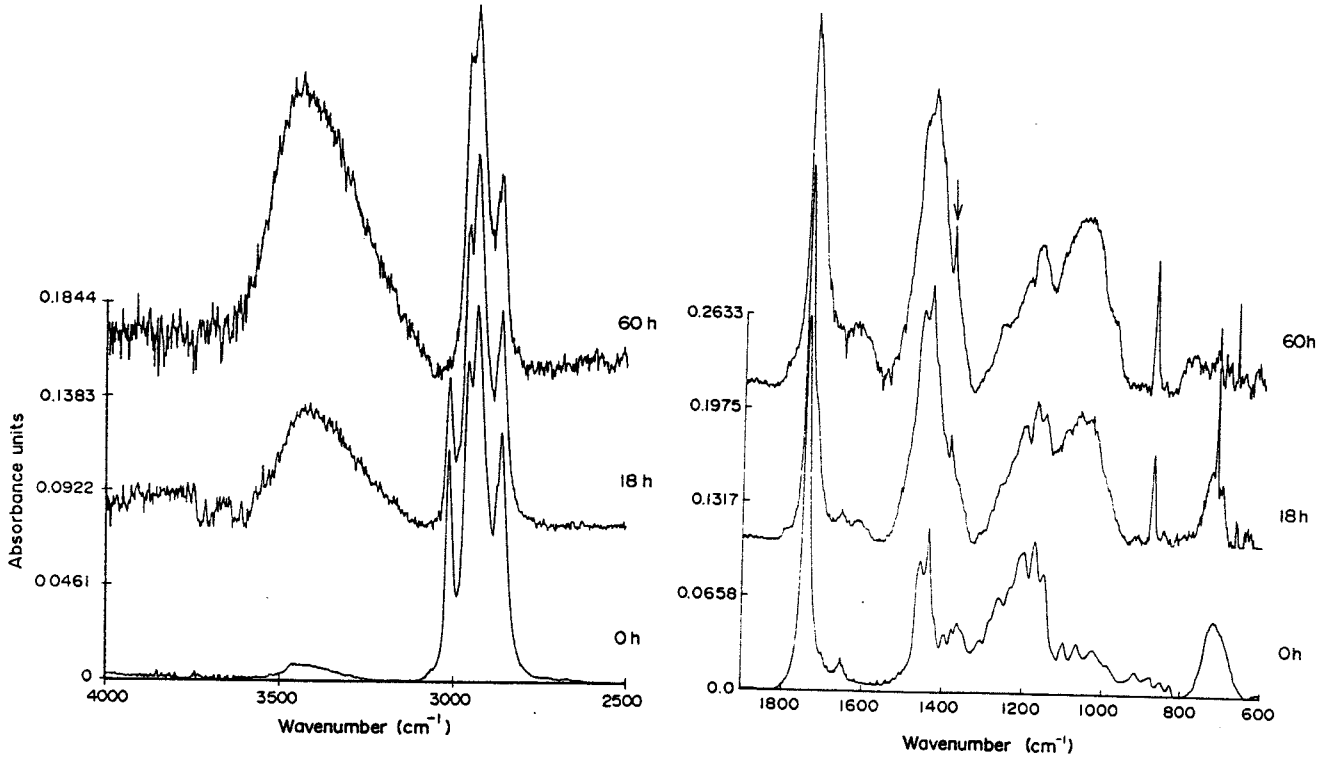

Figure 3.22 FTIR spectrum of methyl linolenate

A plot of the band at 870cm^{-1} vs time is shown in figure 3.23 along with plots of the -OH band and the -C-H band at 3010cm^{-1} all vs time, the plots agree with the proposed mechanism described earlier.

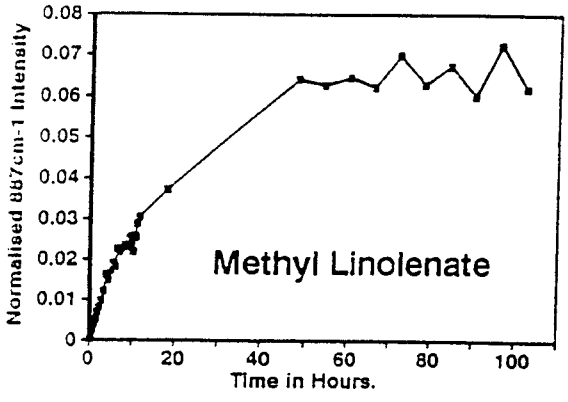

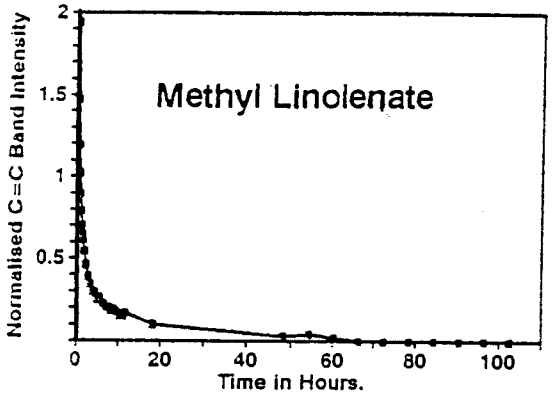

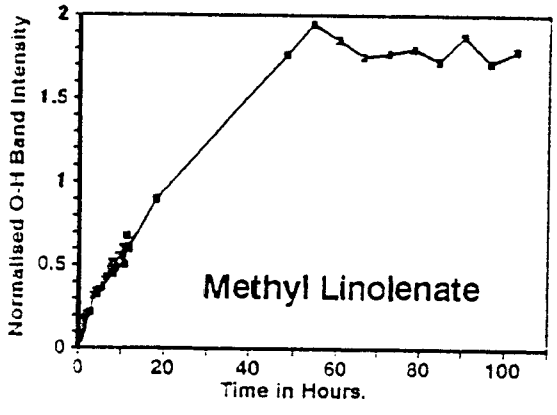

Figure 3.23 (a) Normalized 877cm^{-1} band intensity versus cure time. (b) Normalized C=C band intensity versus cure time. (c) Normalized -O-H band intensity versus cure time.

3.5 Conclusion

FT-Raman and Infra-red spectroscopy have successfully shown how the cures of three model compounds proceed via three very different unsaturation/chain-modification-type mechanisms and rates. Changes appear in the C=C microstructures throughout the cure and are manifest in the peaks at 1670, 1655 and 1640cm^{-1}; these changes have been assigned to *cis/trans* isomerism and to the migration of double bonds during the hydroperoxide formation. Results from the methyl linoleate system highlight several new bands and there is no doubt that these changes correspond to the formation of a conjugated cyclic structure. One school of thought is that this involves the formation of an aromatic peroxide [30].

The initial increase in the level of unsaturation at the early stages of the alkyd cure are still a matter of debate, one explanation behind the effect suggests that it is not a real effect at all, what we are actually seeing is a decrease in the intensity of the band used in the normalization. However by considering the evidence put forward in figure 3.11 it seems likely that this is indeed a real effect. The effect is also apparent in the fatty acid methyl esters.

Broadening of the C=C microstructure (around 1655cm^{-1}) was observed in both the pigmented and un-pigmented cures. These changes have been associated with configurational changes in the resin during the autoxidation process. Shoulders have been noted around the main band-head of 1655cm^{-1} at 1670 and 1630cm^{-1}, these features perpetuate throughout the experiment, and as the coating dries they become more visible.

The 3008cm^{-1} band in the Raman spectra disappears after 150 hours, long before the disappearance of the C=C moiety, which is visible for up to 5 times longer.

The band at 880cm^{-1} in the FTIR spectrum has been tentatively assigned to the -O-O- linkage of hydroperoxide. A band in the FT-Raman spectrum at 873cm^{-1}

correlates well with the IR band. It can be observed that at the point where the unsaturation level begins to decrease, the intensity of this band ($873cm^{-1}$) asymptotes out.

References

1. P. Hendra, M. Sweeney, *Spectroscopy World,* **3**,(2) 22 (1991)

2. O.D. Shreve, *Anal. Chem.,* **24**, 1692 (1952)

3. E.R. Mudler, C.D. Smith, *Ind & Eng. Chem.,* **49**, 210 (1957)

4. L.A. O'Neill, *Paint Technol.,* **27**, 44 (1963)

5. N.S. Baer, N. Indicator, *J. Coating Tech.,* **48**, No. 623, 58 (1976)

6. C.M. Jenden, *Polymer,* **27**, 217 (1986)

7. J. Packansky, C. England, R.J. Waltman, *J. Polym. Sci. :B. Polym. Phys.,* **25**, 901 (1987)

8. J. Packansky, R.J. Waltman, R. Grygier, *Appl. Spectrosc.,* **43**, 1233 (1989)

9. T. de Saussuere, *Ann. Chim. Phys.* **2**, 337 (1820), **49**, 225 (1832)

10. C.F. Schönbein, *J. Prakt. Chem.* **74**, 328 (1858)

11. N.H. Khan, *Can. J. Chem.* **37**, 1029 (1959)

12. D.H. Wheeler, *Prog. Chem. Fats, Lipids,* **2**, 268 (1954)

13. J.E. Jackson, R.F. Paschle, W. Tolberg, H.M. Boyd, D.H. Wheeler, *J. Am. Oil. Chem. Soc.* **29**, 229 (1952)

14. P.L. Nichols Jr., S.F. Herb, R.W. Riemenschneider, *J. Am. Chem. Soc.* **31**, 517 (1954)

15. O.S. Privett, W.O. Lundberg, N.A. Khan, W.E. Tolberg, D.H. Wheeler, *J. Am. Chem. Soc.* **30**, 61 (1953)

16. J.A. Cannon, K.T. Zilch, S.C. Burket, H.J. Dutton, *J. Am. Oil Chem. Soc.* **73**, 247 (1951)

17. J.H. Hartshorn, *J. Coating Technol.* **54**, 53 (1982)

18. E.M. Salazar-Rojas, M.W. Urban, *Prog. Org. Coat.* **16**, 371 (1989)

19. N.J. Leeves, PhD Thesis, Royal Holloway College, Egham (1985)

20. W.J. Muizebelt, J.W. Van Velde, F.G.H. Van Wijk, *Proc. 15th Conf. Org. Coat. Tech.* Athens, July 1989

21. R.A. Hancock, N.J. Leeves and P.F. Nicks, *Prog. Org. Coat.* **17**, 321 (1989)

22. G. Ellis, M. Claybourn, S.E. Richards, *Spectrochim. Acta,* **46A**, 227 (1990)

23. G. Ellis, P.J. Hendra, C.M. Hodges, T. Jawhari, C. Jones, P. Le Barazer, C. Passingham, I.A.M. Royaud, A. Sanchez-Blasquez, G. Warnes, *Analyst,* **114**, 1061

(1989)

24. C. Petty PhD Thesis, Southampton University 1991

25. N.B. Colthup, L.H. Daly, S.E. Wiberley, "Introduction to Infra-red and Raman Spectroscopy", 2nd ed. Academic Press, London (1975)

26. O.D. Shreve, M.R. Heether, H.B. Knight, D. Swern, *Anal. Chem.* **23**, 282 (1951)

27. S.W. Cornell, J.L. Koenig, *J. Appl. Phys.* **39**, 4883 (1968)

28. J.K. Agbenyega, M. Claybourn, in preparation.

29. B. Schrader, "Raman/Infra-red Atlas of Organic Compounds (2nd Edn). VCH, Weinheim (1989)

30. L.J. Bellamy, "IR Spectra of Complex Molecules" (2nd Edn). John Wiley & Sons, New York (1958)

CHAPTER 4: Liquid crystal polymers

4.1 History

Liquid crystalline behaviour[4] was first observed in 1888 by the Austrian botanist REINTZER, when he noted that cholesterol esters formed opaque liquids on melting, which on heating to higher temperatures, subsequently cleared to form isotropic[5] liquids [1].

It was not until the 1940s, and 50s that liquid crystalline behaviour in polymers was studied, most of which were of biological origin [2]. The first synthetic polymer observed to form a liquid crystalline phase was poly(gamma-benzyl-1-glutamate) [3], but it was not until 1965 that liquid crystal polymers similar to those commercialised today were recognised for their unique properties.

The first company to capitalize on these liquid Crystal Polymers (LCP) was Du Pont, with the polymer Nomex™ in 1967. One of the most significant breakthroughs in the liquid crystal industry was again by Du Pont, when they introduced Kevlar™ in 1972, spun from lyotropic[6] aromatic polyamides [4,5].

4.2 Introduction

There has been an explosion of interest in the last few years in the field of liquid crystal polymer technology. This increased activity is the result of a sharp rise in research activity by both industry and universities since the introduction of LCP such Kevlar™ and Vectra™.

liquid crystal polymers have several important properties, making them

---

[4] Liquid crystallinity applies to small molecules and polymers. It refers to a state of matter with a degree of ordering between the almost perfect long-range order observed in crystals, and the randomness observed in ordinary liquids.

[5] Denotes physical properties whose magnitudes are invariant with respect to the direction in which they are measured. (Opposite of anisotropic).

[6] Denotes LC phases that occur as a function of solvation.

commercially attractive. These properties include;

(a) High heat resistance

(b) High chemical resistance

(c) High strength and stiffness properties

(d) Ease of moulding.

They exhibit these properties because they have the unique ability of forming a fourth phase. Most substances can be found only in one of three states of matter; solid, isotropic liquid, or gas, whilst liquid crystals and liquid crystal polymers form solid, liquid crystal, isotropic liquid and gas phases. This new phase between the solid and isotropic liquid is known as the mesophase[7]. These mesophases are free flowing, but also show birefringence as they appear to have properties associated with both crystals and liquid crystals.

Molecules which have the tendency to form liquid crystalline phases have either rigid, lathe-like shapes with a high length to breadth (aspect) ratio, or disc shaped molecular structures. See figure 4.1

[7] From the greek word Mesos meaning "in between". Synonymous with the liquid crystalline phase.

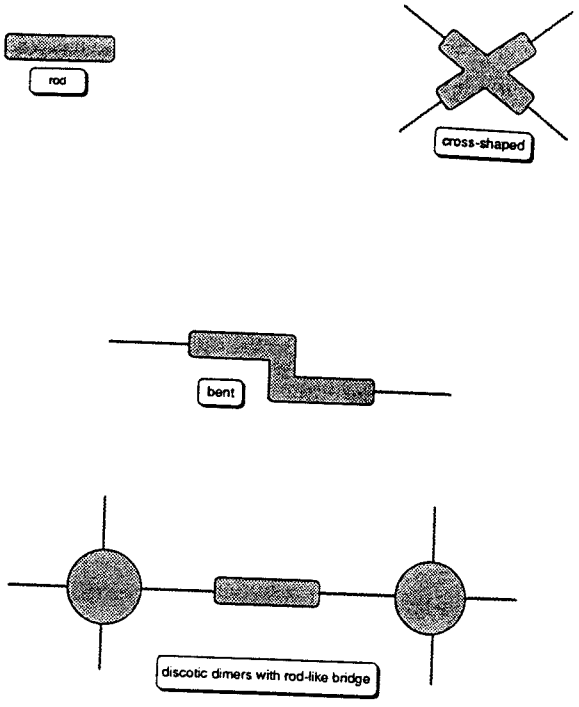

Figure 4.1 Some typical examples of small molecular shapes that form liquid crystalline phases.

Molecules that form liquid crystals or liquid crystal polymers are known as mesogens.

Liquid crystals can be divided into two broad types; those formed when the pure compound is heated are known as thermotropic liquid crystal polymers (LCPs). Whilst those formed when the molecule is mixed with solvent are lyotropic LCPs. Both are characterized by a level of molecular ordering intermediate between that of the solid crystal and the isotropic liquid [6,7]. See figure 4.2.

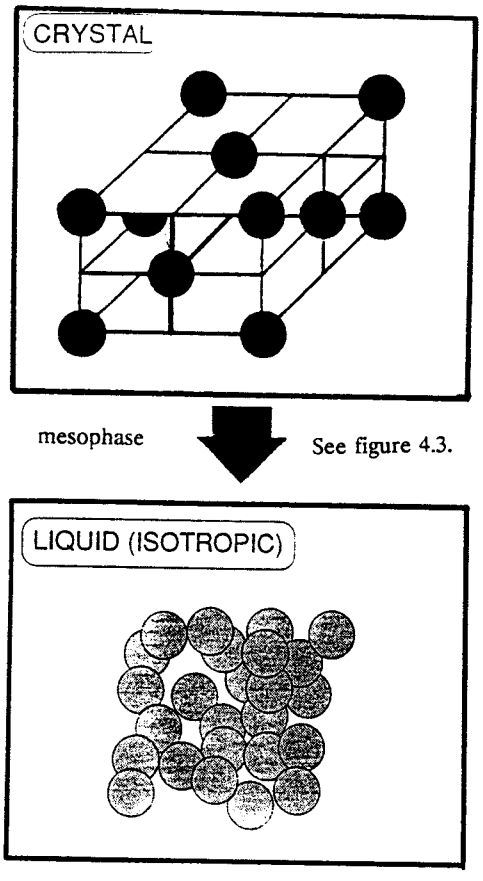

Figure 4.2 The crystal through LC to isotropic liquid phase transition

When the mesogens are arranged in regular layers with respect to there centres of gravity, they are in one of several possible Smectic mesophases[8]. Lateral forces in Smectic phases are much stronger than forces between layers, so slippage of one layer over another is possible, this provides the characteristic liquid like properties of the system, without losing the order within each layer. The most ordered Smectic phase is the Smectic B phase (S_B), which is characterised by hexagonal close packing of the mesogen units. Similar to the S_B phase is S_E which also exhibits 3D order, and has tilted modifications; S_H and S_G. Less ordered smectic phases also exist; S_A and its tilted variation S_C. See figure 4.3.

[8] All the Smectic phases are characterised by both parallel and lateral order

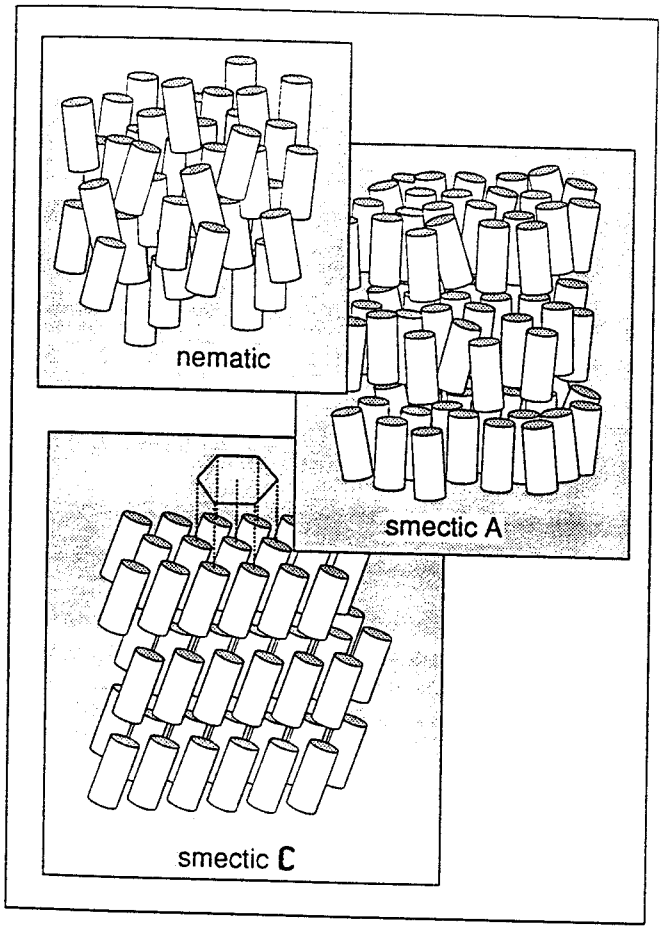

Figure 4.3 Diagram showing the Smectic A & C phases and the Nematic phase

Intermediate in order are the Smectic F and I phases. By far the most common are the Smectic A,B and C phases.

The Nematic[9] phase, also shown in figure 4.3 is more "fluid-like" than the Smectic phases but still exhibits birefringence.

[9] The Nematic phase shows orientation along the long axis of the mesogenic units, but possess no lateral order.

As well as the Smectic and Nematic mesophases, a third phase called the Cholesteric phase exists. See figure 4.4.

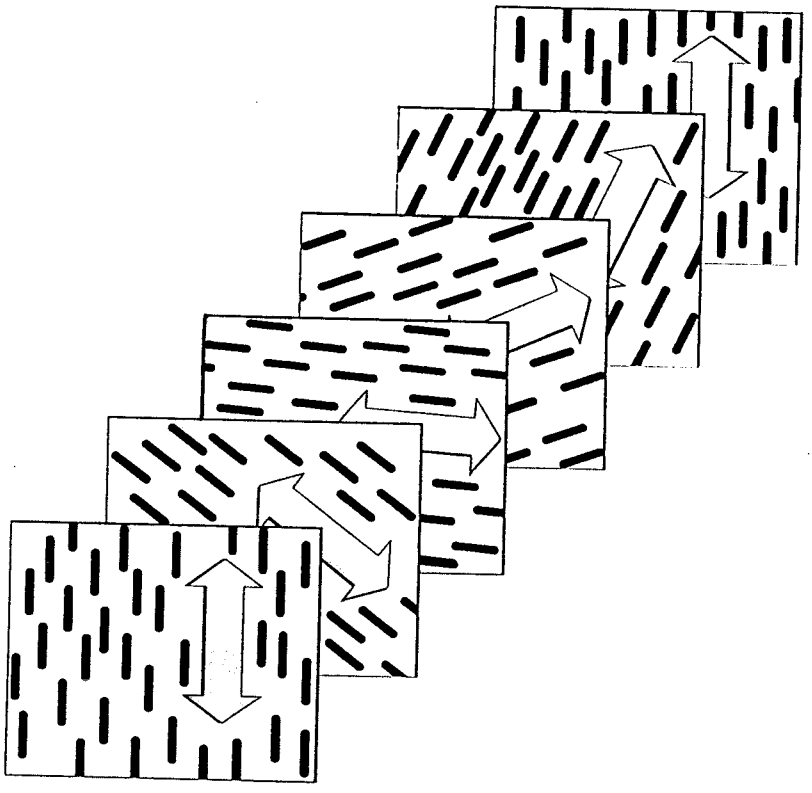

Figure 4.4 A diagrammatic representation of the Cholesteric mesophase

It is often regarded as a modification of the Nematic liquid crystalline structure, where the mesogens are assembled in layers, with each layer rotated through a definite angle relative to the previous layer, thus producing a twist in the molecule, and resulting in a helical-type structure.

4.2.1 Thermotropic liquid crystal polymers

Thermotropic LCPs consist of two main divisions categorized by the position of the mesogenic units within the polymer structure. Those attached to the chain by a flexible spacer are known as side-chain or "comb-like" LCPs [8,9]. Whilst those, that form part of the polymer chain, linked either directly, or by rigid or flexible spacers are known as main-chain LCPs [10,11]. See figure 4.5 for examples of each.

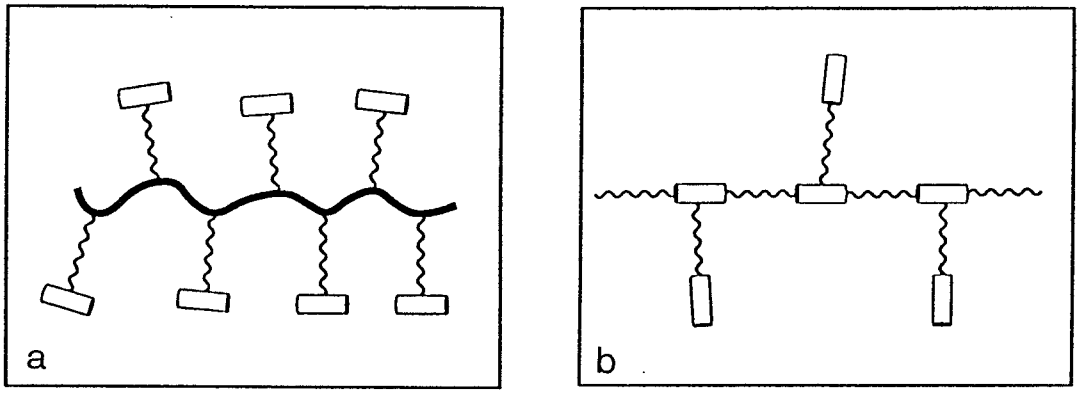

Figure 4.5 (a) Side chain LCP (b) Main chain LCP

4.2.2 Thermotropic main-chain liquid crystal polyesters

ROVIELLO and SIGIRU produced the first thermotropic main-chain LCP in 1975. Subsequently it was found that by linking mesogens together to form polymeric chains, these chains often showed the presence of a liquid crystal

phase appearing at temperatures just above the melting point of the polymer.

Many LCPs synthesised by condensation reactions tend to be very insoluble with high melting points and mesophase ranges[10] [12]. This makes them difficult to process and therefore commercially unattractive. Alternative structure with much lower melting points are more useful. Melting points can be reduced in several ways:

(a) Incorporation of a flexible spacer.

(b) Copolymerization of several mesogenic monomers of different size, to give a random or more irregular structure.

(c) Introduction of lateral substituent to disrupt the chain symmetry.

(d) Synthesis of chains with kinks, such as unsymmetrically linked aromatic units.

Thermotropic (melt state) liquid crystal polymers (with mesogen units in the main-chain) are of strong current interest among polymer scientists, and as such a large variety have been synthesised [13-15]. One of the more popular is shown structurally below;

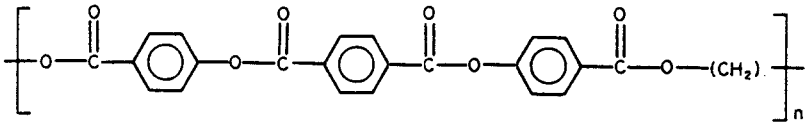

It is based on an alternating sequence containing a mesogenic triad and polymethylene flexible spacer. It has been studied by LENZ et al. [16-20], and BILIBIN et al. [21-24]

Although a large series of these polyesters have been synthesised, a surprising amount of information is still to be gleaned from variations in flexible spacer, addition of lateral substituent, thermal history, etc.

---

[10] Rigid polymers like poly(hydroquinone terephthalate) are non-mesomorphic, with decomposition temperatures in excess of 500°C, and are not melt processable

4.3 Aims

Of primary interest is the development of commercially viable thermotropic, mesophasic liquid crystalline polyesters with lower and wider mesomorphic transition temperatures than those reported in the literature.

In this chapter new experimental results are presented on the characterization (using FTIR, Raman spectroscopy, differential scanning calorimetry (DSC), thermo-optical analysis (TOA), and wide angle X-ray scattering (WAXS)) of a series of thermotropic liquid crystalline polyester, the structures of which are shown in figure 4.6. The procedure followed for their synthesis is described in section 4.5.5. The thermal behaviour at low and elevated temperatures is reported herein.

NAME	ABBREV.	CHEMICAL REPEAT
polytetramethylene terephthaloyl-bis-4-oxy-3-chlorobenzoate	MC4TOB	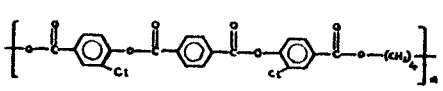
polytetramethylene terephthaloyl-bis-4-oxy-3,5-dichlorobenzoate	DC4TOB	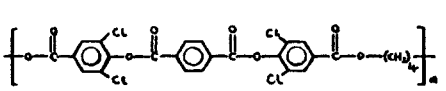
polyheptamethylene terephthaloyl-bis-4-oxy-3-chlorobenzoate	MC7TOB	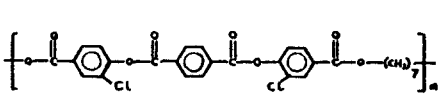
polyheptamethylene terephthaloyl-bis-4-oxy-3,5-dichlorobenzoate	DC7TOB	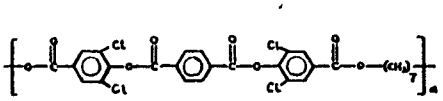

Figure 4.6 Thermotropic liquid crystalline polyesters synthesised whilst in Madrid.

Each of the polymers studied in this chapter namely MC4TOB, MC7TOB, and their equivalents without lateral substituents; P4TOB, and P7TOB are, for simplicity studied separately within this chapter. Further each polymer sub-

section is further divided with respect to method of analysis; DSC, TOA, and WAXS. Sections 4.6.4.4 and 4.6.5.4 have been included to help the reader compare and contrast results obtained for P7TOB/MC7TOB and P4TOB/MC4TOB respectively, rather than leaving all the discussion to the final section. The conclusion and summary section briefly summarize the results with an emphasis on the effects of lateral substitution and flexible spacer lengths.

4.4 Characterization of liquid crystal polymers

4.4.1 Polarizing microscopy

One of the most important methods of analysis of LCPs is to study them visually, using a light microscope. In-fact most of the early work is based on observations from microscopy [25,26].

Providing the sample is optically anisotropic phases can be identified by observing the characteristic textures developed in thin layers of the polymer when viewed through a microscope using a linearly polarizing light source.

A polarizing microscope itself is a standard light microscope fitted with a pair of polarizing filters, one above and one below the specimen [27,28]. If the two polarizers are in the crossed position then no light will pass through the microscope in the absence of a specimen, or if the specimen is isotropic. Inserting a doubly refracting specimen gives rise to beam splitting and interference phenomena which allow light to pass through the instrument, and what is observed are areas of white or bright coloured light on a dark background.

As the temperature of a sample increases it leads to changes from the most ordered to the least ordered state in liquid crystal polymers:

crystal (k) → Smectic (s) → Nematic (n) → Isotropic (i). These phase transitions cause variations in the birefringent properties of the sample and hence changes in the luminosity of the sample. These changes in light intensity detected by the microscope can be related to thermal transitions in the sample. This study is better known as thermo-optical analysis (TOA). In many cases the mesophase to isotropic phase transition is particularly important, since in certain cases only TOA can provide this temperature.

4.4.2 Thermal analysis

In addition to the traditional Differential scanning calorimetry, (DSC) [29,30] the field also includes thermogravimetric analysis, (TGA) thermal analysis, electrical thermal analysis, and effluent gas analysis. By far the most popular of these thermal techniques in the analysis of polymers is DSC and TGA. Crystalline and especially thermotropic liquid crystalline polymers present complex thermograms because of the numerous thermal transitions which are possible. Not only can one study the enthalpy changes associated with heating, annealing and crystallizing, but one can also study a wide variety of responses as a function of temperature for example polymerization, degradation, curing, etc.

In thermogravimetric analysis a sensitive balance is used to follow the weight change of the sample as a function of temperature [29,31]. Typical applications are primarily the assessment of thermal stability in oxygen and nitrogen environments, and decomposition temperatures, again either in oxygen or inert gas environments.

4.4.3 X-ray diffraction analysis

The X-ray diffraction method has been used extensively in the study of thermotropic LCPs. The powder technique is normally employed, for investigating ordered structures, through the interaction of electromagnetic radiation to give interference effects with structures comparable to the

wavelength of the radiation used [31].

In highly crystalline samples the interferences are sharpened so that the radiation is scattered /diffracted only under certain conditions.

Small angle x-ray scatter: is useful in detecting large periodicities which arise from lamellar crystallites, $S_{A\&C}$ phases can be distinguished

Wide angle x-ray scatter: gives information on the spatial arrangement of the atoms. In the case of Nematic or disordered S_A or S_C phases, a broad halo at $2\theta \approx 20°$ appears. Ordered Smectic mesophases, which have true 3D order show reflections between 2θ = 18-30°, and corresponds to lateral order between the molecular chains.

4.4.4 Vibrational spectroscopy

Vibrational spectroscopy in the study of LCPs is not well documented, most studies having been concerned with small and or low molecular weight molecules. Infra-red analyses have been made of side chain LCPs [32], and main chain LCPs [16-18, & 33-35]. Phase transitions have also been followed by FTIR spectroscopy [16,17,35]. Despite the relative popularity of the technique in the analysis of LCPs, the technique is plagued by sample handling problems; common methods of sample preparation include, compression moulding, dissolving the polymer in a solvent, preparing a thin film by microtoming or milling, and pressing a finely ground mixture of the sample with KBr to form a disc. To date only one paper has sighted results obtained from nir FT-Raman analysis [36].

4.5 Experimental

4.5.1 Microscopic studies and thermo-optical analysis

Samples for study were prepared as thin films on standard microscope slides, which were placed in a Mettler FP-8HT high temperature cell. Analysis was carried out using a Reichert polarizing microscope, with a photodetector connected to an X-Y chart recorder to monitor changes in luminous intensity, and a Nikkon FX-35A SLR camera to record photomicrographs of the sample at various temperatures (see section 4.6.6.2).

4.5.2 DSC and TGA

A Mettler TA-3000 with DSC-30 furnace, and Mettler TA-72 software was used to record the DSC thermograms. Calibrations were made using indium (T_m = 156°C/ΔH_m = 28.45J/g), lead (T_m = 327°C/ΔH_m = 23.1J/g), and zinc (T_m = 419.5°C/ΔH_m = 108.37J/g) standards. Samples in the range 7-12mgs, sealed in aluminium pans were heated at rates of 10°C/minute, under nitrogen. Specific details of scan conditions can be found on the appropriate traces. Transition temperatures were taken at peak maxima for both endo and exothermic profiles. Thermogravimetric analysis was performed on a Mettler TG-50 thermobalance, connected to the same thermal analysis device. Samples were heated under nitrogen at heating rates of 10°C/minute.

4.5.3 X-ray analysis

WAXS data were obtained using a Phillips PW1050/70 Geiger counter x-ray diffractometer. The diffractograms were recorded in the 2θ range 2-30° using Ni filtered CuK_α radiation at 2°/minute. Samples were prepared by packing the powder into a 2 x 1.5cm aluminium alloy sample holder. Diffractograms recorded as a function of temperature were made using a Anton Paar high temperature

cell. See appropriate diffractograms for details on heating rates etc.

4.5.4 Infra-red and Raman spectroscopy

Infra-red spectra were recorded on a Perkin-Elmer model 1720 FTIR interferometer, samples were studied as mulls, between highly polished KBr plates, 100 scans were taken at a resolution of 4 or 8cm^{-1}. Data manipulation was carried out using the Perkin-Elmer IRDM and Mattson software.

FT-Raman spectra were measured on a Perkin-Elmer 1720 series FTIR interferometer described in chapter 2. All spectra were corrected for sensitivity variations in the detector, filters and optical components of the interferometer.

4.5.5 Materials and synthesis

All the polyesters were prepared by the method described by BILIBIN et al [23]. In figure 4.7 the reagents used are shown. Their chemical repeat and origin are shown, along with common abbreviations (in brackets).

NAME	ORIGIN	CHEMICAL REPEAT
teraphthaloyl chloride	Merck	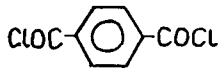
3,5-dichloro-4-hydroxybenzoic acid	Aldrich D6,400-7	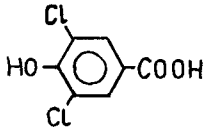
3-chloro-4-hydroxy benzoic hemihydrate	Aldrich C4,460-5	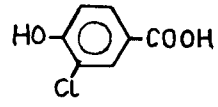
dichloro terephthaloyl-4-bis-oxybenzoic acid (DCTOBA)	-	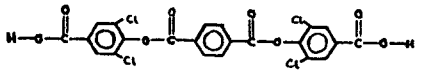
monochloro terephthaloyl-4-bis-oxybenzoic acid (MCTOBA)	-	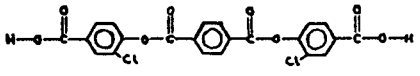
dichloro terephthaloyl-4-bis-oxybenzoyl chloride (DCTOBC)	-	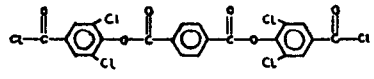
monochloro terephthaloyl-4-bis-oxybenzoyl chloride (MCTOBC)	-	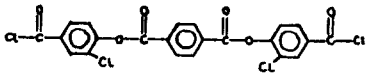

Figure 4.7 Reagents used in synthesis of the LCPs

4.5.5.1 Synthesis of MC7TOB

The general reaction scheme for all the polymers synthesised (see figure 4.6) is shown in figure 4.8.

The first stage involves the preparation of MCTOBA

To a solution of 21.842g of 3-chloro-4-hydroxybenzoic acid in 250ml of 1M NaOH (aq) was added, whilst stirring rapidly, at room temperature, in the course of 10 minutes a solution of 10.2g of terephthaloyl chloride in 100ml of carbon tetrachloride and a 1M solution of NaOH (aq). Stirring was continued overnight.

The resulting white precipitate was filtered under vacuum, and dried overnight under vacuum. The product was then mixed with HCl, filtered, washed with water, then dried under vacuum, to constant weight. (90% yield)

The second stage involves the chlorination of the MCTOBA to MCTOBC

MCTOBA (19.75g) was heated to reflux with thionyl chloride (244ml). The reflux was terminated once all the solid product had dissolved (16 hours). It was then cooled to O°C and filtered under vacuum and dried under vacuum to constant weight. The solid was then recrystallized from chloroform, and dried under vacuum.

The third and final stage of the synthesis in this case involves the polycondenstation of MCTOBC with heptamethylene diol.

MCTOBC (5.00g) was placed into a 3 necked 50ml flask. To this was added heptamethylene diol (1.34g) and diphenyl oxide (23ml). The mixture was purged with nitrogen for 20 minutes at room temperature, before the vessel was submerged to the neck in liquid silicone (80°C). The temperature of the oil was gradually increased to 200°C and left stirring for 14 hours, or until it seemed the mixture was of a sufficient viscosity. On completion of the process the hot viscous solution was decanted into 50ml of toluene. The polymer was filtered and vacuum dried. (99% yield)

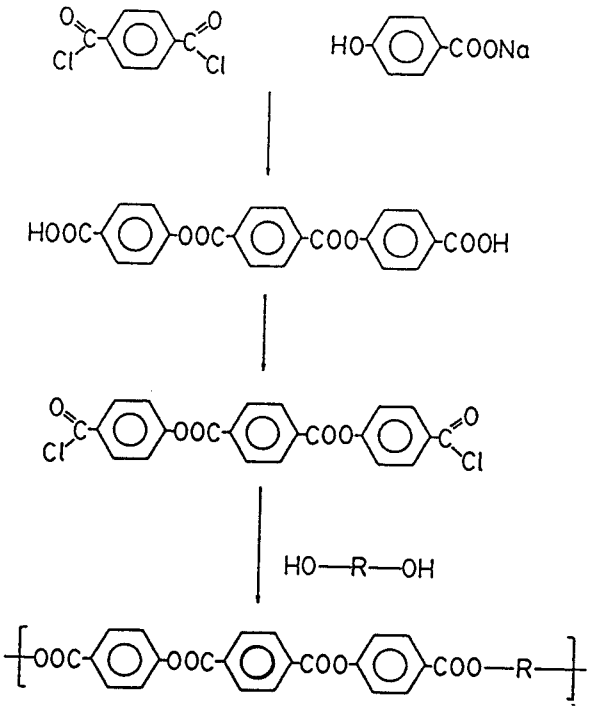

Figure 4.8 General reaction path-way

The polymers described in figure 4.6 were synthesised using a similar method.

The advantage of this method compared with other synthetic routes for the preparation of thermotropic polyesters [19,37] is that it provides a route to high molecular weight polymer. The method also permits for the first time to separate, purify and characterize the mesomorphic dichloride.

4.6 Results and discussion

The structures of the polymers and intermediates were confirmed by elemental analysis, ^{1}H and ^{13}C NMR spectroscopy [38].

4.6.1 Vibrational analysis

This section refers to the vibrational properties of the polyesters studied at room temperature. Infra-red and Raman spectroscopy complement each other to provide a powerful diagnostic tool for the understanding of the structures involved.

It is possible to study structural evolution as a function of temperature through the various phase transitions. Information on order can be obtained from such data. ELLIS et al [39] have studied (using nir FT-Raman spectroscopy) the temperature dependencies of the P7TOB, spectral evidence is presented which is related to both the sample crystallinity and the crystal-to-liquid crystal phase transition. Unfortunately a similar study cannot be performed on the chlorinated liquid crystals because of the elevated transition temperatures involved. High temperature Raman measurements [40] are limited to approximately 190°C above which the thermal background masks the Raman scatter. Results have therefore been limited to the room temperature analysis.

Raman and Infra-red spectra of MC4TOB are shown in figure 4.9. Similar spectra were recorded for P4TOB, MC7- and P7TOB. Raman and infra-red frequency tables are shown in figure 4.10

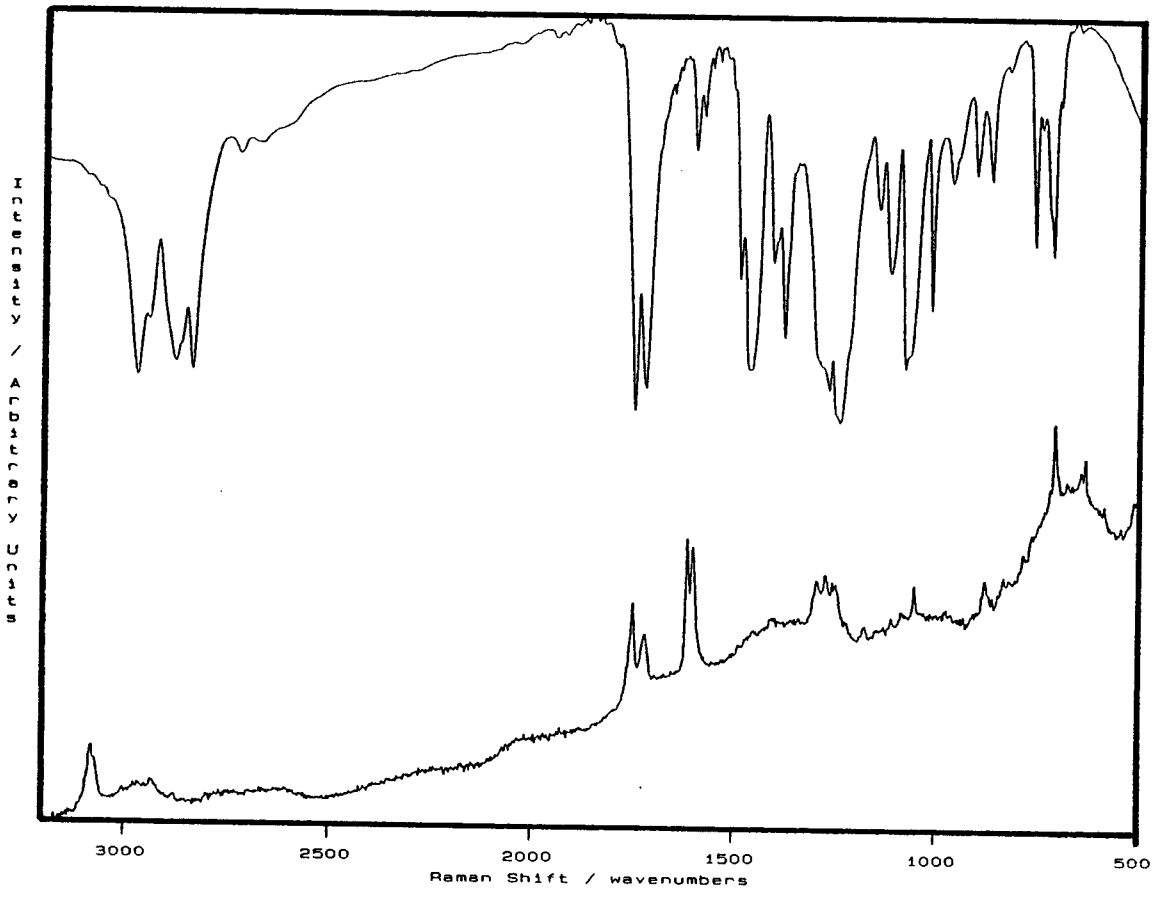

Figure 4.9 The vibrational spectra of MC4TOB, FTIR (upper) 4cm^{-1} resolution, 100 scans, and FT-Raman (lower) 200 scans, 4cm^{-1}, 400mw.

The FTIR spectrum appears to be more complex than the FT-Raman spectrum, due to the band overlap and subsequent band superimposition.

Raman and infra-red frequency assignment for (a) P7- and P4- TOB

Raman	Infra-red	Assignment
1743 m	-	$\nu_{C=O}$
1735 m,sh	1733 s	$\nu_{C=O}$ terephthaloyl
1716 m	1716 s	$\nu_{C=O}$ oxybenzoate
1710 m,sh	-	$\nu_{C=O}$
1605 s	1602 m	$\nu_{C=C}$ ring
1578 w,sh	-	$\nu_{C=C}$ ring
1551 w	-	$\nu_{C=C}$ ring
1488 w	1501 m	
1461 w	1463 s	CH_2 def.
1450 w	-	CH_2 def.
1436 w	-	
1407 vw	1410 m	ring mode
1373 w	1377 m	
1358 w	-	CH_2 def.
1340 vw	-	CH_2 def.
1326 w	-	CH_2 def.
1304 m,sh	1306 m,sh	ring mode, CH_2 twist
1285 m,sh	-	ring -C=O str. + O-C str. +arom.CHbend
	1275 s	C(O)-O str.
1269 s	-	C(O)-O str.
1230 w	-	
1206 w	1205 m	ring mode
1196 w,sh	-	ring mode
1179 w,sh	-	ip ring CH bend
1163 m	1163 s	ring mode
1139 vw	-	
1124 w,sh	-	C-O str.

	1115 m	ip ring CH str. or C-O-C sym. str.
1107 w	-	ip ring CH str. or C-O-C sym. str.
1078 m	1078 s	ester C(O)-O str. or C-C str. in C-C chain
1066 m,sh	-	ester
1017 w	-	C-O asym. str. or ring mode, C-O-C sym.
1002 vw	-	O-CH_2 str.
963 vw	961 w	C-O asym. str., oop C-H wag (arom)
951 vw	-	-
936 vw	-	-
921 vw	-	-
888 m	886 m	CH_2 rock, ring breathing (ν_2)
879 vw,sh	875 m	CH_2 rock
858 w	-	CH_2 rock
836 w	-	CH oop def
827 w,sh	831 w	CH_2 rock
814 w,sh	-	oop CH wag
763 m	760 m	ring CH oop bend
719 m	719 s	ring CH oop bend or C-O-C def. or C=O oop bend/ring CH oop bend, CH_2 rock
686 vw	694 m	CH oop def arom.

670 vw	-	
663 m	-	
645 w,sh	646 w	ring mode
629 m	-	ring C-C-C ip bend
609 vw	-	

Raman band assignments for MC4- and MC7- TOB

Raman	Infra-red	Assignment
1750 m	1747 m	$\nu_{C=O}$ terephthaloyl
1720 w	1720 m	$\nu_{C=O}$ terephthaloyl
1614 s	1599 m	$\nu_{C=C}$ ring
1599 s	1579 m	$\nu_{C=C}$ ring
-	1490 m,sh	-
1446 w	1461 s	CH_2 def. (bending)
1392 w	1407 m,sh	ring mode
-	1377 s	-
1273 m	1268 s	C(O)-O str.
1254 m	-	C(O)-O str.
	1240 s	$\nu_{C=O}$ str. ester
1179 w	-	ip ring CH bend
-	1146 m	ring mode
-	1117 m	ip ring CH str. or C-O-C sym. stretch
1078 w	1078 s	ester C(O)-O str. or C-C str. in C-C chain
1052 m	-	ester

-	1014 s	C-O asym. str. or C-C str.
963 vw	962 w	C-O asym. str., oop CH wag (arom).
-	903 w	-
879 m	-	CH_2 rock
-	866 m	CH_2 rock
-	759 m	ring CH out of plane bend
-	712 m	ring CH out of plane bend
706 m	-	C-O-C def.
631 m	-	ring C-C-C ip bend.

vs = very strong, s=strong, m=medium, w=weak, vw=very weak, sh=shoulder

Figure 4.10 The Raman and IR frequencies for (a) P7- & P4-TOB, and (b) MC4- & MC7-TOB.

Consider the selection rules for the polymers (viewed as one dimensional crystals). The polymers are centrosymmetric and as such the symmetric *gerade* (g) Raman-active normal frequencies, and the antisymmetric, *ungerade* (u) infra-red active modes should not coincide. It is common knowledge that the splitting between g and u modes can occur only if the intramolecular coupling is sizeable. If the vibrational motions are uncoupled, accidental degeneracy may occur and some of the IR and Raman-active modes may coincide [41,42].

4.6.1.1 C-H stretchings

Infra-red analysis

The C-H groups located in the positions 2,3,5 and 6 in the aromatic ring of the polyester without substitution result in the weak absorptions near 3100cm^{-1}, from the appearance of the band, one can deduce the vibrations are highly localized and decoupled. Asymmetric and symmetric C-H vibrations appear at around 2934 and 2852cm^{-1} respectively [43,44].

In the MC7- and MC4-TOB the C-H groups located in positions 2,5 and 6 appear at a slightly lower frequency of vibration than would initially be expected (2980-2900cm^{-1}) due to the electron withdrawing properties of the chlorine atoms. Methylenic asymmetric and symmetric C-H stretches give rise to IR absorptions at 2883 and 2845cm^{-1} respectively.

Raman analysis

The Raman spectra of the P7- and P4- TOB, show C-H stretching vibrations around 3077cm^{-1} (aromatic), and 2936 and 2856cm^{-1} (methylenic). In the case of MC7- and MC4-TOB, the aromatic C-H vibration appears around 3082cm^{-1}, whilst the aliphatic C-H antisymmetric and symmetric stretching vibrations appear around 2914 and 2857cm^{-1} respectively.

4.6.1.2 C=O stretching vibrations

These bands appear between 1710-1750cm^{-1}. The strong multiplet observed in the spectra is not easily accounted for. It occurs in both the infra-red and Raman spectra of the polyesters. As expected the band is stronger in intensity in the IR analysis, although the Raman band is relatively strong.

The interpretation of the spectra in the C=O stretching range can be rationalized once several basic features characteristic of these ester systems are accepted.

The following account provides a general understanding of the phenomenon and applies to all the polyesters studied in this and chapter 5.

Consider first, the coplanarity and conformational rigidity of the central benzene 1,4-diester, such a structure has been the matter of some interest [45,46,47]. Calculations have shown [47] the molecule to be coplanar, because the P_z electrons of the C=O group are conjugated with those of the benzene ring. Coplanarity favours conjugation, lengthens the C=O bond length and shortens the ring -COOR bond length [47]. Since the calculated barrier height is reasonably high, in this thesis it is assumed that the OOC-C_6H_4-COO unit is rigidly coplanar at all temperatures.

The next step involves the conformation, either *cis* or *trans* of the C=O moieties around the benzene ring. The mutual exclusion between infra-red and Raman active modes observed in the spectra of model compounds [38] and the results of X-ray diffraction studies, again on model molecules [38], indicate the centrosymmetric *trans* configuration as the most likely.

Now let R and Ar indicate the saturated and aromatic residues that may be attached to the ester group. According to JONES [48] molecules of the type R-CO-O-R' absorb near 1735cm^{-1}, molecules of the type Ar-CO-O-R (with conjugation) absorb near 1720cm^{-1}, the downward shift is ascribed to the decrease in bond order (hence increase in the bond length) because the C=O is conjugated with the aromatic ring. Still not explained is the fact that molecules of the type Ar-CO-O-Ar' absorb at a higher frequency of vibration near 1745cm^{-1}. This may be due to the effect of the P_z electrons adjacent to the -O- group affecting the electronic distribution, and hence the dynamic properties of the system, seemingly making the C=O bond stiffer than in any other case.

Rotation about either side of the -O- group may change such effects. Following these observations the multiplet structure observed in these systems at round 1745 and 1720cm^{-1} in the Infra-red, and 1750-1709cm^{-1} in the Raman, are therefore ascribed to the existence in the sample, at room temperature of more than one structure characterized by different rotational states about the -O-Ar' bond. It has also been postulated that because of strong intermolecular interactions more than one different crystalline structure exists in the sample [49]. If more than one crystalline phase exists in the solid sample as prepared, the evolution of the spectrum as a function of temperature should show several discontinuities at transition temperatures. This is not observed in the case of P7TOB [39], but is in the case of P4- and MC4-TOB, (see later).

4.6.1.3 C-O stretching and COC deformations

The region 1350-900cm^{-1} is complex in both spectroscopic techniques, the modes are strong, surrounded by and overlapped with many medium-strong bands ascribed qualitatively to C-C bond stretchings. The band between 1163-1140cm^{-1} which is strong in both spectroscopies is a characteristic of *para-* substituted aromatic moieties in polymer chains, and is thought to be due to a ring stretching vibration [41] in the terephthaloyl segment. The large electrostatic bond dipole moment on the C-O bonds (and large dipole moment changes during vibration) induce a strong polarization of the neighbouring C-C bonds, thus giving rise to strong absorption bands. It is very difficult to clearly assign bands in this region, however the band around 1270cm^{-1} has been tentatively assigned to the *internal* C-O group. The vibration of the *external* C-O groups are hidden in the very strong and complex spectral pattern in this region [41].

4.6.1.4 Out-of-plane C-H deformations

From a survey of spectroscopic data in the literature [41] an absorption band between 690-720cm^{-1} is due to a C=O out-of-plane deformation mode. An adsorption band between 740-749cm^{-1} has been assigned to the out-of-plane deformation mode of the C-H next to the -O- of the ester group, and the band near 720cm^{-1} to the out-of-plane deformation mode of the C-H next to the C=O group.

4.6.2 Thermogravimetric analysis

Before the analysis by DSC, the thermal stability of the polymers was studied, in order to gain some idea of the thermal stability, and upper heating limits in the DSC analysis figure 4.11 shows the results obtained in the study. Results are compared to the polymers without lateral substitution, namely polytetramethylene terephthaloyl-*bis*-4-oxybenzoate (P4TOB) and polyheptamethylene terephthaloyl-*bis*-4-oxybenzoate (P7TOB), courtesy of J. del Pino, and Dr. J. Lorente respectively.

POLYMER	DECOMPOSTION TEMPERATURE (°C) (under nitrogen)
P4TOB	350
MC4TOB	350
DC4TOB	350
P7TOB	347
MC7TOB	340
DC7TOB	345

Figure 4.11 The decomposition temperatures of some thermotropic liquid crystalline polyesters (heating rate, 10°C/minute, under nitrogen).

The DC4 and MC4 polymers are both stable upto 350 °C, with a 10% weight loss at 390 °C. P4TOB (without lateral subsitituents) is also stable upto 350 °C. It is therefore reasonable to say that the introduction of the 2 chloro atoms in positions -3,3- of the *p*-hydroxybenzoic acid in the mesogen does not modify the thermal stability of the polymer. Variations in flexible spacer length does however affect the thermal stability of the polyesters. Looking down the table in figure 4.11, the thermal stability of the substituted polymers show a certain trend. As the flexible spacer length increase, the thermal stability decreases. What we are seeing is a dilution of the effective number of aromatic mesogenic groups in the macromolecules. The elevated thermal stability in the case of the substituted polyester with 4 methylene units is due to the short chain flexible spacer being more rigid than flexible spacers of greater length[11]. The short chains are more rigid, as they do not impart as much flexibility on the system. Thus the point of degradation increases due to the restricted motion of the polymer flexible segments.

In the presence of air the thermal stability of the polymers decreased dramatically. The decompostion profiles were complex, which suggests chain scission at polymer chain ends [39].

4.6.3 Analysis of P7TOB

4.6.3.1 DSC

The DSC heating curves of virgin P7TOB are characterized by the presence of 4 different transitions at 60-70, 115-150, 173 and 295 °C. See figure 4.12a. The first endotherm is very broad and shallow corresponding to the glass transition. The fairly broad transition between 115-150 °C is an exothermic band with a low

[11] Each C-C bond can be *trans* or be in one of 2 different gauche states about the preceding C-C bond.

enthalpy of 2.6J/g, corresponding to the crystallization of the sample. The third band near 173°C ΔH = 10.3J/g is due to an endothermic process; the crystal - liquid crystal transition (T_1). The final endotherm at 295°C corresponds to the isotropization of the mesophasic sample, (T_i) with an enthalpy of 13.3J/g.

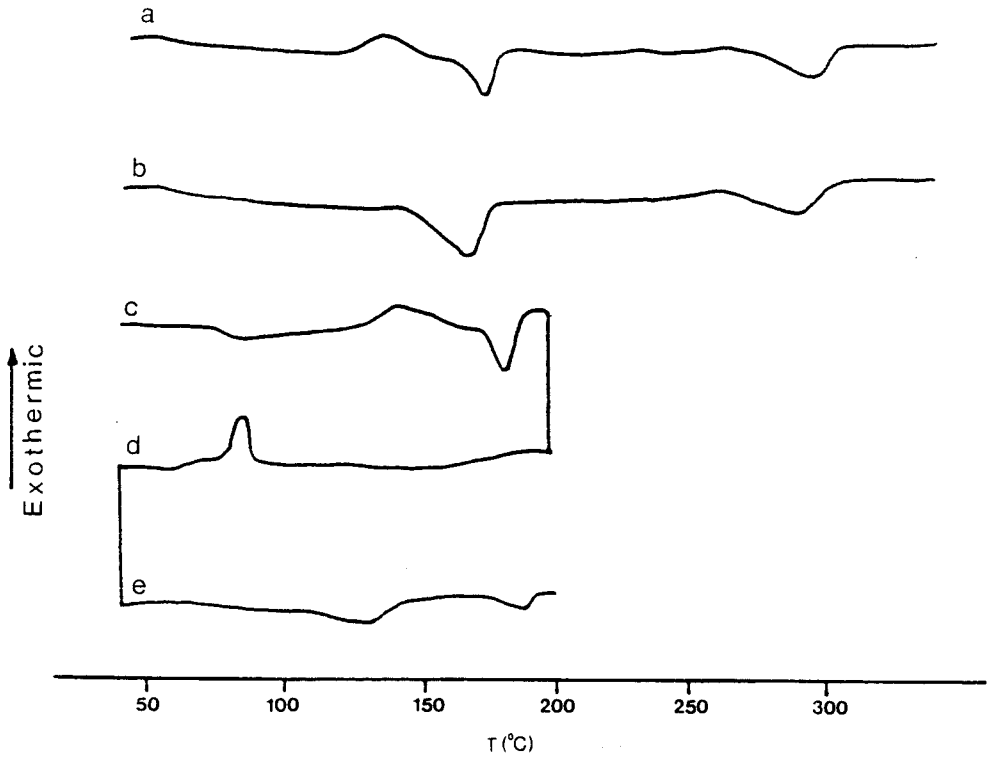

Figure 4.12 The DSC traces of P7TOB

The crystallization between 115-150°C proceeds at a much lower enthalpy than the crystal to mesophase transition, (2.6J/g compared with 10.3J/g respectively), this must be due to the fact that the virgin polymer is already crystalline to a certain degree. X-ray analysis confirms this hypothesis with a crystallinity index of 0.23.

In an attempt to increase the homogeneity of the polymer, a sample was

crystallized from a solution of trifluoroacetic acid, figure 4.12b shows the DSC trace, note the absence of the crystallization exotherm seen in figure 4.12a. The endotherm occurs at a similar temperature to the one in figure 4.12a but with an increase in enthalpy, to 13.3J/g, signifying an increase in the degree of crystallinity.

To study the effect of thermal history on the polymer the sample from (a) was heated to the mesophase (figure 4.12c) and then cooled to room temperature at a rate of 10°C/minute (figure 4.12d). The crystallization exotherm shows a high undercooling at 80°C. When the sample was heated for a final time (figure 4.12e) two endotherms at 130 and 180°C appeared. When compared to the original thermogram it can be seen the onset of the transitions have decreased from 173 and 295°C respectively, indicating how important the thermal history is to the polymer properties.

4.6.3.2 Thermo-optical analysis

The analysis of a film prepared by cooling a film from 200°C shows the existence of three transitions (figure 4.13a). These transitions were also detected by the calorimetric study (see previous figure). The first transition corresponds to a light loss in the TOA, this occurs between 100-200°C and is due to the melting of small and/or imperfect crystallites. A sharp light gain can be observed between 165-185°C corresponding to the crystal to liquid crystal phase transition, photomicrographs taken in this range show the existence of a smectic mesophase. The isotropic liquid is clearly visible at 310°C. On cooling from the isotropic melt (4.13b) a mesophase starts to nucleate at 290°C.

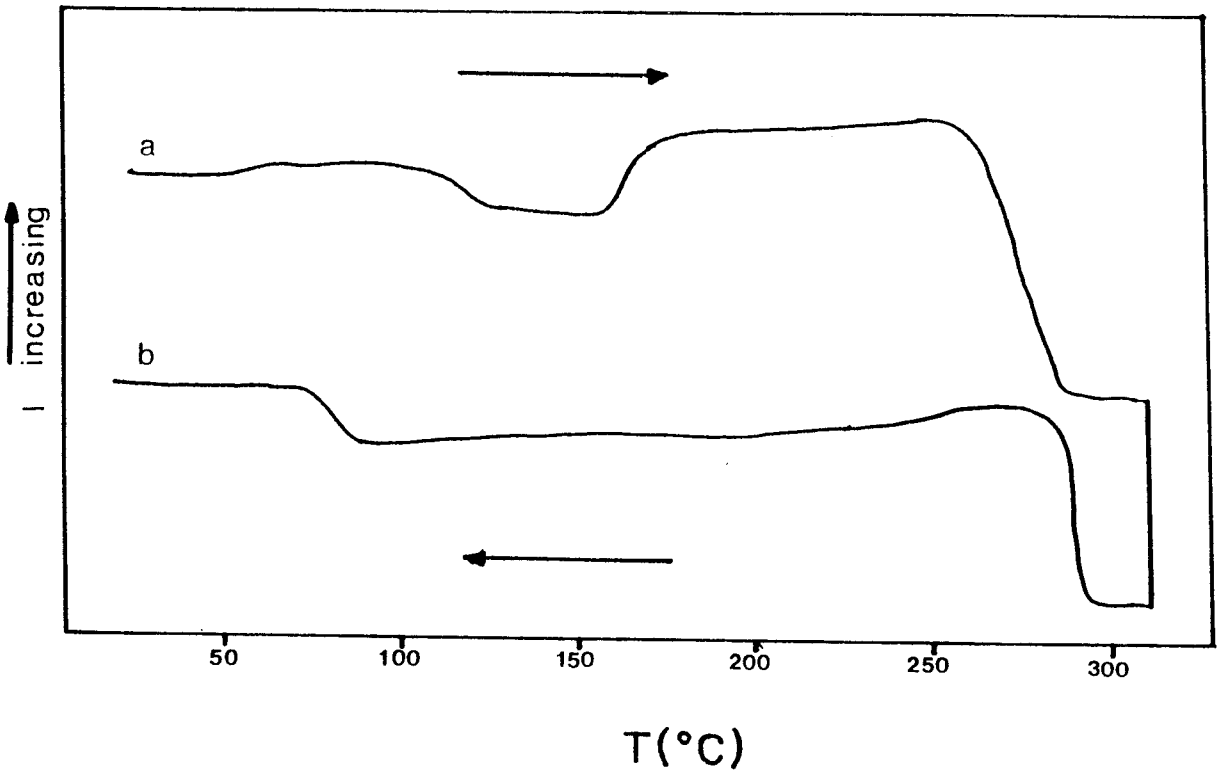

Figure 4.13 The thermo-optical analysis of P7TOB

4.6.3.3 X-ray analysis

X-ray diffraction patterns recorded on (a) virgin P7TOB (b) heat treated (to 200 °C then cooled) P7TOB and (c) Quenched into liquid nitrogen from 200 °C, are shown in figure 4.14.

Figure 4.14 (a) shows the typical pattern of a semicrystalline polymer. The scattering patterns in (b) and (c) are quite different.....

In figure 4.14 (a) strong reflections occur at 2θ = 3.8, 19.7, and 23.4°. An amorphous halo is centred around 2θ = 28°. The reflection at 2θ = 3.8° (corresponds to a Bragg d spacing of 23.24Å) is characteristic of a smectic mesophase, thus confirming the findings proposed by TOA. The x-ray data does not however provide any conclusive information about the nature of the smectic mesophase.

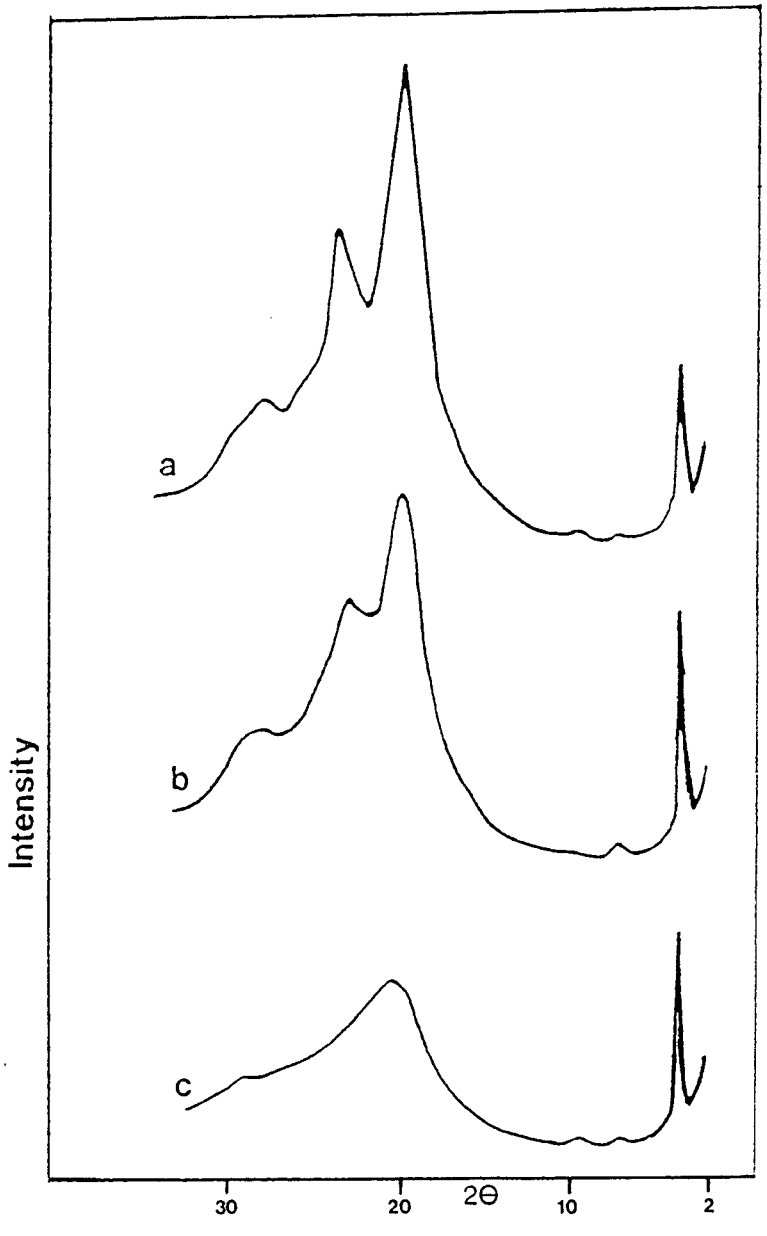

Figure 4.14 The WAXS of P7TOB; (a) original sample (b) heat treated to 200°C and then cooled to room temperature and (c) heated to 200°C and quenched into liquid nitrogen.

In (b) 3D order has been preserved with reflections similar to those in (a) but slightly more diffuse. Whilst in (c) all evidence of crystalline order has disappeared and we are left with a reflection at 2θ = 3.8° indicative of a smectic mesophase (this supports the findings in the section 4.6.3.2 and the TOA data). It is therefore possible to "freeze-in" the mesophase. This phenomenon has been noted in other thermotropic polymers [49,50].

The x-ray diffraction pattern of the sample crystallized from solution is shown in figure 4.15 (a), strong reflections are observed at 2θ = 20 and 24° corresponding to 3D, crystalline order. No reflection at small angles was observed. When the sample was heated to 200°C the liquid crystal phase was observed, 2θ = 3.8° (figure 4.15b). These results indicate that in the virgin polymer straight from the reaction vessel, the liquid crystal and crystalline phases co-exist, and depending on the thermal history imposed on the sample, it is possible to isolate the LC phase (figure 4.14c). Only when the sample is recrystallized from solution is it possible to isolate the crystalline phase.

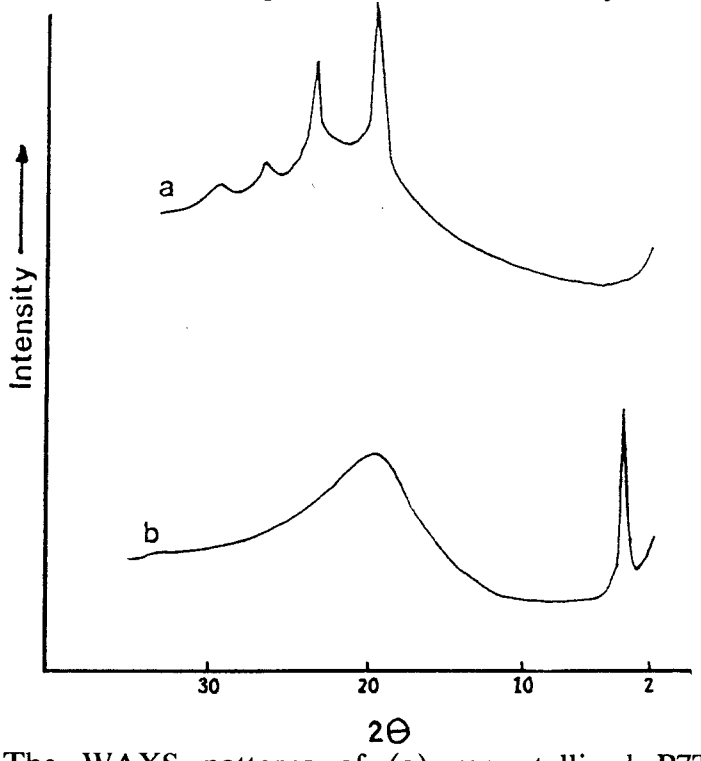

Figure 4.15 The WAXS patterns of (a) recrystallized P7TOB, and (b) recrystallized P7TOB (heated to 200°C and then cooled)

4.6.4 Analysis of MC7TOB

4.6.4.1 DSC

The virgin polymer shows a very different thermogram to the P7TOB. Figure 4.16a is characterized by the endotherm doublet, around 110-140°C. A T_g can be detected at 49°C. No T_i was noted. The sample was then annealed at 280°C for 5 minutes, before being allowed to cool at a rate of 10°C/minute. The cooling thermogram (figure 4.16b) shows a broad exotherm at 80°C, due to a recrystallization process.

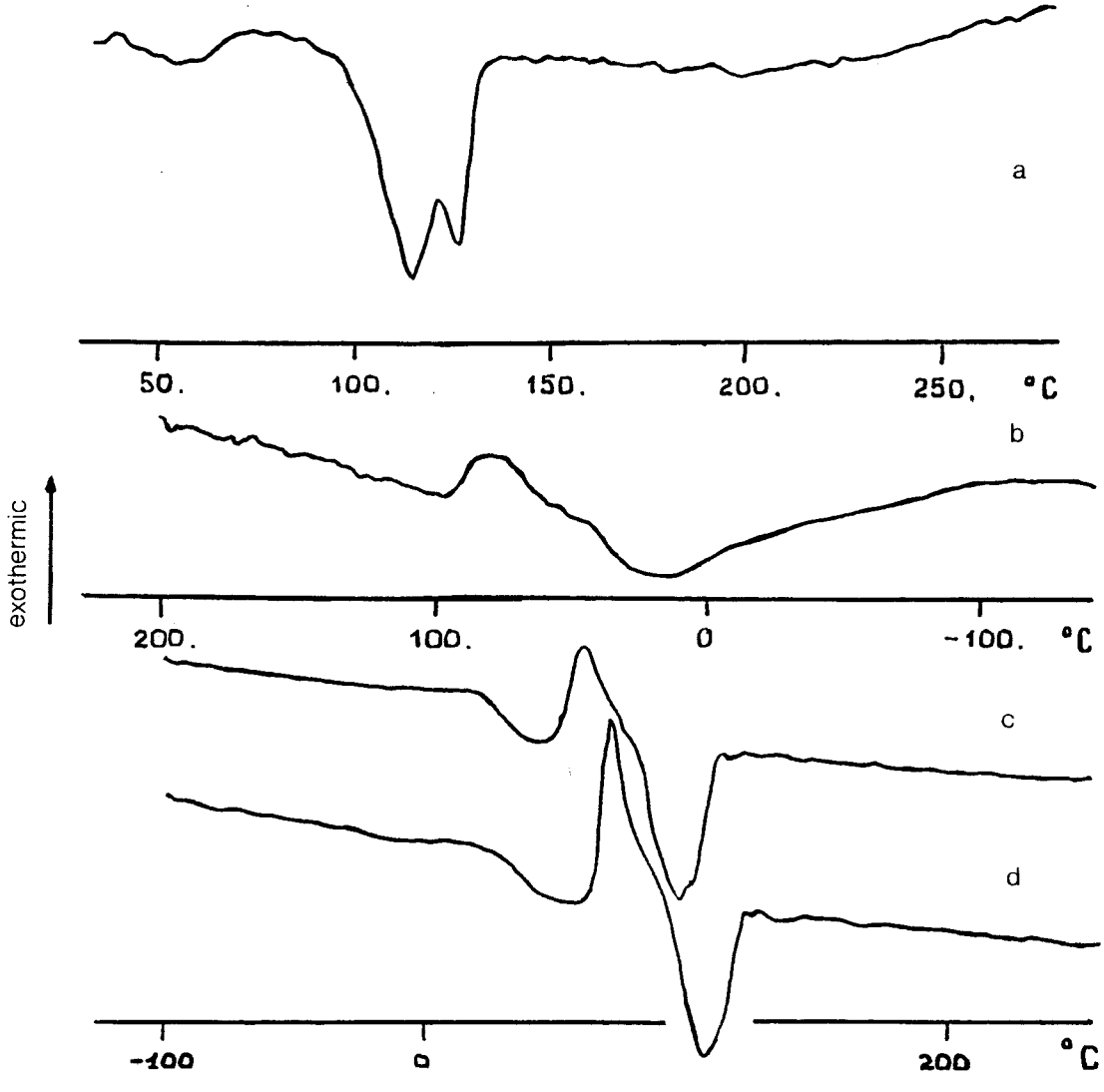

Figure 4.16 The DSC thermograms of MC7TOB

The subsequent heating run (figure 4.16c) shows a well defined T_g at 40°C, This is followed almost immediately by a crystallization exotherm, peak maximum at 60°C. These crystallites finally melt at approximately 105°C. A small shoulder can be observed at a slightly higher temperature indicating the presence of a second crystalline phase. The sample was annealed again at 280°C for 5 minutes before being quenched into liquid nitrogen. The resulting thermogram is shown in figure 4.16d. Again a T_g can be observed at approximately 50°C, followed by a crystallization exotherm at 70°C and a melting endotherm at 110°C.

When compared to with the first trace the melting endotherm in (d) now appears as one band, due to annealing effects. Throughout the thermal treatments, transitions have remained within a narrow temperature band. No liquid crystalline phase was noted. However supercooling of the melting endotherms was noted, this appears to be a common feature of liquid crystalline polymers [20].

4.6.4.2 Thermo-optical analysis

The TOA of the polymer film prepared by cooling a sample from 150°C shows a single light intensity loss between 140-150°C probably due to the melting of the crystallites to form an isotropic liquid. Upto 140°C and the onset of visual melting, four leaf clover patterns are observed characteristic of 3D order, formed when the film was cooled down from the melt.

4.6.4.3 X-ray analysis

The WAXS pattern of MC7TOB is shown in figure 4.17a It is characterized by 4 reflections at 2θ = 14° (sharp and strong), 19°(broad), 24°(strong) and 26°(shoulder). Reflections at 2θ = 19, 24 and 26° are characteristic of 3D crystalline order. The origin of the reflection at 2θ = 14 which corresponds to a Bragg d spacing of 6.37Å is still unknown. When the sample is recrystallized from trifluorocetic acid the same reflections are observed, the only difference

being in the intensity of the band at $2\theta = 14°$ (figure 4.17b).

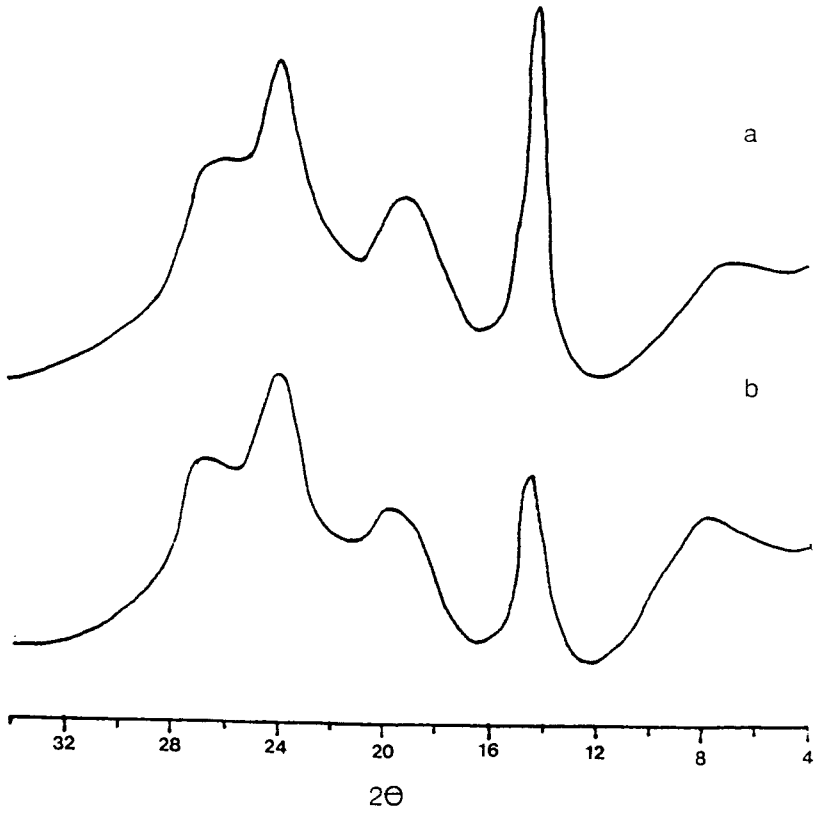

Figure 4.17 WAXS patterns of MC7TOB

Particular attention has been given to the thermal treatment of the polymer. Figure 4.18 shows the polymer heated from room temperature to 130°C. Figure 4.18c shows evidence of the melting of the crystalline region with the appearance of broad poorly bands. All evidence of the 3D network has disappeared by 120°C, leaving a broad halo. Slow cooling the sample from the melt (figure 4.87f) fails to produce the crystalline phase observed in the untreated sample. Results confirm DSC and TOA, namely the absence of liquid crystalline order.

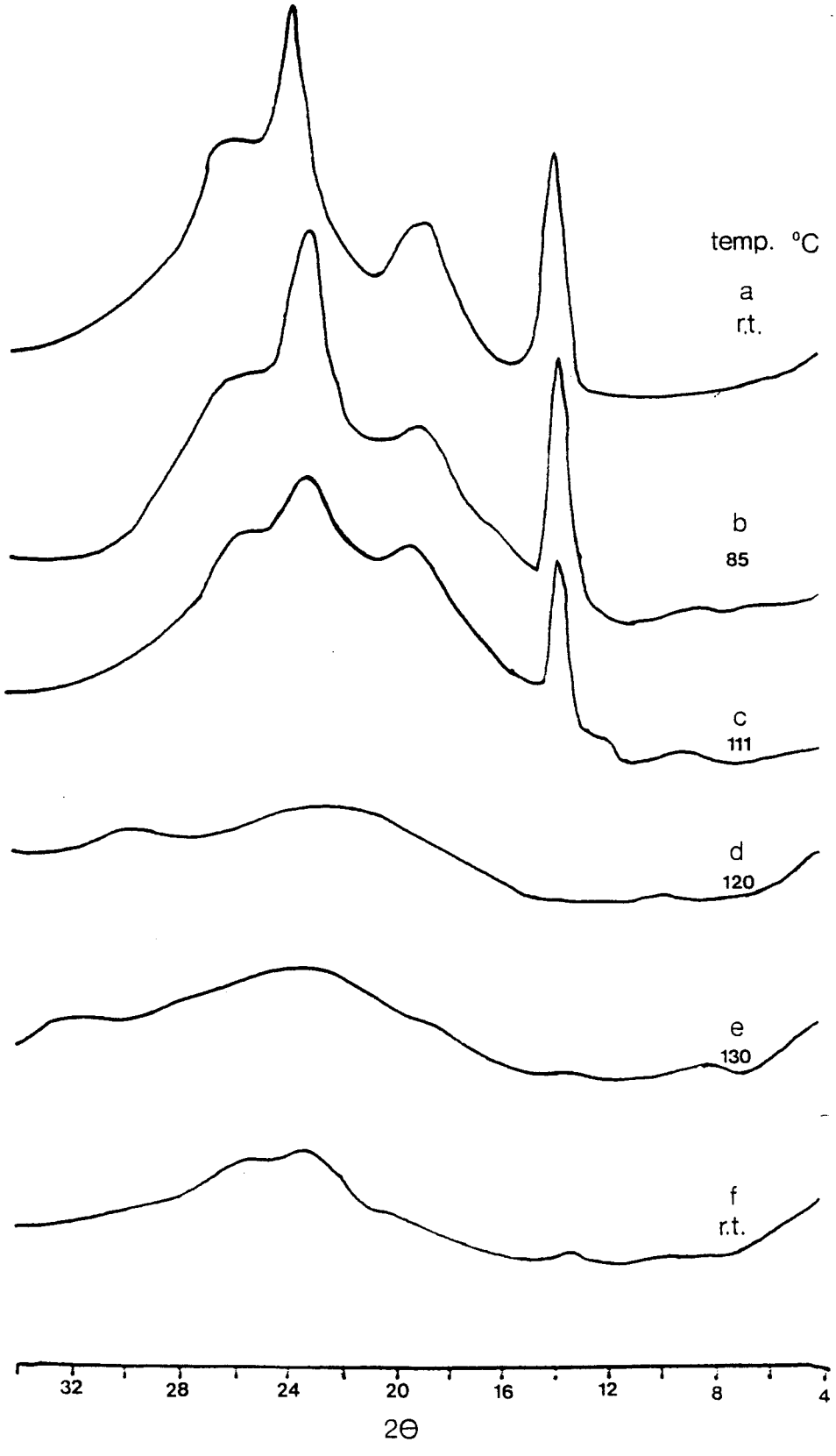

Figure 4.18 The WAXS patterns of MC7TOB as a function of temperature

4.6.4.4 Comparison of P7TOB and MC7TOB

By the simple addition of lateral substituents into the planar mesogenic triad of the P7TOB the smectic mesophase and any evidence of liquid crystallinity is lost.

As already mentioned the seven unit flexible spacer imparts a greater degree of flexibility into the chain than say, a 4 methylene unit flexible spacer. Compounding this with the disruption of the smectic layers with the chlorine atoms (which tend to force the chains apart, there-by reducing the intermolecular forces of attraction), completely destroys the liquid crystalline phase. In more favourable cases the disruption of the chain symmetry has the effect of lowering and narrowing phase transitions, in terms of temperature [20].

The loss of the clearing point and mesophase is not surprising as they have been observed in similar polymer systems [20,50]. As a result of the loss of the mesophase the properties of MC7TOB are entirely different to those of P7TOB. MC7TOB has properties typical of any semi-crystalline polymer, in the fact that a "single" melting endotherm is observed followed by the melting of the crystals.

The results suggest either the addition of smaller lateral substituents or a reduction of the flexible spacer chain length.

4.6.5 Analysis of P4TOB

4.6.5.1 DSC

The original polymer sample with no thermal treatment, shows a complex endotherm centred around 280°C, with a slight shoulder at around 210°C. This complex endotherm is due to the crystal-to-mesophase transition, as will be demonstrated in subsequent sections. The sample starts to degrade at 350°C and so it is impossible to detect the isotropization by the DSC method.

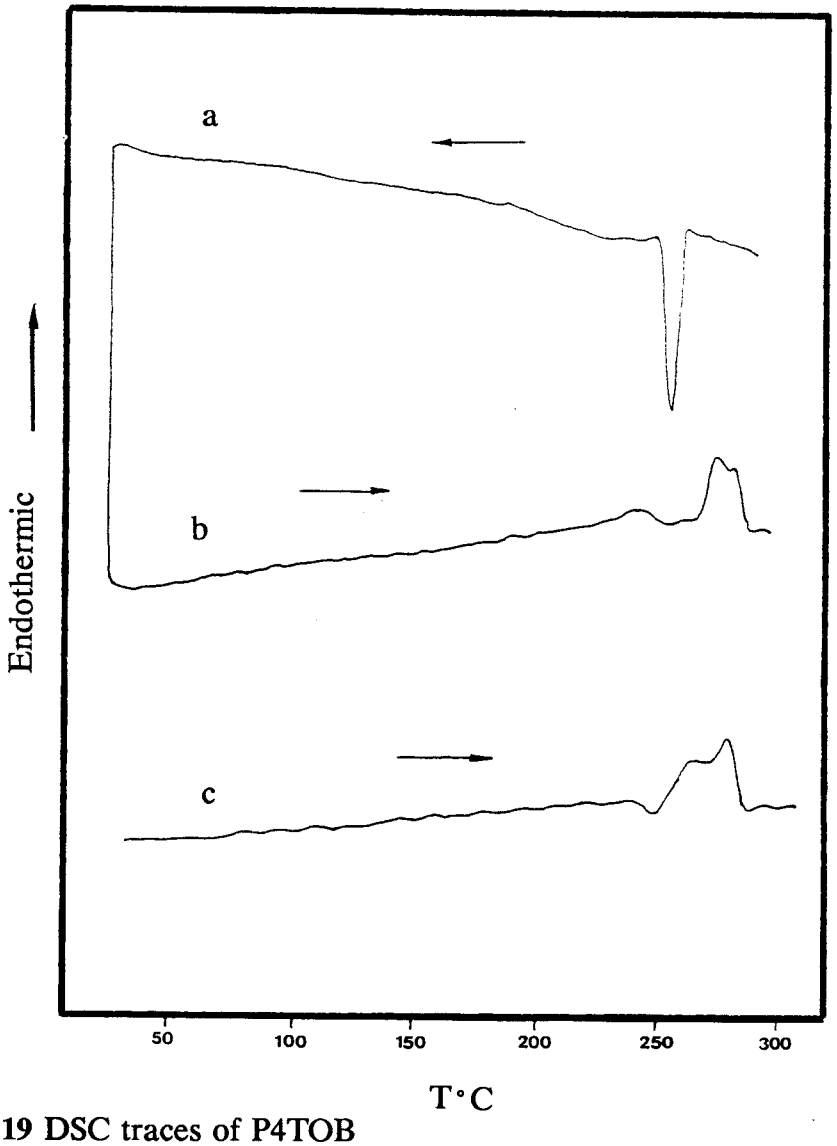

Figure 4.19 DSC traces of P4TOB

Figure 4.19 shows the DSC traces of P4TOB for several different thermal treatments. In 4.19a, as the polymer is slow-cooled from 300°C the thermogram showed a sharp exotherm at 257°C and a broad shoulder centred around 220°C. This shoulder is due to a concentration of low molecular weight species. Figure 4.19b shows the subsequent heating cycle. The first observable endotherm is due to the melting of these low molecular weight species observed in (a). The second endotherm centred around 275°C corresponds to the melting of the crystalline region. This sample was then quenched from 300°C into liquid nitrogen. Figure 4.19c shows the heating trace of the quenched sample, a T_g is detectable at 75°C, this is followed by a complex endotherm at 280°C.

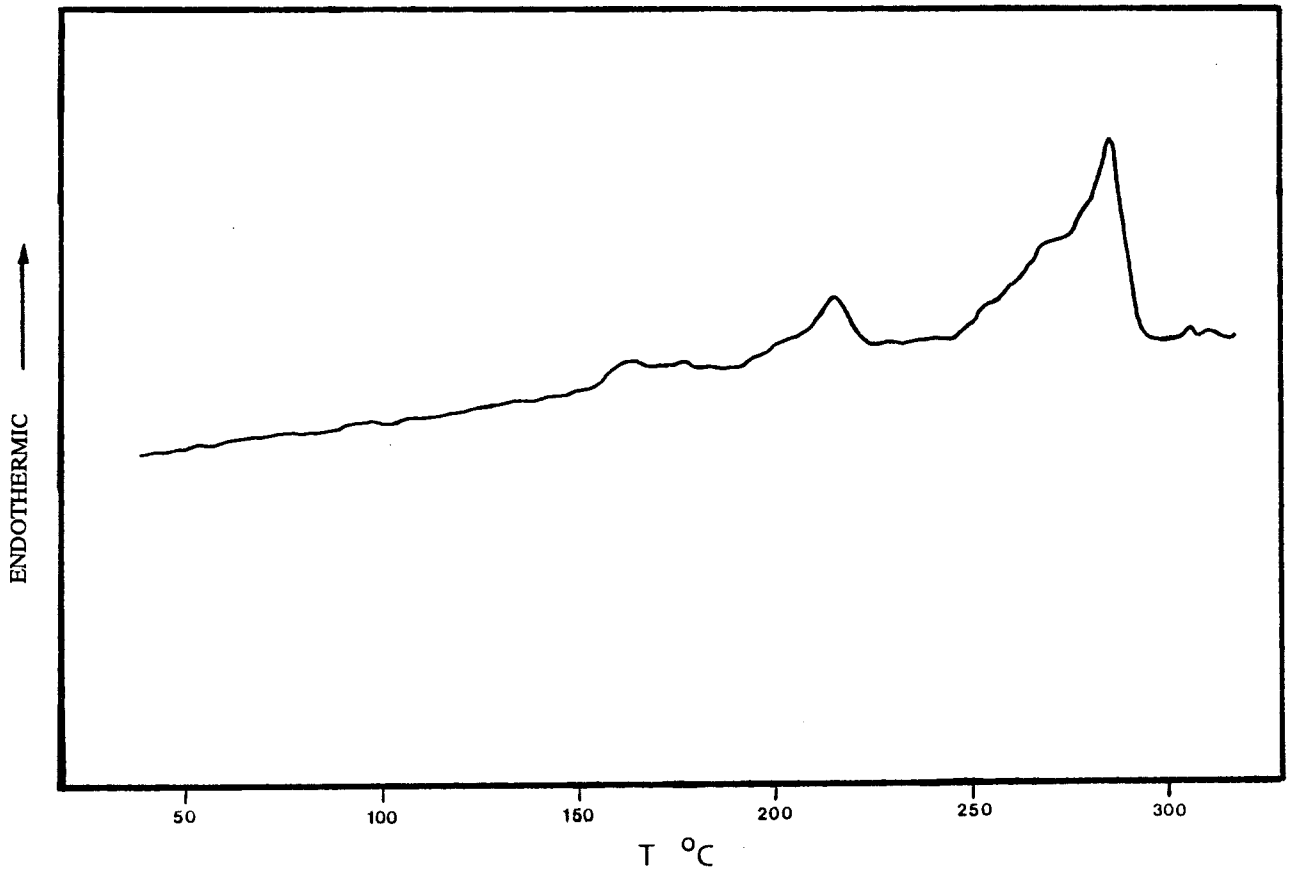

Figure 4.20 The DSC traces of recrystallized P4TOB

A sample of P4TOB was also prepared by solvent evaporation, in order to obtain a less heterogeneous sample. The DSC trace is shown in figure 4.20, two endotherms can be observed, one at 215°C, ΔH = 5.2J/g, and the second at 285°C, ΔH = 24.2J/g. The second endotherm, which will be demonstrated later

by WAXS is due to a solid-solid transformation.

4.6.5.2 Thermo-optical analysis

Figure 4.21 shows the TOA of a film prepared by cooling a sample from 310°C. On heating a light gain is observed at 280°C with the appearance of a marbled texture, typical of a nematic mesophase. On cooling the birefringence decreased at 240°C.

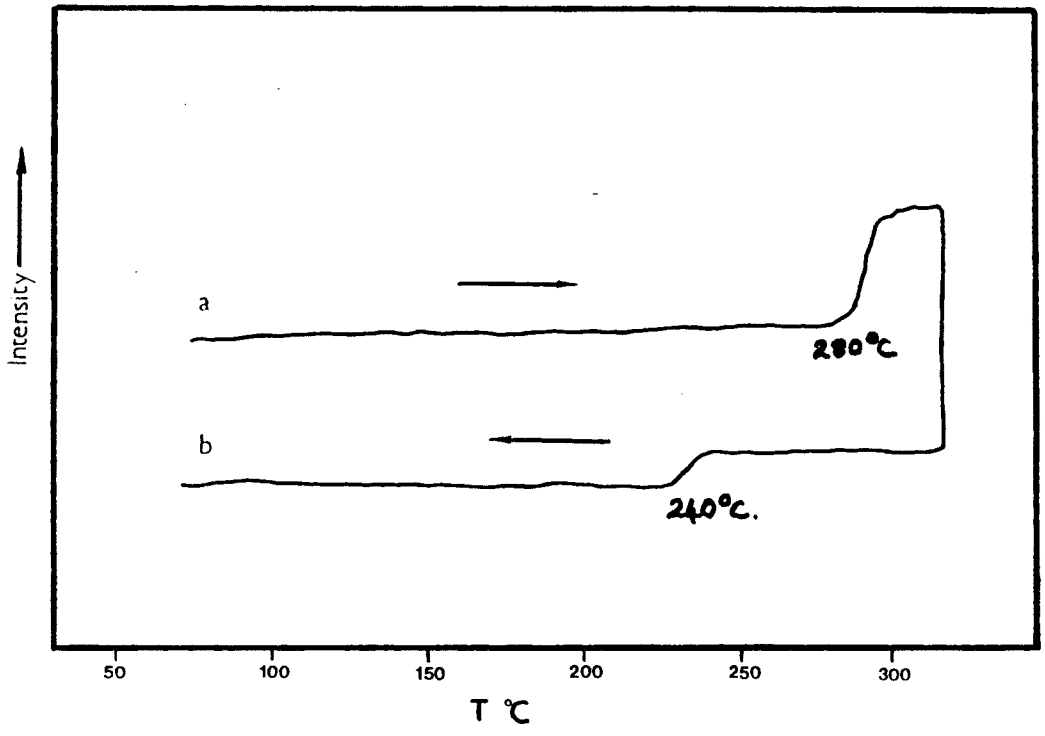

Figure 4.21 TOA analysis of P4TOB

4.6.5.3 X-ray analysis

Figure 4.22a shows the WAXS diffractogram of P4TOB at room temperature, as can be seen several reflections are observed; 2θ = 19.4, 23.4, 27.8 and 29.5°, associated with 3D order. When the sample was heated to the mesophase, (290°C) only a broad halo was observed (figure 4.22c). Combined with TOA

data this halo is due to the nematic mesophase. When the sample was cooled from 290°C to room temperature the diffractogram obtained is shown in figure 4.22b. This diffractogram shows a completely different pattern to that of 4.22(a). The peak observed at 23.4° has completely disappeared. These findings provide evidence of a second polymorph in P4TOB whose stability is temperature dependent. When an original sample was quenched into liquid nitrogen from 300°C the diffractogram obtained was identical to that shown in 4.22b, and when this sample was heated again to 300°C, the diffractogram remained unchanged upto 290°C, which corresponds to the nematic mesophase. These observations confirm that the endotherm at 220°C observed in the DSC does not correspond to a solid-solid transformation, but is in actual fact due to a difference in molecular weight.

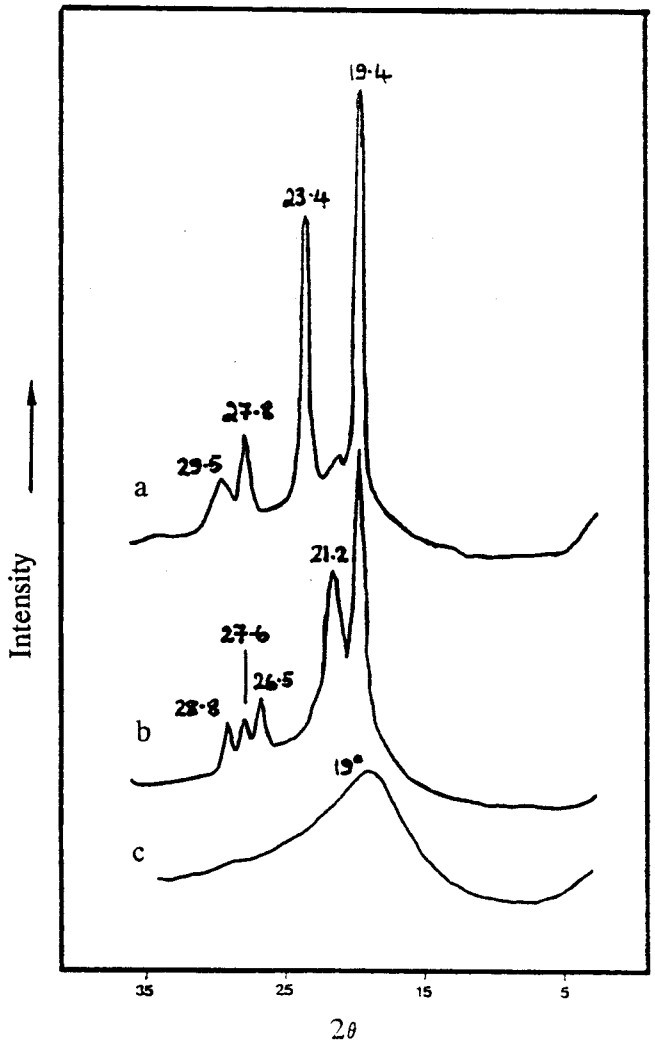

Figure 4.22 WAXS diffractograms of P4TOB

4.6.6 Analysis of MC4TOB

4.6.6.1 DSC

Figure 4.23 shows the thermal treatment of the polymer, figure 4.23a represents the original sample, a broad and shallow endotherm is observed at 223°C, ΔH = 6.0J/g. The absence of an observable crystallization band leads one to believe the original polymer already has a considerable degree of low molecular weight crystalline regions. Following the melting of the low molecular weight material it crystallizes at a slightly higher temperature, 238°C, ΔH = 3.9J/g indicating not all the crystals that melted recrystallized. The second observable melting endotherm occurs at 274.1°C with a substantial increase in the enthalpy, ΔH = 29.5J/g, indicating the predominance of this "second" crystalline phase. The sample was then annealed for 5 minutes at 320°C, figure 4.23b shows the cooling cycle of the annealed material. A recrystallization process takes place at 208°C, ΔH = 25J/g which corresponds to the phase II region. This sample was then heated, (figure 4.23c) the melting endotherm of phase I at 226°C has a ΔH = 4.4J/g. The lower enthalpic value indicates a lower degree of order in the system. This melting endotherm is followed by an immediate crystallization at 237°C and then the melting of phase II at 265.7°C, again with a lower enthalpic value when compared to figure 4.23a. The sample was then annealed at 320°C for a second time, before being quenched into liquid nitrogen. The final trace, figure 4.23d shows the result. For the first time in the MC4TOB sample we have evidence of a mesophase (between 274 & 319°C). As we shall see from TOA data the mesophase is nematic in order.

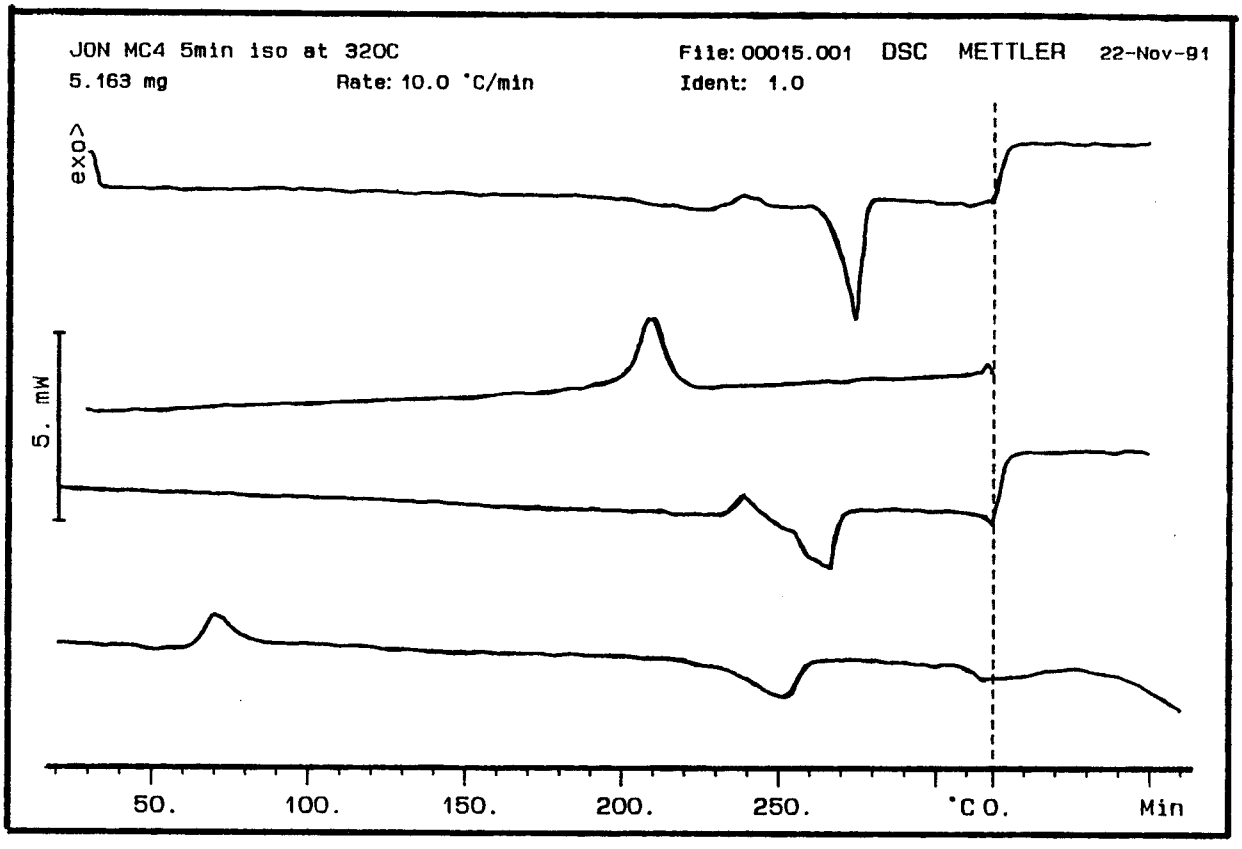

Figure 4.23 The DSC traces of MC4TOB

4.6.6.2 Thermo-optical analysis

The TOA of MC4TOB shows several interesting features. A sample prepared from 300°C shows an important light gain at 300°C corresponding to the mesophase, which exists upto 318°C, see figure 4.24 a,b & c. On cooling birefringence exists down to 190°C, see figure 4.25 a,b & c. The patterns are typical of a nematic mesophase.

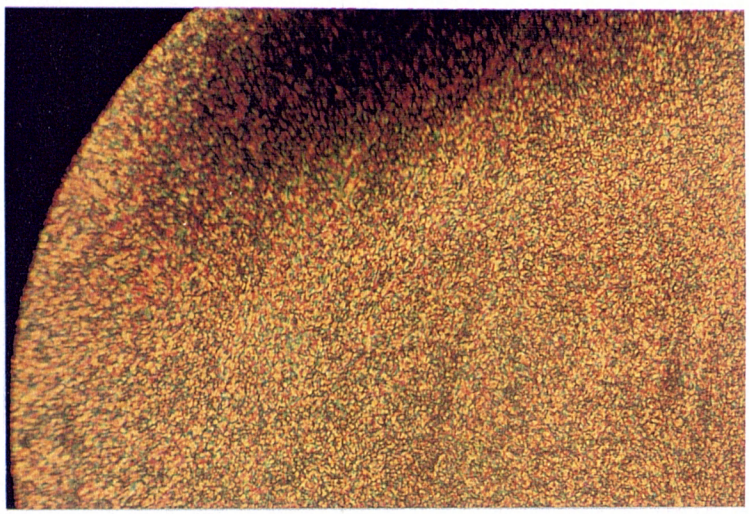

a - RT

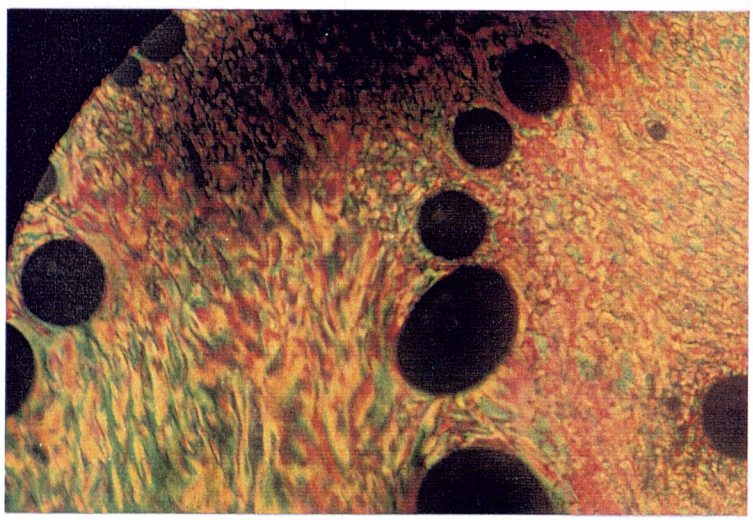

b - 300 °C

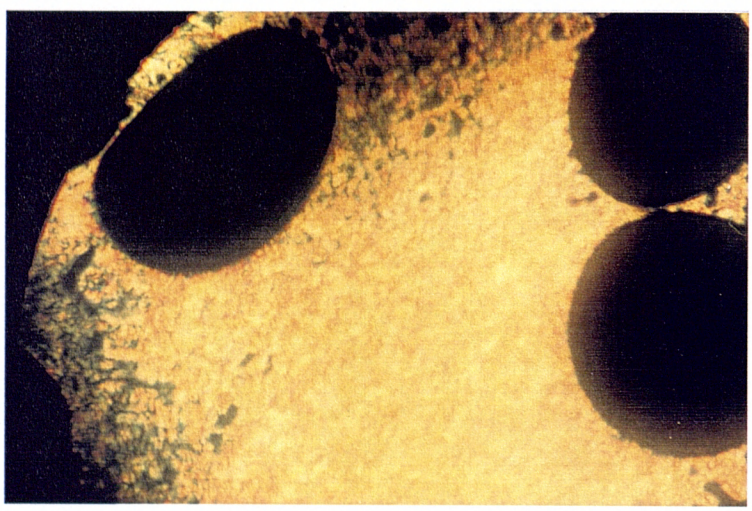

c - 315 °C

figure 4.24

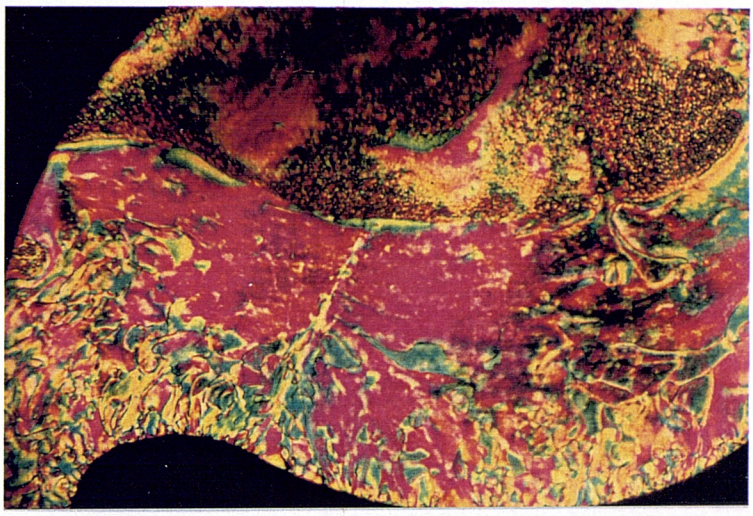

a - 280°C

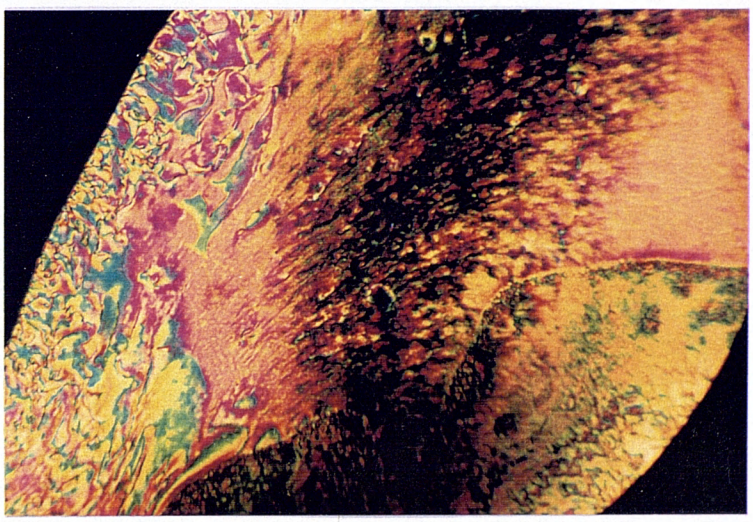

b - 250°C

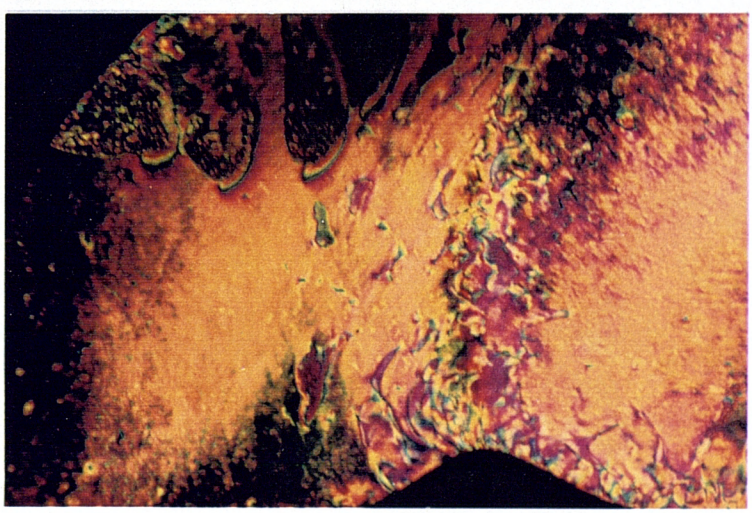

c - 190°C

figure 4.25

4.4.6.3 X-ray analysis

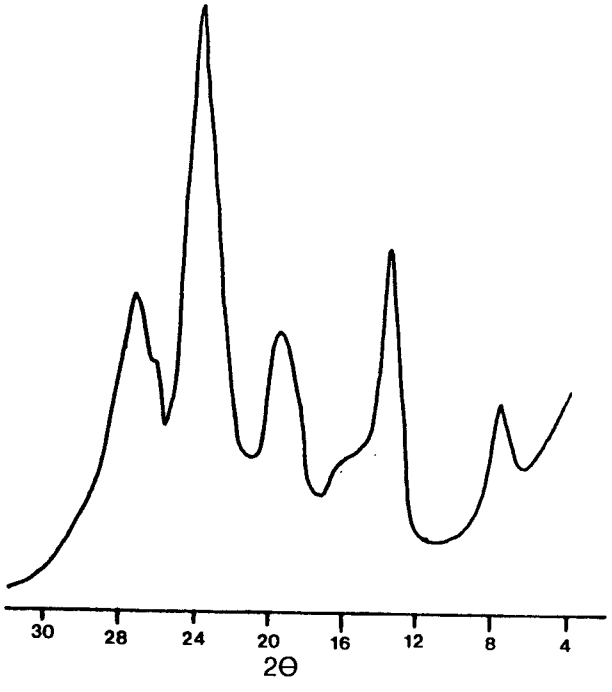

Figure 4.26 The WAXS pattern of MC4TOB

Figure 4.26 shows the WAXS pattern of the polymer, and shows strong reflections at 2θ = 8, 14, 19, 24, and 27°, associated with 3D order. When the sample is heated, (figure 4.27) the crystalline form apparent at room temperature exists up to 205°C, where-upon it changes dramatically to form a new pattern. This "new" crystalline phase shows strong reflections at 2θ = 11, 14, 16, 17, 18, and 24°, again associated with 3D order. The broad halo observed at 296°C is ascribed to the nematic mesophase. This crystal-crystal (k-k) phase transition confirms the results obtained in the DSC ie. the existence of two phases. This effect is quite common in polymers of this type [16,17].

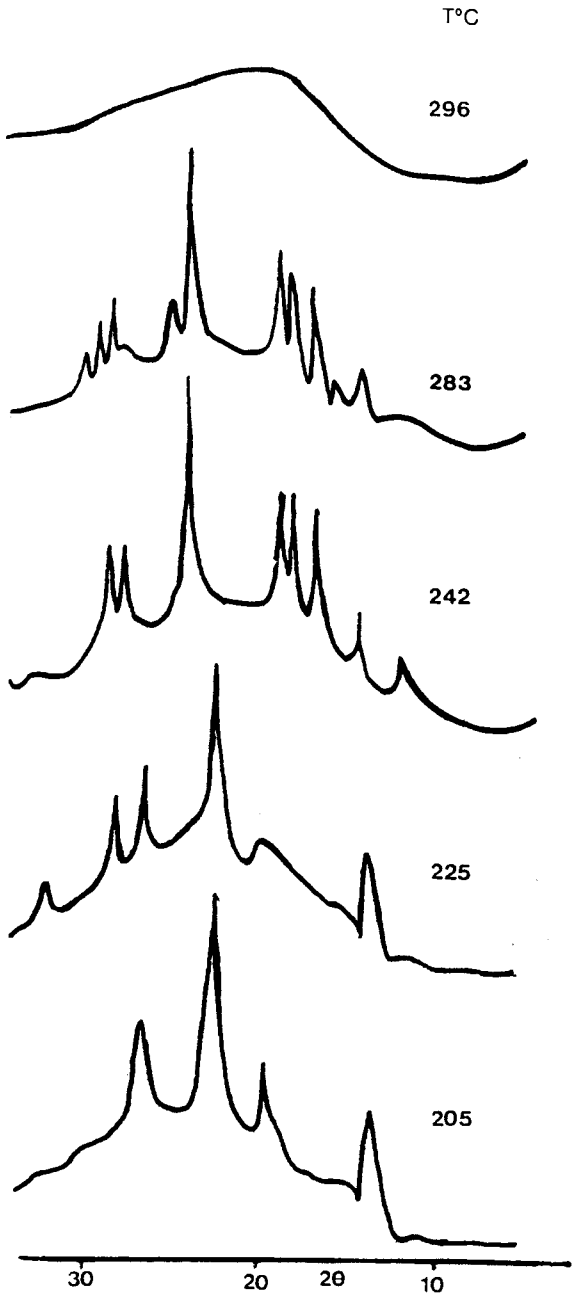

Figure 4.27 The WAXS patterns of MC4TOB as a function of temperature

4.4.3.4 Summary and analysis of P4TOB and MC4TOB

Both P4TOB and MC4TOB exhibit a liquid crystalline phase. However in the case of MC4TOB the liquid crystal phase is only observed once the polymer has been thermally treated, see section 4.6.6.1. The thermo-optical analysis data suggests the mesophases are both nematic in character. Compared with data from P4TOB the lateral substituents in MC4TOB have successfully reduced the T_m by 10 °C and T_i by 30 °C. As expected however, the stability of the mesophase has also been affected, it has decreased from a stability range of 65 to 45 °C.

4.7 Summary and Conclusions

POLYMER	T_g (°C)	T_l (°C)	ΔH_l (J/g)	T_i (°C)	crystallinity
P7TOB	44	175	9.7	295	0.23
MC7TOB*	49	110	not available	un-detected	0.18
P4TOB	75	280	46.9	350	0.46
MC4TOB	50	274	25.7	319	0.42
DC7TOB*	un-detected	96	not available	un-detected	un-detected

Figure 4.28 Summary of calorimetric data

* = no liquid crystalline phase observed so $T_l \equiv T_m$.

When longer flexible spacer units are introduced several effects are observed; the T_g of the polymer is lowered as the flexible spacer length increases, this is due to internal plasticization effects. From figure 4.28, increasing the spacer length from 4 to 7 in the unsubstituted polymers has the effect of decreasing the T_g from 75 °C to 44 °C.

As the spacer length is increased there is an enhancement of the ordering and the nematic phase gives way to a smectic phase. This effect is observed when moving from P4TOB to P7TOB. Ordering can be encouraged still further by increasing the spacer length. As already discussed in section 4.6.2 an increase in flexible spacer length, decreases the degradation and isotropization temperatures, crystallinity effects also apply to this argument.

Polymers with spacers having an even number of CH_2 units have higher melting points and high clearing temperatures T_i, than those with odd numbers, see figure 4.28. This suggests that the spacer length influences the ordering in the liquid crystal phase. The long range ordering will tend to try and maintain the

orientation of the mesogen parallel to the director axis and this may be easier for even numbered methylene unit spacers if they are in the all *trans* zig-zag conformation, as shown in figure 4.29. [51].

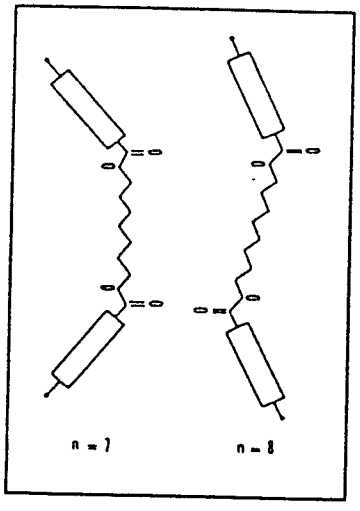

Figure 4.29 Arrangement of consecutive mesogenic units for odd- and even-numbered methylene units in the spacer

Introduction of lateral substituents in the mesogen also affects the polymer properties; the bulky side groups tend to force the chains apart, thereby reducing the intermolecular forces of attraction. The introduction of chlorine atoms into the mesogen lowers T_m and T_i in the case of P4TOB, whilst in MC4TOB and the dichloro- derivatives the inability to pack the molecules regularly is so enhanced, that no mesophase is observed. MC7TOB has properties similar to that of a semicrystalline polymer, whilst DC7TOB "seems" amorphous.

References

1. F. Reinitzer, *Montash. Chem.* **9**, 421 (1888)

2. G. Oster, *J. Gen. Physiol.*, **33**, 445 (1950)

3. G.L. Wilkes, *Mol. Cryst. Liq. Cryst.*, **18**, 165 (1972)

4. R.E. Wilfong, J. Zimmerman, *J. Appl. Polym. Sci.*, **17**, 2039 (1973)

5. P.W. Morgan, *Macromol.* **10**, 1381 (1977)

6. A. Ciferri, W.R. Krigbaum, R.D. Meyer (eds), "Polymer Liquid Crystals", Academic Press, New York (1982)

7. A. Blumstein (eds), "Polymeric Liquid Crystals", Plenum Press, New York (1985)

8. A. Blumstein, *Macromol.* **10**, 872 (1977)

9. W.J. Jackson Jr., *Macromol.* **16**, 1027 (1983)

10. W.J. Jackson Jr., H.F. Kahfus, *J. Polym. Sci. Chem. Ed..*, **14**, 2043 (1976)

11. B.P. Griffin, C.K. Michael, *Br. Polym. J.*, **12**, 147 (1980)

12. R.W. Lenz, *J. Polym. Sci. Polym. Symp.* **72**, pp1-8 (1985)

13. J.I. Lin, S. Anyoun, C. Ober, R.W. Lenz, *Br. Polym. J.*, **132**, (1980)

14. J. Economy, *J. Macromol. Sci. Chem.*, **121**, 1705 (1984)

15. R.W. Lenz, *J.Polym. Sci. Symp.*, **72**, 1 (1985)

16. G. Galli, E. Benedetti, E. Chiellini, C. Ober, R.W. Lenz, *Polym. Bull.*, **5**, 497 (1981)

17. E. Benedetti, F. Galleshi, E. Chiellini, G. Galli, R.W. Lenz, *J. Polym. Sci. Part B:. Polym. Phys.*, **27**, 25 (1989)

18. Z. Jedliński, J. Franek, A. Kukzycki, A. Sirigu, C. Carfanga, *Macromol.*, **22**, 1600 (1989)

19. C. Ober, J.-I. Jin, R.W. Lenz, *Polym. J.*, **14**, 9 (1982)

20. G.Galli, E. Chiellini, C. Ober, R.W. Lenz, *Macromol. Chem.*, **183**, 2693 (1982)

21. B.Z. Volchek, N.S. Kholmuradov, A.V. Purking, A.Yu. Bilibin, S.S. Skorokhodov, *Polym. Sci. USSR*, **27**, 90 (1985)

22. ibid, *Polym. Sci. USSR.*, **28**, 1674 (1986)

23. A.Yu. Bilibin, A.V. Ten'Kovtsev, O.N. Piraner, S.S. Skorokhodov, *Polym. Sci.*

USSR, **26**, 2882 (1984)

24. A.Yu. Bilibin, O.N. Piraner, *Macromol. Chem.,* **192**, 201 (1991)

25. F.C. Frank, *Discuss. Faraday Soc.,* **25**, 19 (1958)

26. G.W. Gray, "Molecular structure and properties of liquid crystals", Academic Press, New York (1962)

27. N.H. Hartshorne, A. Stuart, "Crystals and the polarizing microscope", 4th edn., Arnold, London (1970)

28. A.F. Hallimond, "The polarizing microscope", 3rd edn., Vickers, York (1970)

29. M.J. Richardson, "Quantitative differential scanning calorimetry", chapter 7 in J.V. Dawkins, ed., "Developements in polymer characterisation - 1", Applied Science, London (1978)

30. E.A. Turi, ed., "Thermal characteristics of polymeric materials", Academic Press, New York (1981)

31. D.S. Brown, R.E. Wetton, Chapter 6 in J.V. Dawkins, ed., "Developements in polymer characterisation - 1", Applied Science, London (1978)

32. V.P. Shibaev, N.A. Platé, A.L. Smolyansky, A.Ya. Voloskov, *Macromol. Chem.* **181**, 1393 (1980)

33. C. Noel, F. Laupetre, C. Fredrich, B. Fayolle, L. Bosio, *Polymer,* **25**, 808 (1984)

34. B.M. Landreth, S.I. Stupp, *Appl. Spectrosc.* **40**, 1032 (1986)

35. P.P. Wu, S.L. Hsu, O. Thomas, A. Blumstein, *J. Polym. Sci. Part B: Polym. Phys.,* **24**, 827 (1986)

36. G. Ellis, J. Lorente, C. Marco, M.A. Gómez, J.G. Fatou, P.J. Hendra, *Spectrochimica acta* **47A**, No. 9/10 1353 (1991)

37. B.W. Jo, J-I. Jin, R.W. Lenz, *Eur. Polym. J.,* **18**, 233 (1982)

38. J.K. Agbenyega, J. del. Pino, J.G. Fatou, C. Marco, P.J. Hendra, *In preparation*

39. G. Ellis, C. Marco, J. Lorente, J. del Pino, M.A. Gomez, J.G. Fatou, J.K. Agbenyega, P.J. Hendra. "A vibrational study of main chain thermotropic polyesters". Paper presented at conference, Caracas, Venezuela, September 1992

40. J.K. Agbenyega and P.J. Hendra, "The Raman spectra of polymers", to be published by John Wiley and Sons Ltd. 1993

41. N.B. Colthup, L.H. Daly, S.E. Wiberley (eds.), "Introduction to infra-red and Raman spectroscopy", Academic Press, New York 1975

42. D.I. Bower, W.F. Maddams, "The vibrational spectroscopy of polymers", Cambridge, 1989

43. S. Wunder, M. Bell, G. Zerbi, *J. Chem Phys.* **85**, 3287 (1987)

44. G. Zerbi, P. Roncore, C. Longhi, S. Wunder, *J. Chem. Phys.* **89**, 166 (1987)

45. A. Tonelli, *J. Polym. Sci. (B)* **11**, 441 (1973)

46. J.P. Hummell, P.J. Flory, *Macromol,* **13**, 479 (1980)

47. A. Ghanem, P. Meurisse, F. Lampretre, C. Noel, *Mol. Cryst. Liq. Cryst.* **122**, 339 (1985)

48. N. Jones in "Techniques of organic chemistry", (ed. A. Weissberger) **9**, Wiley-Interscience, New York, 1956

49. V. Frosini, S. De Petris, E. Chiellini, G. Galli and L.W. Lenz, *Mol. Cryst. Liq. Cryst.* **98**, 223 (1983)

50. R.W. Lenz, K. Feichtinger, *Polym. Props. Am. Chem. Soc. Div. Polym. Chem.,* **20**, (1) 114 (1979)

51. W.R. Krigbaum, J. Watanabe, T. Ishikawa, *Macromol.* **16**, 1271 (1983)

CHAPTER 5: Crystallizable blends

5.1 Introduction

The aim of this research, sponsored in part by ICI Paints Research Centre, Slough was to develop a crystallizable polymer blend system for surface coatings, from readily available starting materials. Why crystallizable? To achieve a similar resistance to chemical and physical attack, a non-crystallizable polymer would have to have a molecular weight several orders of magnitude greater than that of an equivalent crystallizable polymer blend system. Also the crystallizable polymers are much easier to process [1]. As with epoxy resin films the polyester/epoxy blend systems, (depending on the composition and thermal treatment) form hard, clear polymer films.

By mixing the finely powdered polyester (in the first instance polybutylene terephthalate, (PBT)) into a liquid epoxide resin (epikote 880™) at elevated temperatures in the presence of a crosslinker, (soluble in the epoxide) 3,3-diaminodiphenyl sulphone, a homogeneous solution is assured. Fully crosslinked films are then formed by exposing the semi-crosslinked film to elevated temperatures for a specified time.

The structures of the starting materials are shown in figure 5.1.

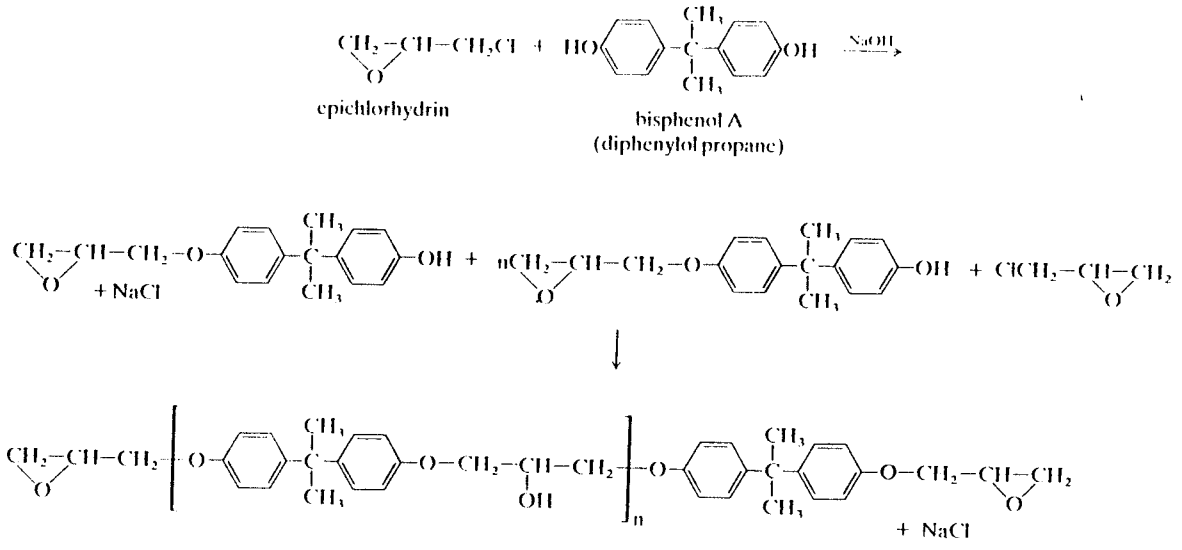

Epikote 880

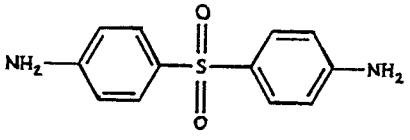

DIAMINO DIPHENYL SULPHONE

Figure 5.1 Structures of the starting materials

The generally accepted mechanism for amine curing of epoxy resins described by CHAIO [2] involves three major reactions, as shown in figure 5.2.

(i) primary amine - epoxy addition

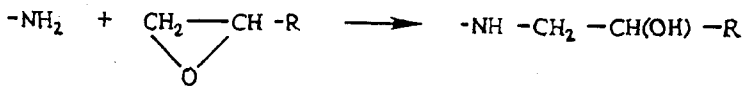

(ii) secondary amine - epoxy addition

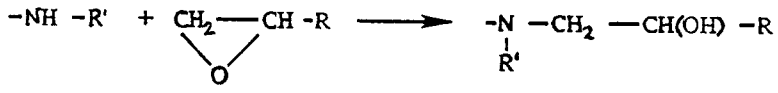

(iii) hydroxyl - epoxy (etherification)

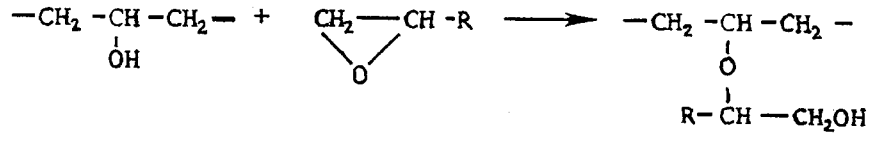

Figure 5.2 The amine cure of an epoxy resin

In the initial stages of the cure the dominant reaction is the primary amine-epoxy addition [3]. After approximately 60% of the primary amine groups have reacted, the concentration of secondary and hydroxyl groups is then large enough, for the corresponding reactions to take place. these reactions are diffusion controlled, due to the, by then high and increasing viscosity of the resin as it cures [4].

Raman spectroscopy has rarely been attempted on epoxy based resins, because they exhibit strong fluorescence when exposed to visible radiation. The limited number of papers that do exist, in this field all mention the necessity to "burn-out" the fluorescence. The first cited material detailing a conventional Raman study of an epoxy was by CANALS et al [5]. Following this publication a flurry

of papers detailing vibrational analyses of these 3 membered rings appeared [6-10]. LU and KOENIG [11] studied the commercial resin Epon 825, and observed the changes in the Raman spectrum after curing with ethylene diamine. They assigned several bands that are sensitive to the curing mechanism. JANARTHANAN and THYAGARAJAN [12] investigated the effect of temperature on a commercial epoxy resin from Ciba-Geigy, and were able to assign temperature sensitive phenyl-hydrogen vibrational modes.

The near infra-red (NIR) region offers an alternative analytical approach. The absorption bands seen in the NIR region are mostly first or second overtones of the frequencies observed in the conventional region. Essentially only overtone bands of hydrogen containing groups (C-H, O-H, N-H) exhibit appreciable absorption in this region, therefore, the NIR spectrum is often less complex than the conventional one [13]. The NIR is particularly suitable for the cure analysis of epoxy resins [14] as the absorptivities for bands in this region are very low. This therefore allows optimum path lengths in the range 1-10mm, thus facilitating easy sampling. Since the spectra in the NIR are less complex than their mid-IR counterparts, quantitative analysis becomes more accurate and reliable. Further, interference from water vapour is reduced, so purging is not required, and glass may be used as the sample container.

DANNENBERG [14] was the first to use NIR to follow the amine curing of an epoxy resin. He performed a study of the cure of Epon 828 a commercial diglycidyl ether of bisphenol-A resin, with ethylene diamine as the curing agent.

Recently AGBENYEGA et al [15] reported on the NIR FT-Raman analysis of an epoxy resin. The curing of Araldite, at ambient temperature, was followed in order to explore the potential of the NIR FT-Raman approach. Spectra of the cure show variations in the relative intensities of the band at 1608cm^{-1}, specific to the aromatic ring moiety. Figure 5.3 shows a plot of this band versus time of cure, it is evident that the cure process is virtually complete after 10 hours.

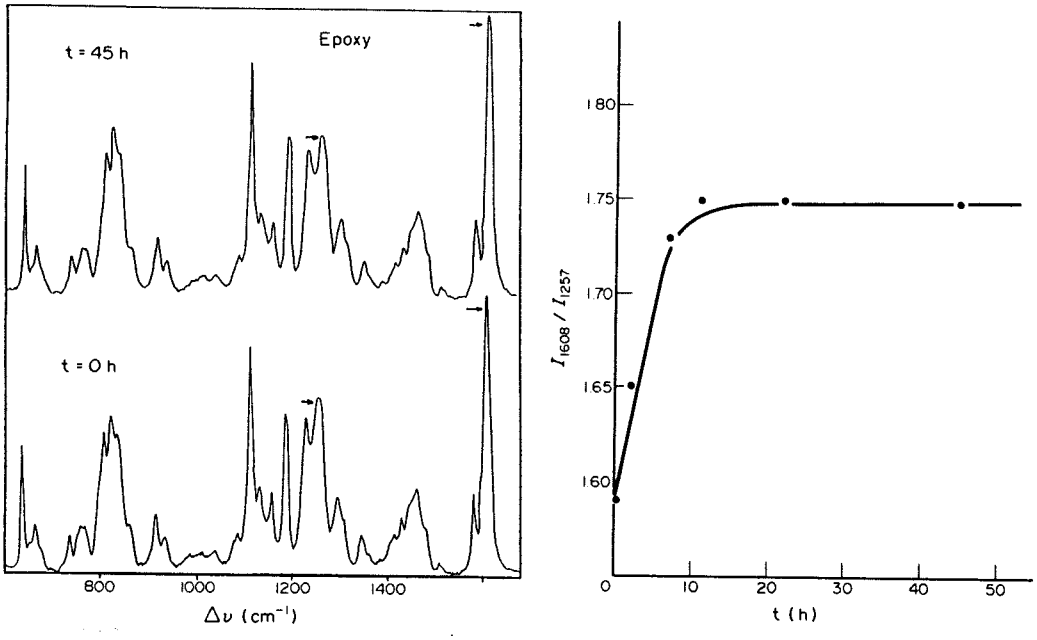

Figure 5.3 The curing process of an epoxy resin

WALTON and WILLIAMS [16] observed the kinetic FT-Raman spectra of a commercially based Ciba-Geigy resin with diamino-diphenyl sulphone as the crosslinker. After curing they found a number of bands decreased, which was consistent with the accepted mechanism of cure. However they were unable to collect spectra of samples cured for extended periods of time due to the dark brown colouration and the subsequent thermal and fluorescence emissions.

5.1.1 The structure of semi-crystalline polymers

The semi-crystalline polymer is classed as a two-phase system, consisting of an ordered crystalline phase co-existing with a completely disordered amorphous phase.

Polymer crystals can be formed in one of two ways;
1. Crystallization from dilute solution, or by
2. Crystallization from the melt.
We shall be concerned with the latter, and the crystallization from the melt state. The classical model of the semi-crystalline polymer will be briefly reviewed and the inadequacies of the model discussed.

The structure of a polymer crystallized from the melt is less well ordered than its solution grown counterpart [17]. X-ray diffractograms show an appreciable degree of diffuse scattering associated with a substantial amorphous content. The crystal habit is lamellar in nature and usually crystallizes into organized spherulites [18-20]. Crystallization is initiated from a central "nucleus" which may arise from the melt itself (homogeneous nucleation) or from a foreign particle (heterogeneous nucleation). The resulting spherulite develops from lamellae which grow radially from the nucleation point, branching and twisting as they do so [21] (figure 5.4). The controversy about the nature of the fold surface in melt crystallized polymers has led to several structural models. The average length of the polymer molecule is far in excess of the lamellar thickness and so models describing the chain folding back into the lamella or in contrast traversing the inter-lamellar regions have been put forward. The adjacent re-entry model proposed by Hoffman and Lauritzen [22,23] is well known and consists of regular fold periods. Later this was somewhat modified by other workers [24] who suggested that the folds were irregular, and GEIL [25] who stipulated that the crystallization conditions dictated the size of the re-entry network. Problems arise

when the re-entry model is modified to account for changes in physical properties. For example, to explain mechanical properties tie molecules bridging the lamellae are usually assumed! [26-28] To an extreme in Flory's model [29] where-by each chain randomly passes from one lamella to another. More recently a chain folded model has been proposed containing partially adjacent and partially random re-entry and which seems plausible [30].

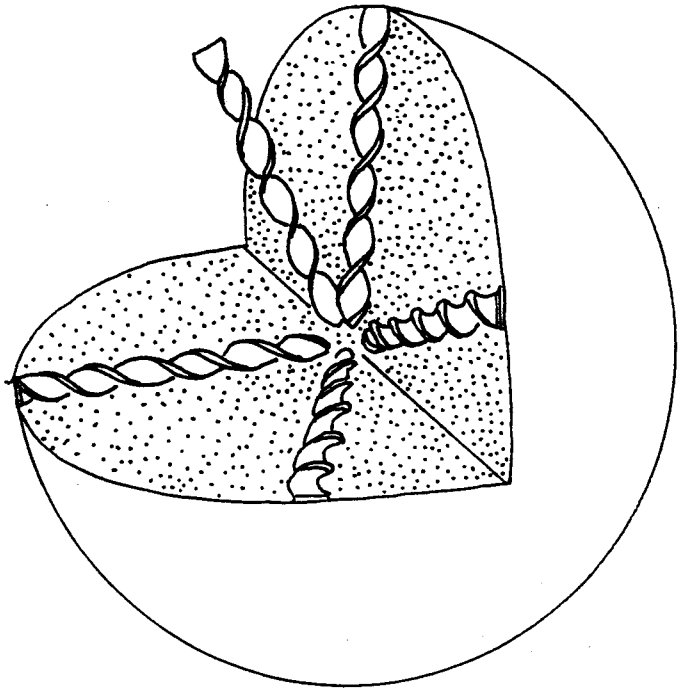

Figure 5.4 A schematic representation of the structure of a polyethylene spherulite

There is general agreement to support the theory of a two phase system; a well ordered crystalline region containing chains normal to the lamellar surfaces sandwiched between disordered amorphous material. It is assumed of course that the fold containing zone can be simply described as disordered and that the transition from crystalline to amorphous layers is sharp. In reality this is

nonsense, for it is well known that defects and imperfections are commonplace in the crystalline zones, thus reducing the order. MANDELKERN [31] is therefore suggesting a 3-phase model, consisting of crystalline, interfacial and amorphous zones. If the *trans* sequences persist as they emerge from the lamellae there is simply no room for them to be in any other phase than a crystal. If one persists with this view, the only satisfactory conclusion is that as one progresses along a chain from the centre of the lamella core, its order gradually decreases as one approaches the lamellar "surface". This being the case, there is an infinite number of describable phases. This cannot be true because by definition a "phase" is that part of a system which is chemically and physically uniform throughout [32]. Consequently it is much better to envisage a polymer where the properties are equated to those of partially ordered crystalline material gradually progressing towards less ordered material with properties characteristic of a more disordered amorphous phase.

5.2 Aims

The study of miscibility in polymer blends where one component is crystallizable and the other highly crosslinked has received relatively little attention. NASI and ROBESON examined the miscibility of a range of anhydride cured epoxy resins with poly(ε-caprolactone) (PCL) of various molecular weights and with different end-groups [33]. They concluded that above a critical molecular weight and composition the blends have a two-phase structure and that the PCL end-groups reacted with the anhydride curing agent to produce a block co-polymer.

From the thermodynamic point of view, an increase in molecular weight for either of the components of a miscible blend would decrease the cloud-point temperature. Therefore, the occurrence of partial miscibility in such polymer blends containing one component with an infinite molecular weight (ie. highly crosslinked) is surprising and requires further comment.

As shall be seen later differential scanning calorimetry and electron microscopic studies provide evidence for the phase separation in some of the blends as the crosslinking reaction progresses.

The aim of this project is to clarify using nir FT-Raman spectroscopy the complex interrelationship between morphology, composition and thermal history of the polyester (polybutylene terephthalate)/epoxy resin (epikote 880) blend.

5.3 Experimental

5.3.1 Chemicals

Polybutylene terephthalate (M_n=20 000) was supplied by ICI Paints Research Centre, Slough.

Epikote 880 is a liquid bisphenol-A Epichlorohydrin epoxide resin supplied by Shell Chemicals. Epikote 880 is the standard liquid resin used in many applications, these include casting, impregnating, cured at room or elevated temperatures, for the electrical and electronic industries, adhesives, grounding compounds and other compositions for the building and civil engineering industries.

5.3.2 Instrumentation

5.3.2.1 Raman spectroscopy

FT-Raman spectra were recorded on a Perkin-Elmer model 1760 FTIR interferometer. The laser excitation was provided by a Nd^{3+}:YAG laser operating in the TEM_{00} mode at 1.064μm. Laser powers typically of the order of 400mW were used. Samples were studied at $4cm^{-1}$ resolution and accumulated over 200 scans. Processing of the data was executed on the Perkin-Elmer IR data manager and Mattson software.

5.3.2.1 Differential scanning calorimetry

The instrument used was a Perkin-Elmer DSC-2 device (see chapter 2). The accuracy in temperature output is estimated to be ± 1K. Pure indium was used for temperature calibration (T_m = 429.76K). The melting point of the polymer was deduced by super-imposing the leading edge of an indium fusion peak onto the observed peak recorded under the same conditions.

5.4 Results and Discussion

Preliminary measurements involved feasibility studies of the use of FT-Raman spectroscopy in determining the properties of crystallizable polyesters, such as polybutylene terephthalate, polyethylene terephthalate, and polyethylene terephthalate copolymers, with different thermal histories and confirming the results with differential scanning calorimetry.

5.4.1 Raman study of Polybutylene terephthalate

Figure 5.5 shows the FT-Raman spectrum of polybutylene terephthalate.

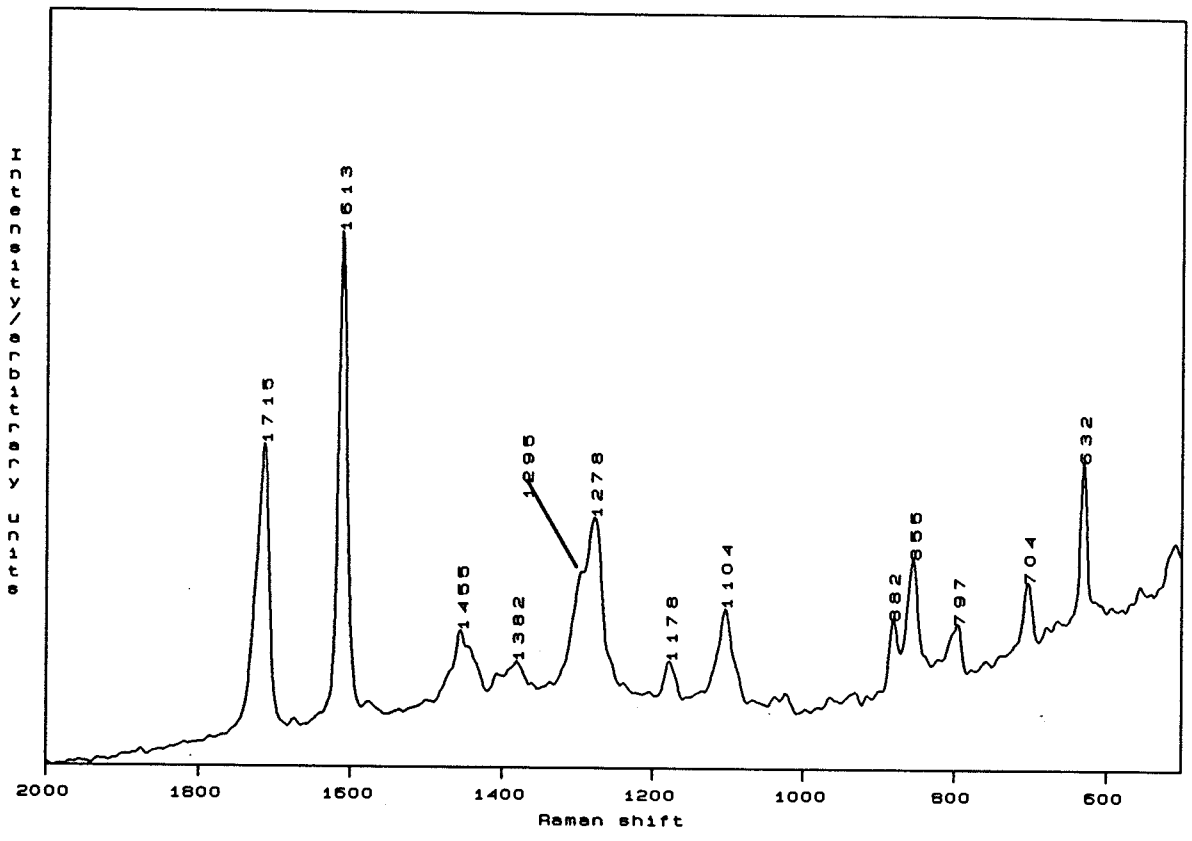

Figure 5.5 The FT-Raman spectrum of polybutylene terephthalate, quenched from the reaction vessel.

The sample was prepared by quenching polybutylene terephthalate from above its melting point (T_m = 224 °C) into liquid nitrogen. The spectrum is essentially that of the amorphous polymer, as determined by WARD and WILDING [34]. The corresponding x-ray diffractogram along with a sample slow cooled is shown in figure 5.6.

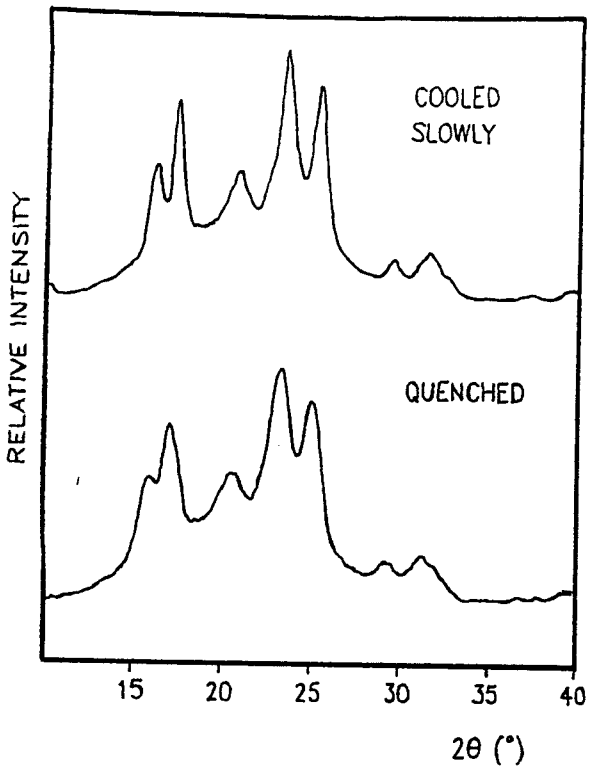

Figure 5.6 X-ray diffractograms of polybutylene terephthalate subjected to two different thermal treatments.

As expected, the slow cooling of the sample resulted in sharper diffraction peaks, indicating the formation of larger and more regular crystallites. Three intense peaks characterize the diffraction pattern, lying at 2θ angles of 17.38°, 23.41°, and 25.33°. The position of the diffraction peaks is the same in both instances, and is typical of the α relaxed form [35-37].

It is assumed that [38] the vibrational assignments can be made on the basis of an isolated chain molecule. Further, the molecule can be separated into vibrations originating probably from the *para*-disubstituted benzene ring and from the aliphatic residue. This model excludes the role of the carbonyl groups attached to the benzene ring. However reports have shown [35] the terephthalate residue to be stabilised by conjugation. This means that the internal vibrations of the benzene ring will be affected by changes in the terephthalate residue as a whole.

The strongest feature in the Raman spectrum of polybutylene terephthalate at 1613cm^{-1} is assigned to a ring C-C stretching vibration. The second prominent feature is the spectrum (which is characteristic of the family of glycol terephthalate polymers (n-GT) of which polyethylene terephthalate (2GT) is a member) is the carbonyl stretching vibration at around 1718cm^{-1}. A table of the band assignments can be found in figure 5.7.

Raman (cm^{-1})		**Band assignments**
amorphous	**annealed**	
1719 m	1718 m	C=O str.
1615 s	1616 s	ring C-C str.
1456 w	1460 w	glycol C-H def.
1411 ws	1412 ws	ring C-C str.
1285 m,sh	1282 m,sh	ring carbonyl str., O-C- str., ring C-H in plane bend.
1176 w	1182 w	ring CH in plane bend
1112/1104 m	1108 m	ring CH in plane bend or C-O C-O str.
1048 w	-	C-C str.
884 w	888 w	CH_2 rock
860 m	859 m	C-C breathing
798 w	800 w	CH out of plane
708 w	708 w	ring C-C-C out of plane
634 m	635 m	ring C-C-C in plane bend

s=strong, vs=very strong, m=medium, m,sh=medium shoulder, w=weak

Figure 5.7 Raman band assignments of polybutylene terephthalate

The band at 1104cm^{-1} has been related to the planarity of the terephthalate residue. This frequency appears at 1097cm^{-1} in the planar form of polyethylene terephthalate [34] and 1120cm^{-1} in non-planar amorphous polyethylene terephthalate and polypropylene terephthalate. It is therefore concluded that the intermediate value obtained in polybutylene terephthalate is evidence of a non-planar terephthaloyl residue.

5.4.2 A Raman study of thermally treated polybutylene terephthalate

Figure 5.8 shows the spectra of heat treated samples of polybutylene terephthalate, band assignments can be made from the fact that polybutylene terephthalate can exhibit 2 crystal structures; the application of uniaxial stress on polybutylene terephthalate has been found to induce a reversible crystal:crystal phase transition [39]. Studies have shown [36] that the glycol residue in the unstrained state is close to *gauche-trans-gauche* and that this changes to an all *trans* sequence on straining. The proposed structure also indicates substantial non-planarity in the terephthaloyl segment, due to rotation of the carbonyl groups out of the plane of the benzene ring. Annealed samples of polybutylene terephthalate, figure 5.8 a,b,c,d and e and oriented samples of polybutylene terephthalate at zero strain show bands at 808 and 884cm^{-1} which are completely absent in the spectrum of the strained sample. It is therefore clear that these bands are associated with the *gauche-trans-gauche* glycol residue in the crystalline polymer. Marked changes are also observed in the region around 1400cm^{-1}. Bands at 1457 and 1445cm^{-1} both vary in intensity as the degree of crystallinity changes.

These bands have been assigned to CH_2 bending modes of the aliphatic segment [34].

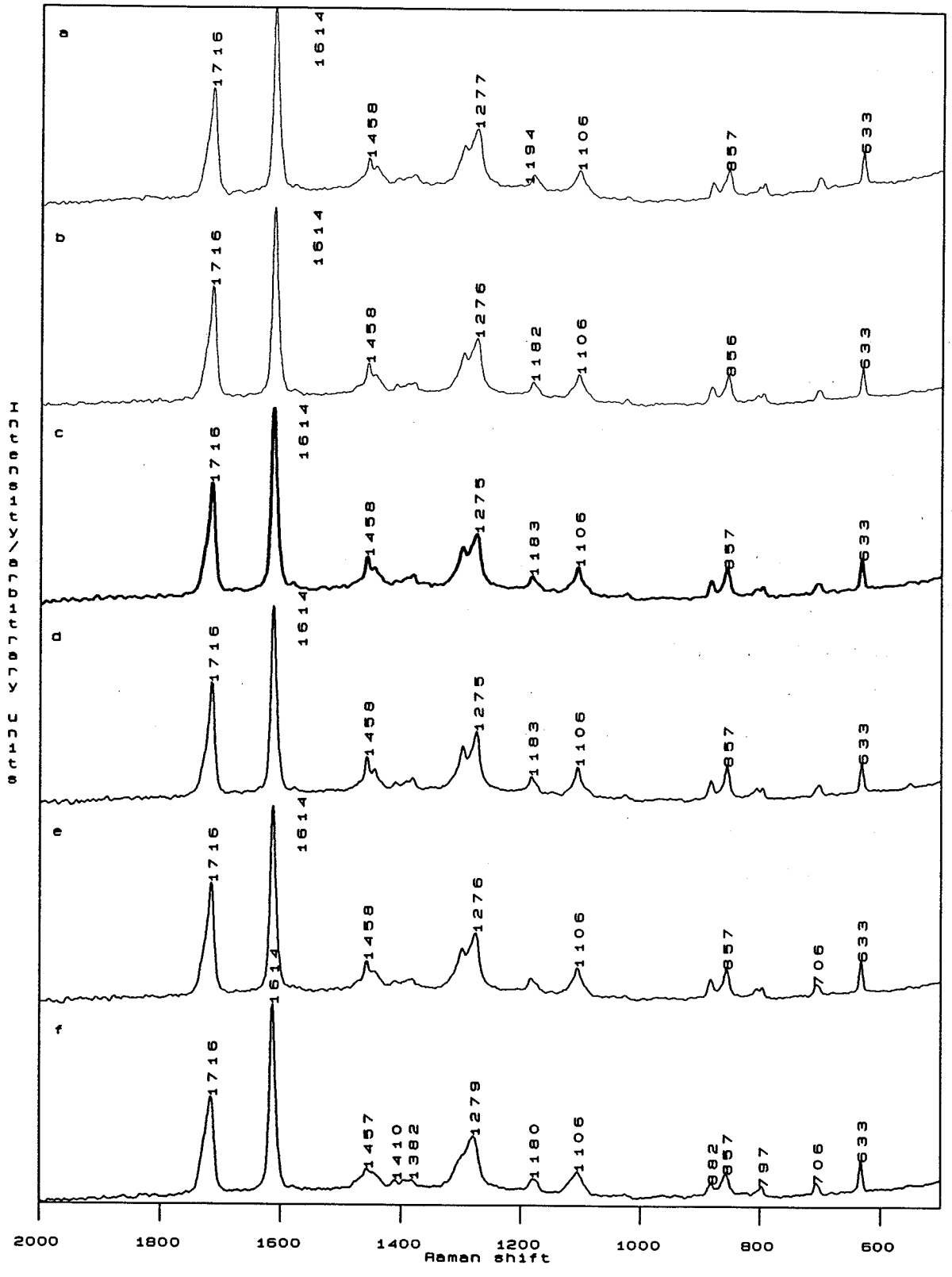

Figure 5.8 FT-Raman spectra of PBT annealed at various temperatures for 10 minutes

Concentrating our attention on the band at 1715cm^{-1} due to the C=O stretching vibration, it can be seen how this band is sensitive to crystallinity changes. As the degree of order in the material increases then the full width at half height (FWHH) decreases. MELVEGER [40] has proposed that this narrowing correlates with the density of the sample, whilst PURVIS and BOWER [41] relate the band width to the degree of crystallinity, rather than directly to the density. As already mentioned in chapter 4 the successive carbonyl groups on the benzene ring are in the *trans* conformation [42] and the moiety exists in a planar conformation. PURVIS and BOWER claim there is a departure from the planarity when the benzene ring is in the amorphous phase, ie. there may be a rotation of the C-C=O bonds out of the plane of the benzene ring. MELVEGER suggests that the amorphous polymer (n-GT) consists of a series of rotational isomers, ie. the carbonyl groups can be rotated out of the benzene plane to varying degrees. This distribution of rotational isomers tends to cause broadening of the C=O stretching band, since each state has its own characteristic C=O stretching frequency. The fact that the C-C stretching band of the aromatic unit is not sensitive to crystallinity changes, supports the argument of free rotation around the benzene plane [40].

Figures 5.9 a,b and c show plots of the FWHH of the C=O band versus temperature, samples were annealed for 5, 10, and 60 minutes respectively.

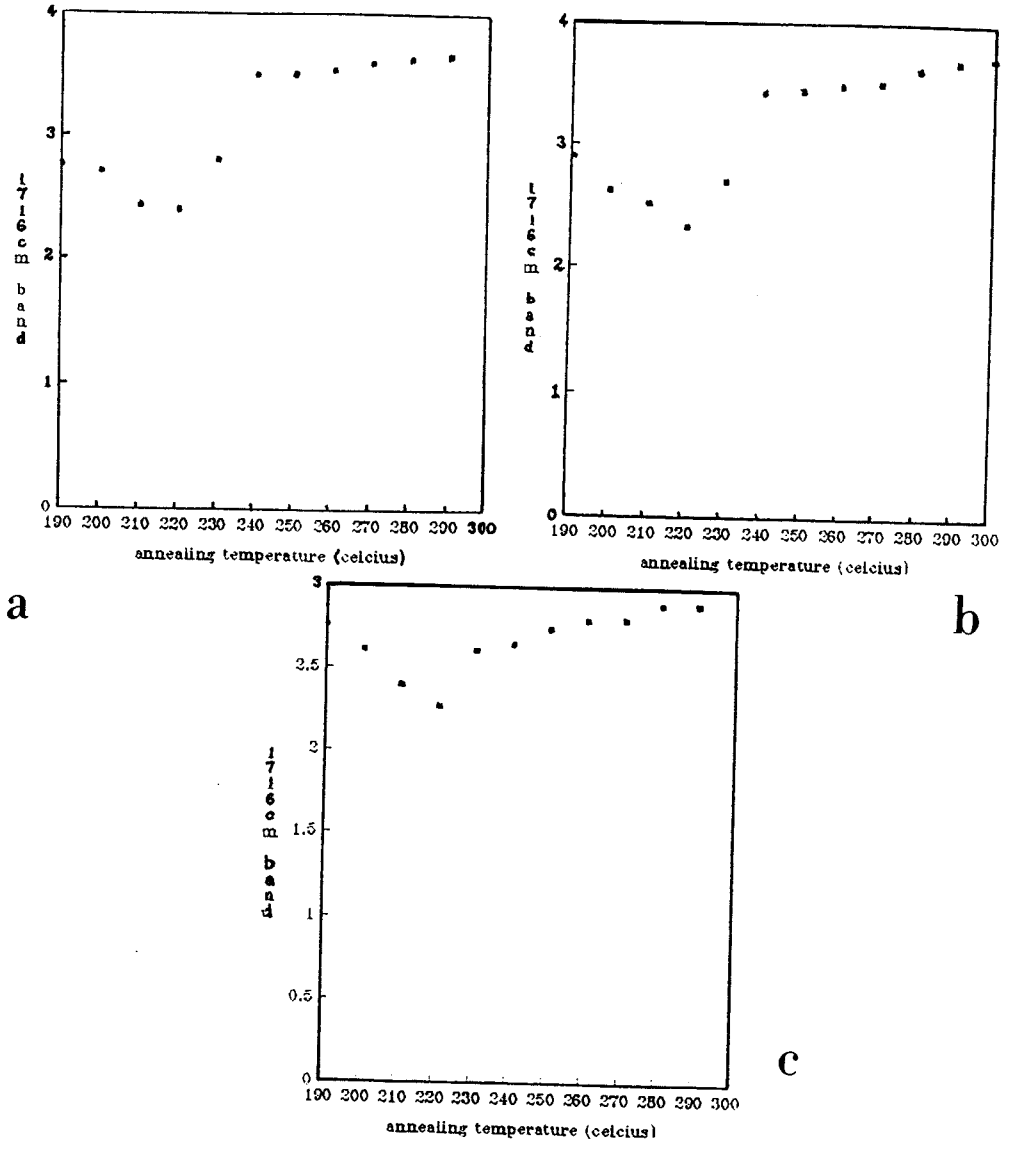

Figure 5.9 The effect of temperature on the FWHH of the C=O band, annealed for (a) 5 minutes, (b) 10 minutes, (c) 60 minutes.

Annealing effects are observed up to 230°C, since the width of the carbonyl band decreases, suggesting an increase in the degree and rate of crystallization in the sample. Above 230°C the relative degree of crystallization decreases, this effect is observed as a widening of the FWHH. This property, of an optimum temperature for annealing is well known [18].

Calorimetric data shows a sharp melting endotherm at 224°C. Above this temperature traces show only a diffuse endotherm.

5.4.3 Diamino diphenyl sulphone (DDS)

The FT-Raman spectrum of DDS is shown in figure 5.10, and the band assignments are given in figure 5.11.

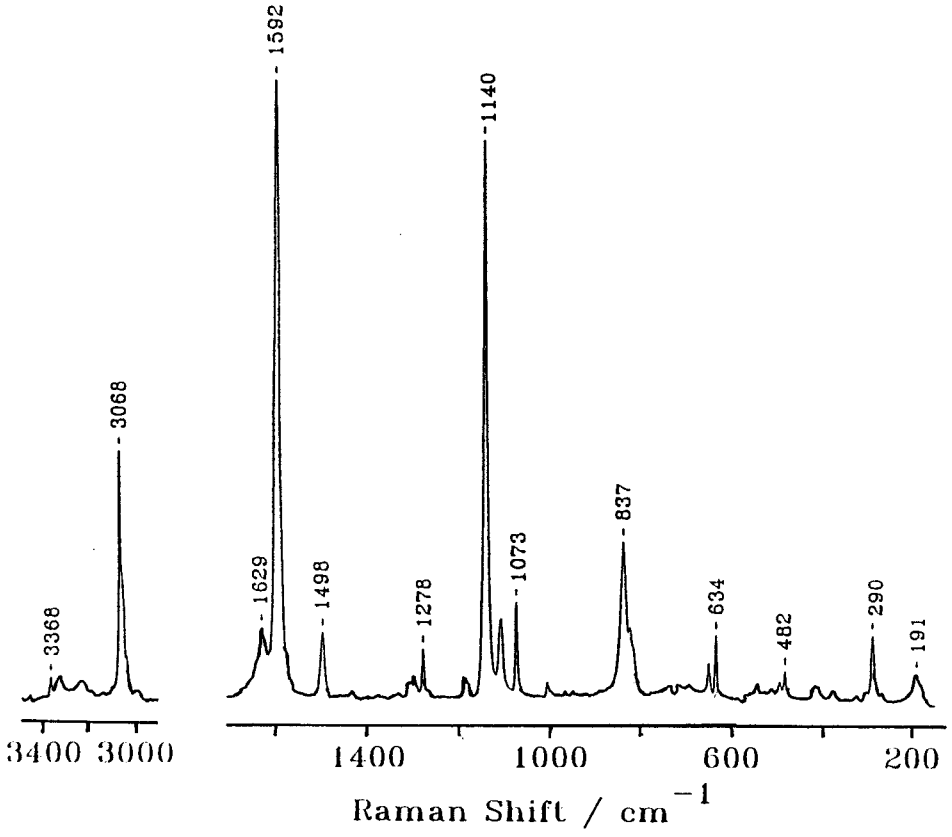

Figure 5.10 The FT-Raman spectrum of diamino diphenyl sulphone (DDS)

The results are consistent with those given by WALTON and WILLIAMS [16]. Bands at 3367, 3330, and 1629cm^{-1} are due to the asymmetric and symmetric NH_2 stretch and symmetric NH_2 deformation respectively. It is these bands that we would expect to decrease during the curing reaction with the epoxy resin. Unfortunately these bands are very weak and when mixed with the epoxy resin, are overlapped, by much stronger bands, thus making it impossible to follow the consumption of the crosslinker.

Raman band (cm^{-1})		Assignment
3367	vw	NH_2 asym. str.
3330	w	NH_2 sym. str.
3065	m	aromatic CH str.
1629	w	NH_2 sym def.
1597	s	benzene ring str.
1500	w	*p*-sub. benzene ring str.
1280	w	SO_2 asym. str.
1140	s	SO_2 sym. str.
1107	w	C-S-C asym. str.
1073	w	C-S-C sym. str.
822	m	adjacent H wag of *p*-sub benzene
634	w	*p*-sub. benzene
482	vw	SO_2 deformation
289	w	C-S-C deformation
191	w	-

s=very strong, vw=very strong, m=medium, w=weak.

Figure 5.11 Diamino diphenyl sulphone, Raman band assignments

5.4.4 Epikote 880

The FT-Raman spectrum of Epikote cured and un-cured is shown in figure 5.12, strong Raman lines which are characteristic of epoxy resin are found at 640, 823, 1114, 1185, 1232, and 1608cm^{-1}. These bands compare favourably with those of bisphenol-A [43].

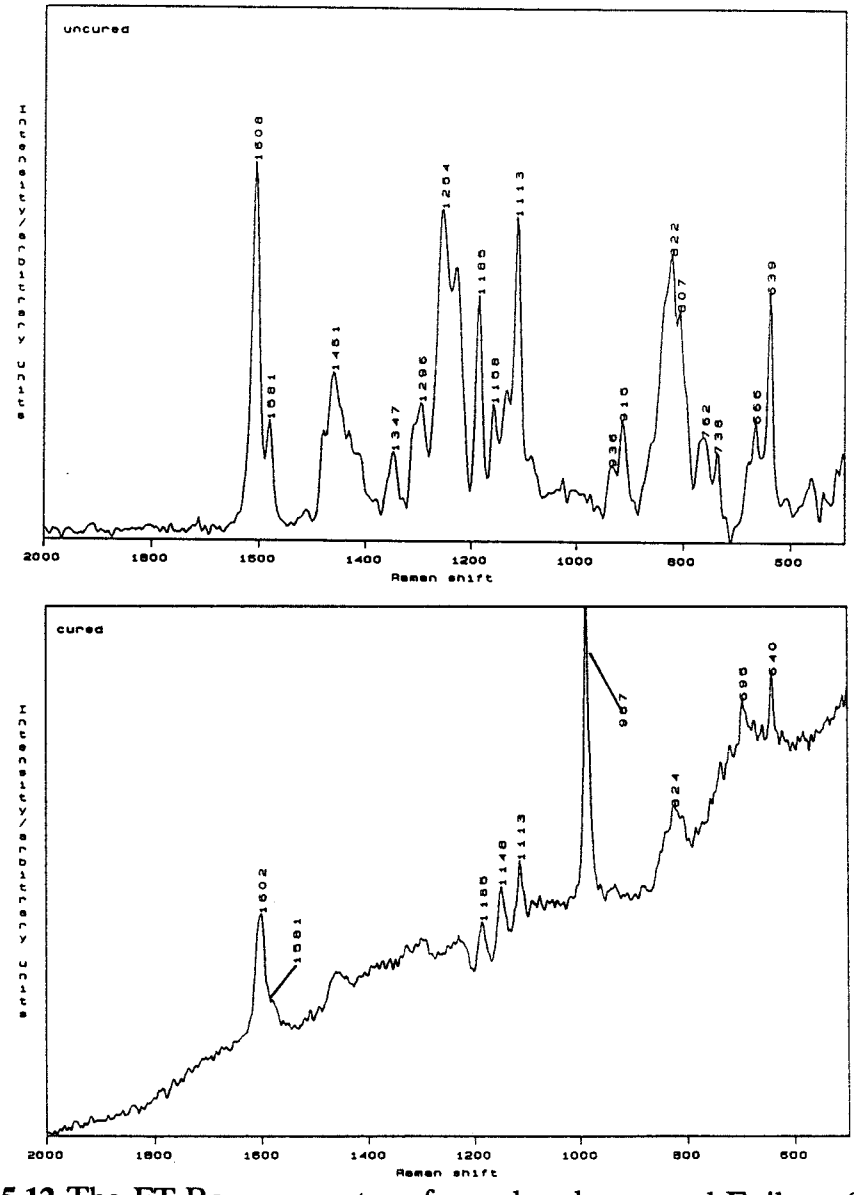

Figure 5.12 The FT-Raman spectra of cured and un-cured Epikote 880

The bands at 640 and 1185cm^{-1} are believed to be due to the group vibration of -C(CH$_3$)$_2$- [44,45]. The bands at 823, and 1114cm^{-1} have been assigned to the out-of-plane and in-plane deformation modes for 1,4-substituted aromatic rings [45].

The band at 1230cm^{-1} has been assigned to the rocking vibration of -CH_3 and the 1608cm^{-1} band to the presence of aromatic rings [43].

Raman bands at 762, 807, 1158, 1254, and 1430cm^{-1} are much weaker in the spectrum of the cured samples than their un-cured counterparts. Since the curing of epoxy resins involve the opening-up of the epoxy ring to form cross-links and -OH and -OCH_2- groups, any decrease in the intensity of a band with cure can be related to the epoxy group.

5.4.5 Polybutylene terephthalate /Epikote blends

A range of cured blends (of different composition and thermal history) were supplied by Dr. Riaz Choudery of ICI Paints, Slough, for the FT-Raman analysis. Blends of composition 75% PBT/25% epoxy, 50% PBT/50% epoxy, and 20% PBT/80% epoxy are reported herein. These samples had the following thermal histories;

Cured at: 217°C/ 30 minutes/ slow cooled
230°C/ 30 minutes/ slow cooled
250°C/ 15 minutes/ slow cooled
and their quenched equivalents.

The spectra of the slow cooled and quenched 50/50 blends can be found in figures 5.13 a, b, and c, 75/25 blends in figure 5.14 a, b, and c, and the 20/80 blend in figure 5.15 respectively. Comparing the spectrum of the cured epikote with that of the blend it can be deduced that the bands at 1721, 1297-1276, and 808cm^{-1} are due purely to the presence of the polybutylene terephthalate. The crystalline sensitive region, 1300-1278cm^{-1} and the carbonyl stretching region, around 1720cm^{-1} were chosen to study the properties of the semi-crystalline polymer in the blend as the epoxy crosslinked under the presence of the crosslinker, diamino diphenyl sulphone.

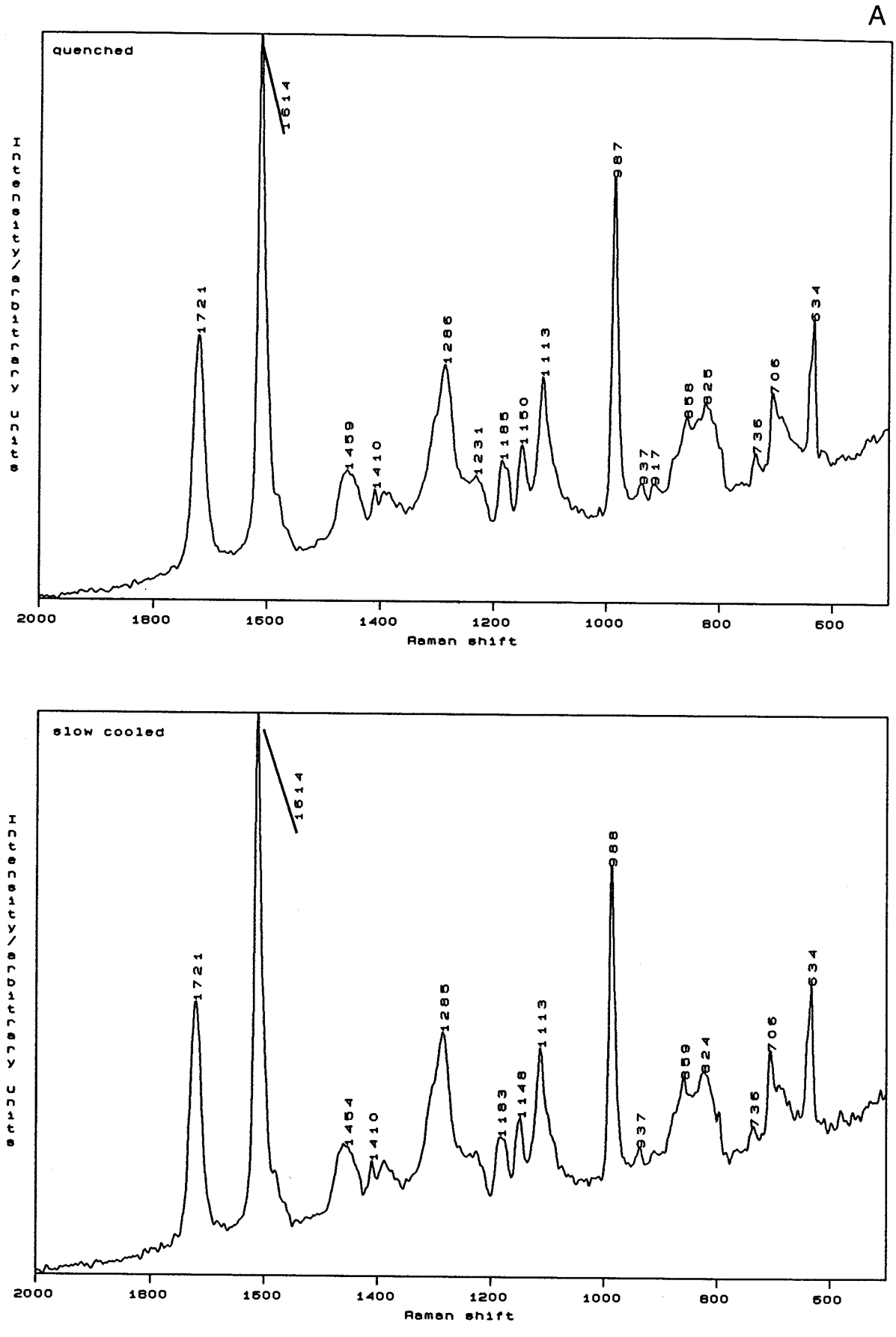

Figure 5.13 50% PBT/217°C/30 minutes

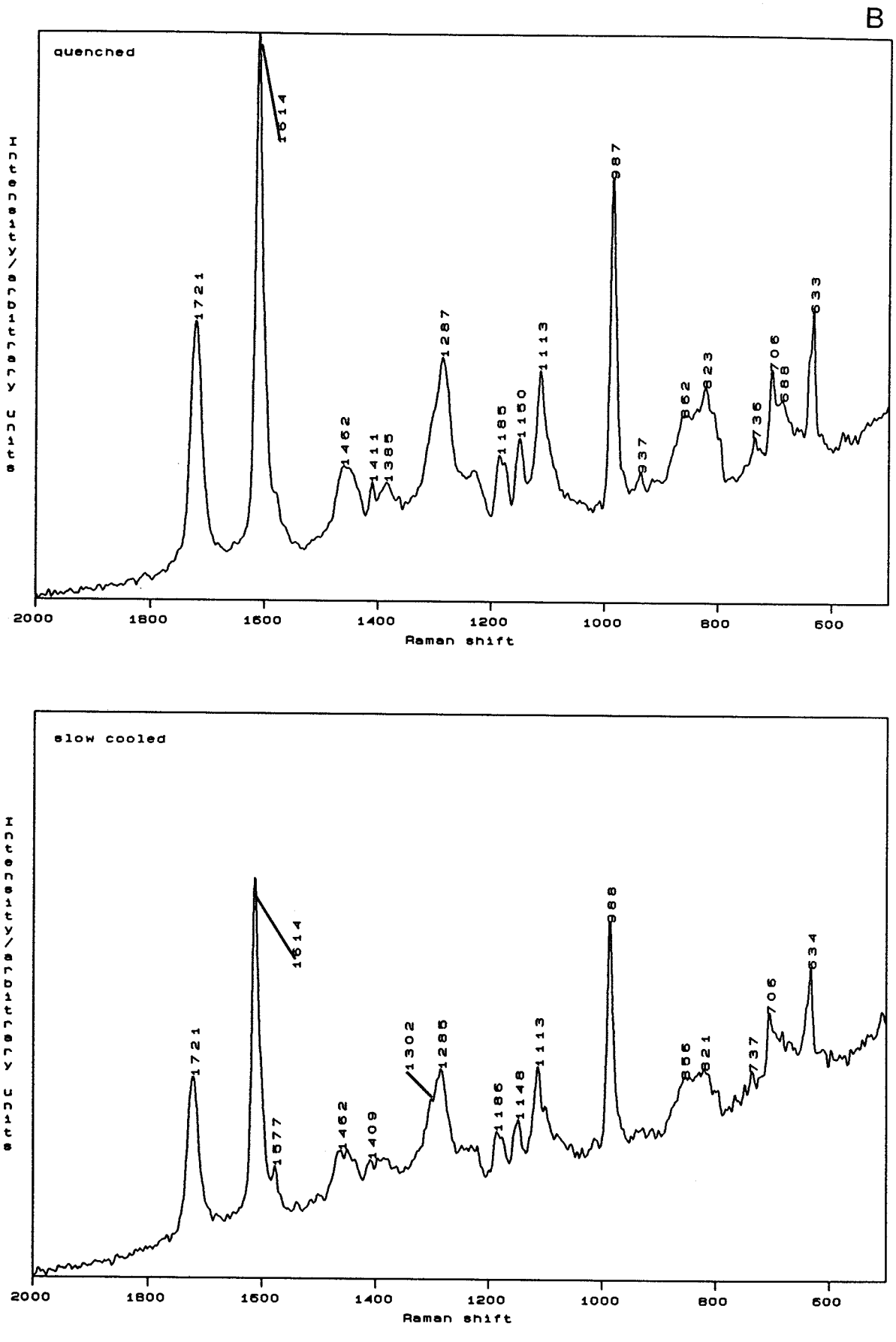

Figure 5.13 50% PBT/230°C/30 minutes

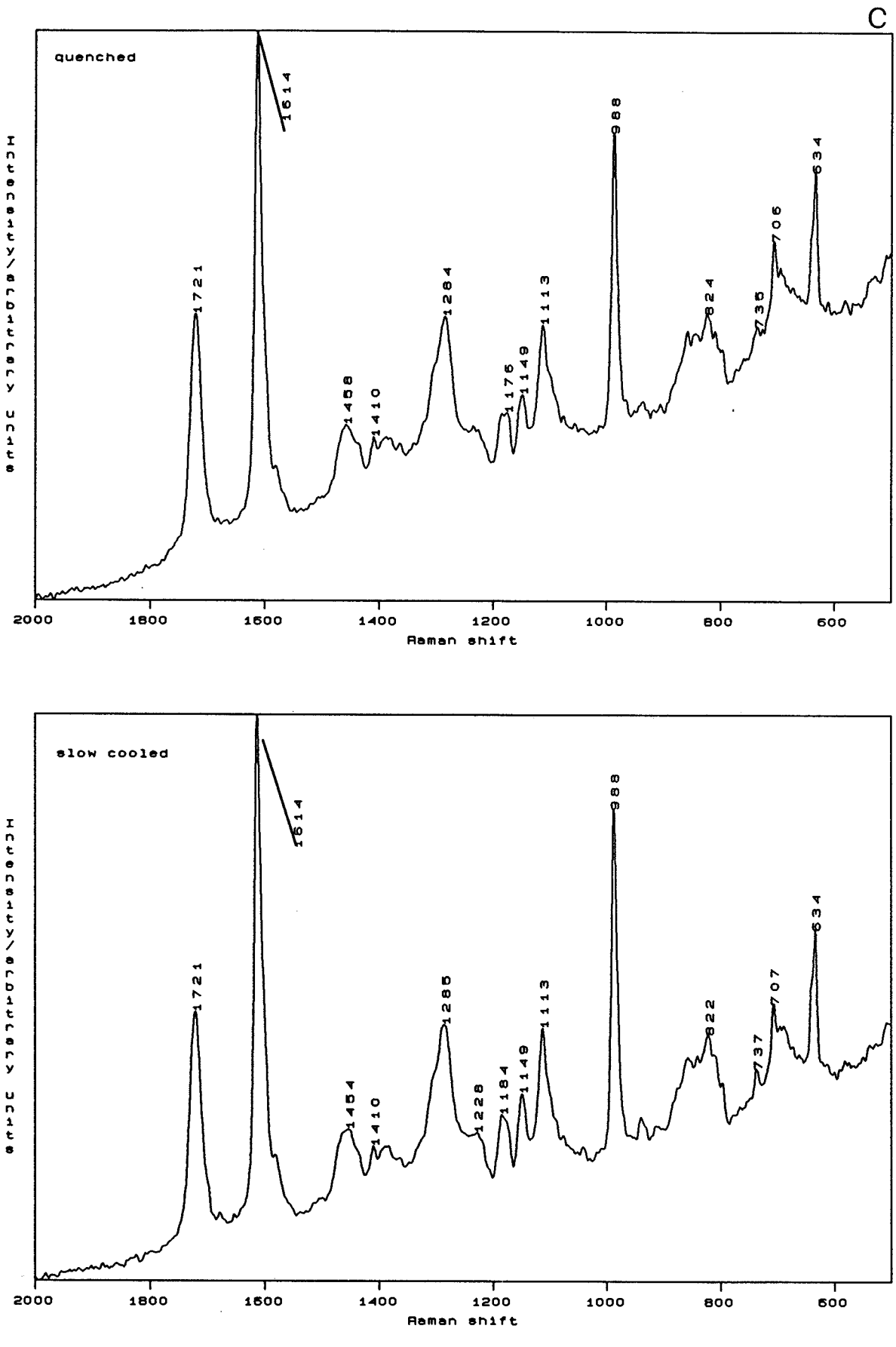

Figure 5.13 50% PBT/250°C/15 minutes

Page 170 was not
included in
the bound thesis.

The general appearance of the Raman spectra of the 50/50 blends, shown in figure 5.13 a, b, and c, suggest they are essentially amorphous, the crystalline sensitive band around 1285cm^{-1} is not resolved, as it is in annealed samples. Further, there are no apparent differences between the samples slow cooled and those quenched. The measurement of the FWHH of the carbonyl band supports these findings and goes on to indicate, when compared with data from the homopolymer a similar degree of crystallinity in the sample held isothermally at 230°C for 10 minutes. These results suggest a penetration of the polybutylene terephthalate into the crosslinked epoxy network. DSC analysis confirms the amorphous nature of the blend [46].

Figure 5.14 a, b, and c shows the FT-Raman spectra of the 75/25 blend systems, the FWHH of the carbonyl band is noted on each figure. Unlike their 50/50 counterparts these samples show a considerable degree of crystallinity. Figure 5.14a shows that of the sample cured at 217°C for 30 minutes, the band at around 1300-1276cm^{-1} is well resolved in the slow cooled sample but only slightly in the quenched sample. The crystalline sensitive band at around 808cm^{-1} is apparent in the slow cooled sample. The FWHH also suggests a greater degree of crystallinity in the slow cooled sample. These effects are well known and are due to the crystallization of the sample as the temperature decreases at a specific rate.

Figure 5.14b shows the sample annealed at 230°C for 30 minutes. As with the homopolymer equivalent the slow cooled sample shows a smaller degree of crystallinity than may be originally expected, the 1300-1276cm^{-1} region is very poorly resolved, and the band at 808cm^{-1} is difficult to detect. The FWHH tends towards a value of the amorphous homopolymer. These findings suggest a destruction of the nuclei at temperatures above the melting point of the polybutylene terephthalate, and a formation of an essentially amorphous polymer that is able to penetrate the epoxy network.

Figure 5.14c shows the sample held isothermally at 250°C for 15 minutes. As

expected, holding the blend at a temperature above the melting point of the polybutylene terephthalate serves to destroy any nucleation sites, as a result in the slow cooled sample the degree of crystallinity is also low.

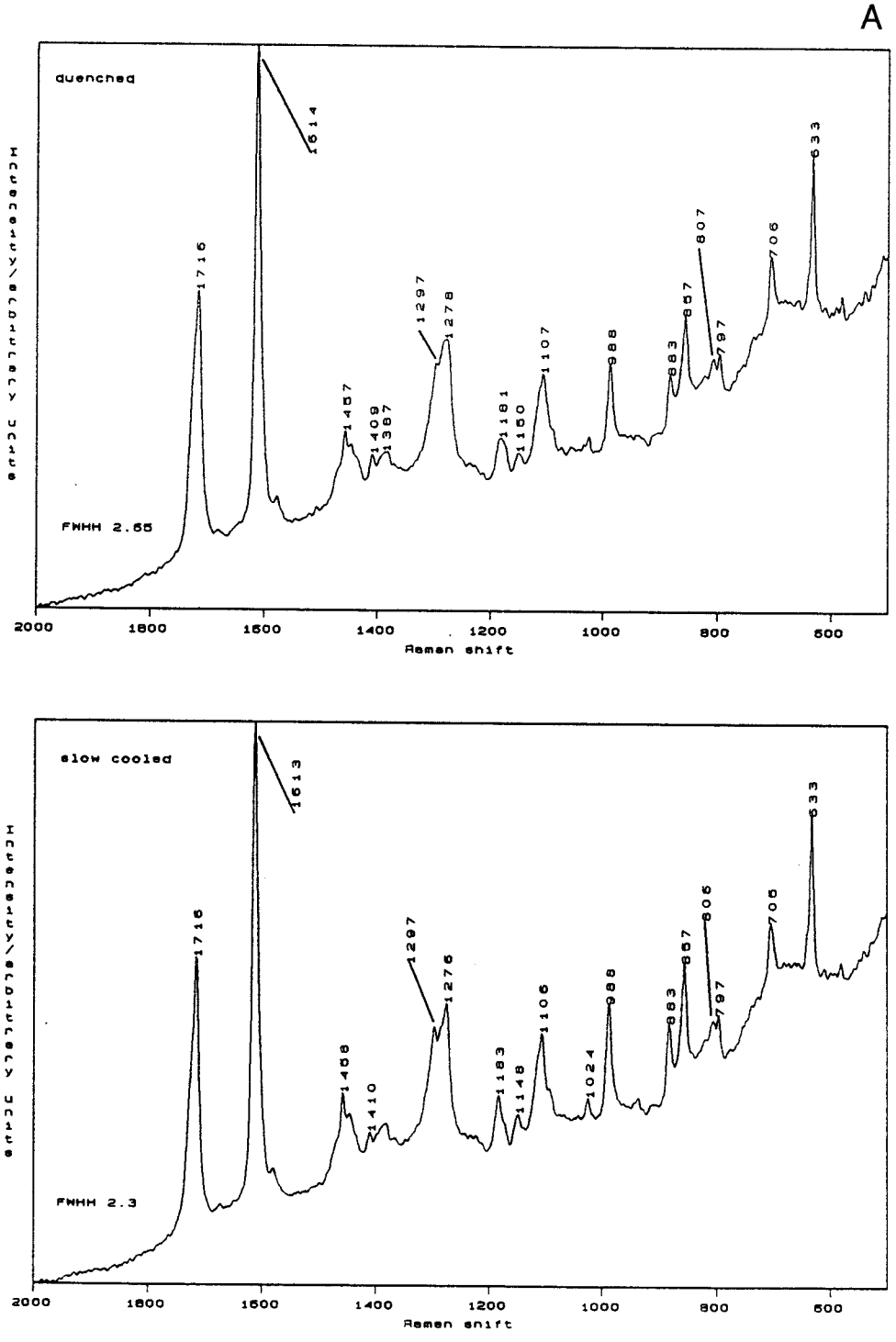

Figure 5.14 75% PBT/217°C/30 minutes

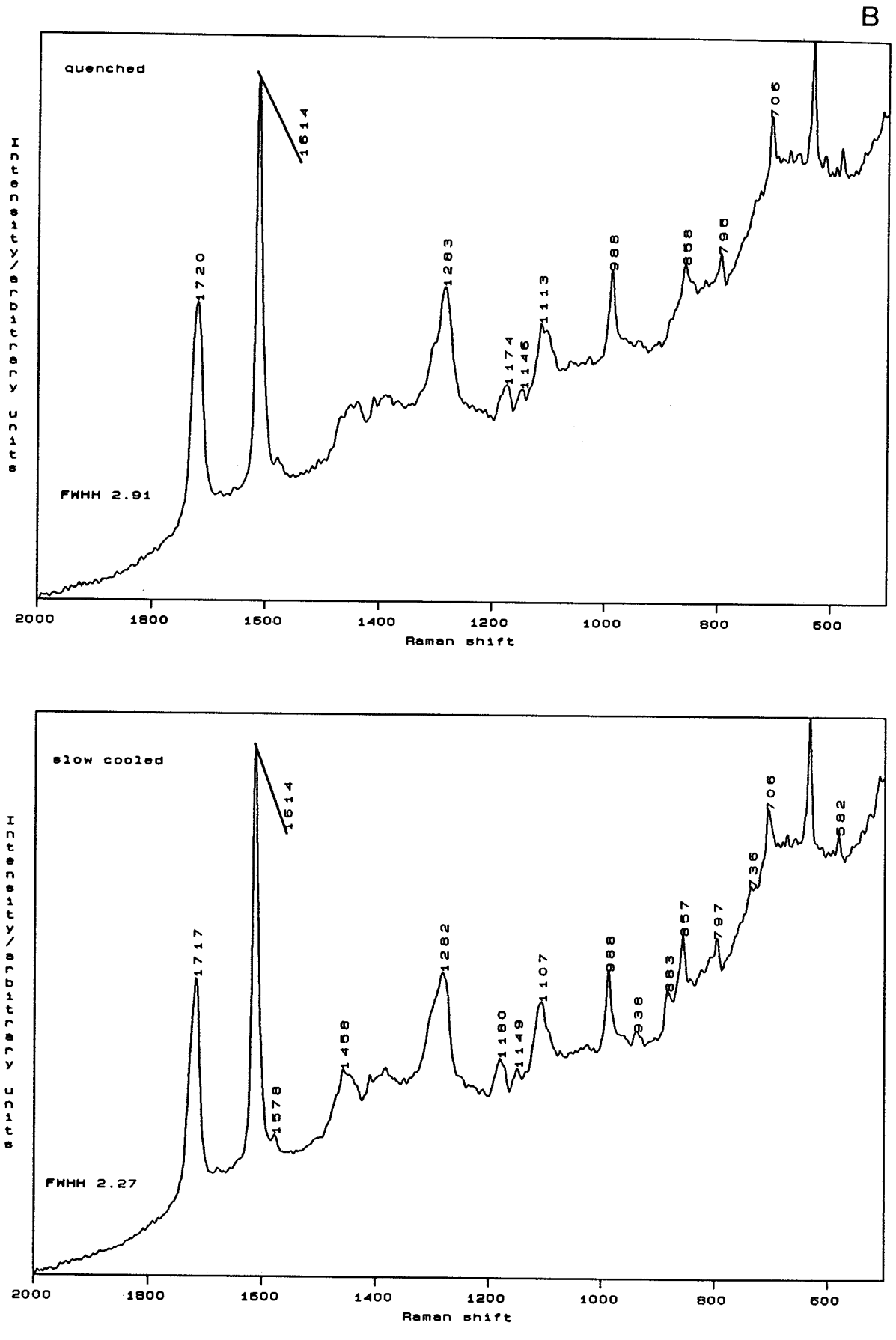

Figure 5.14 75% PBT/230°C/30 minutes

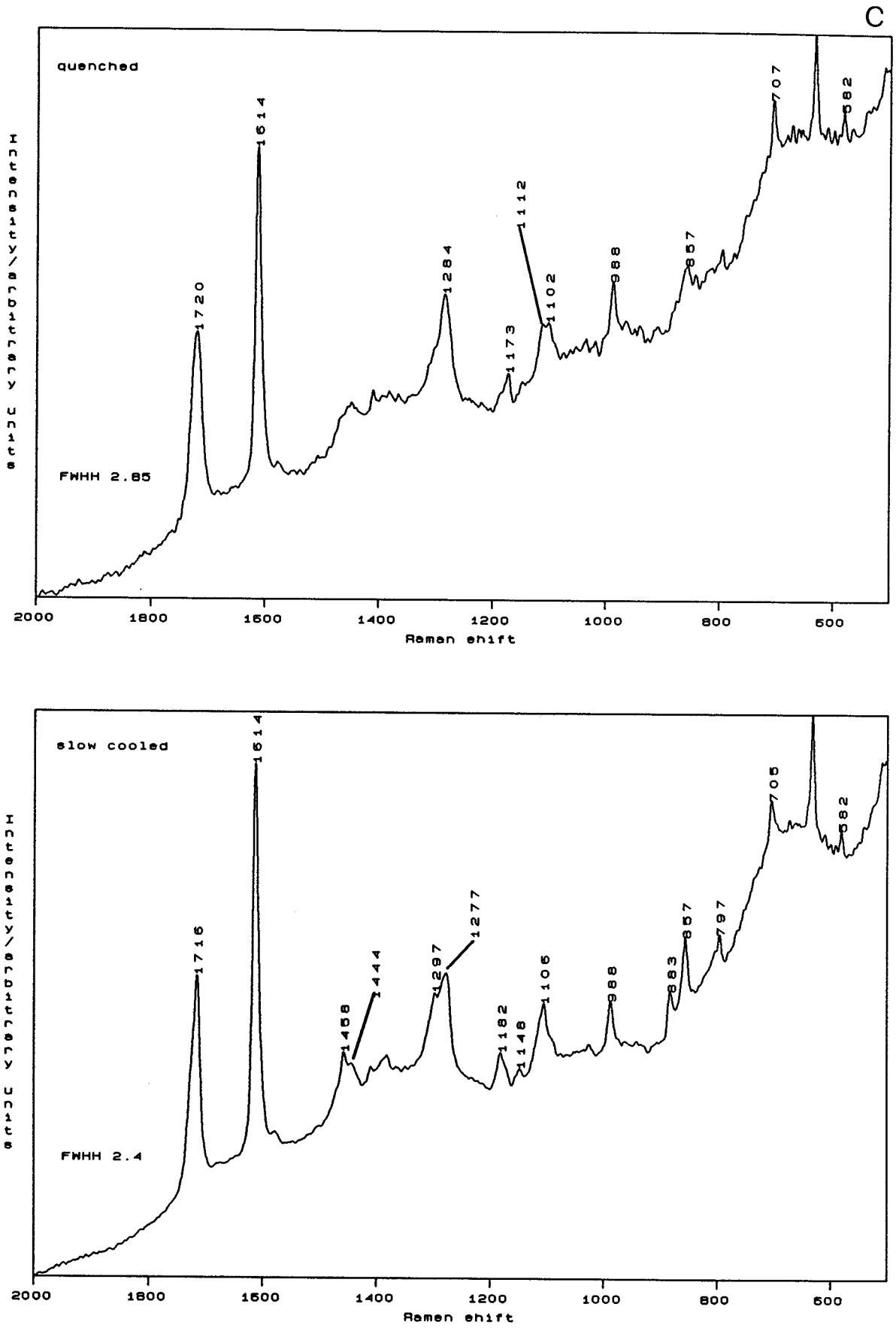

Figure 5.14 75% PBT/250°C/15 minutes

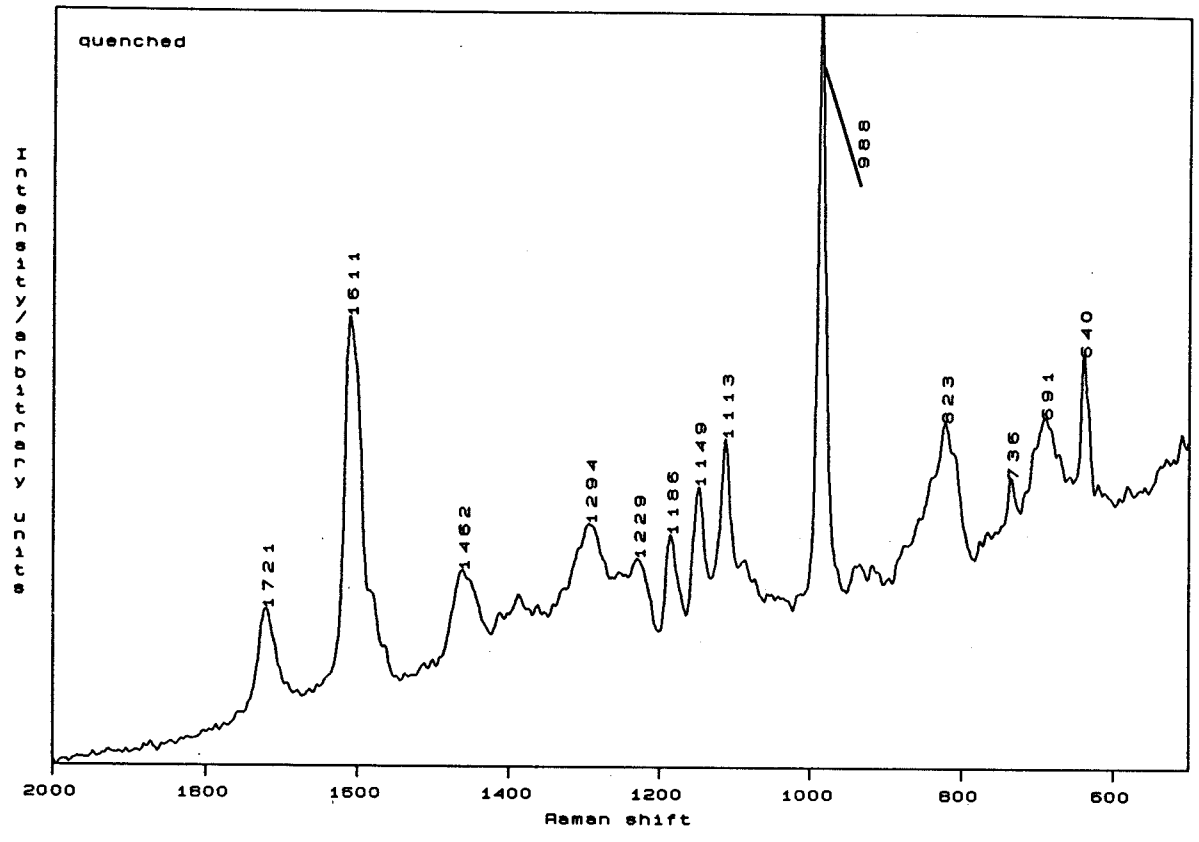

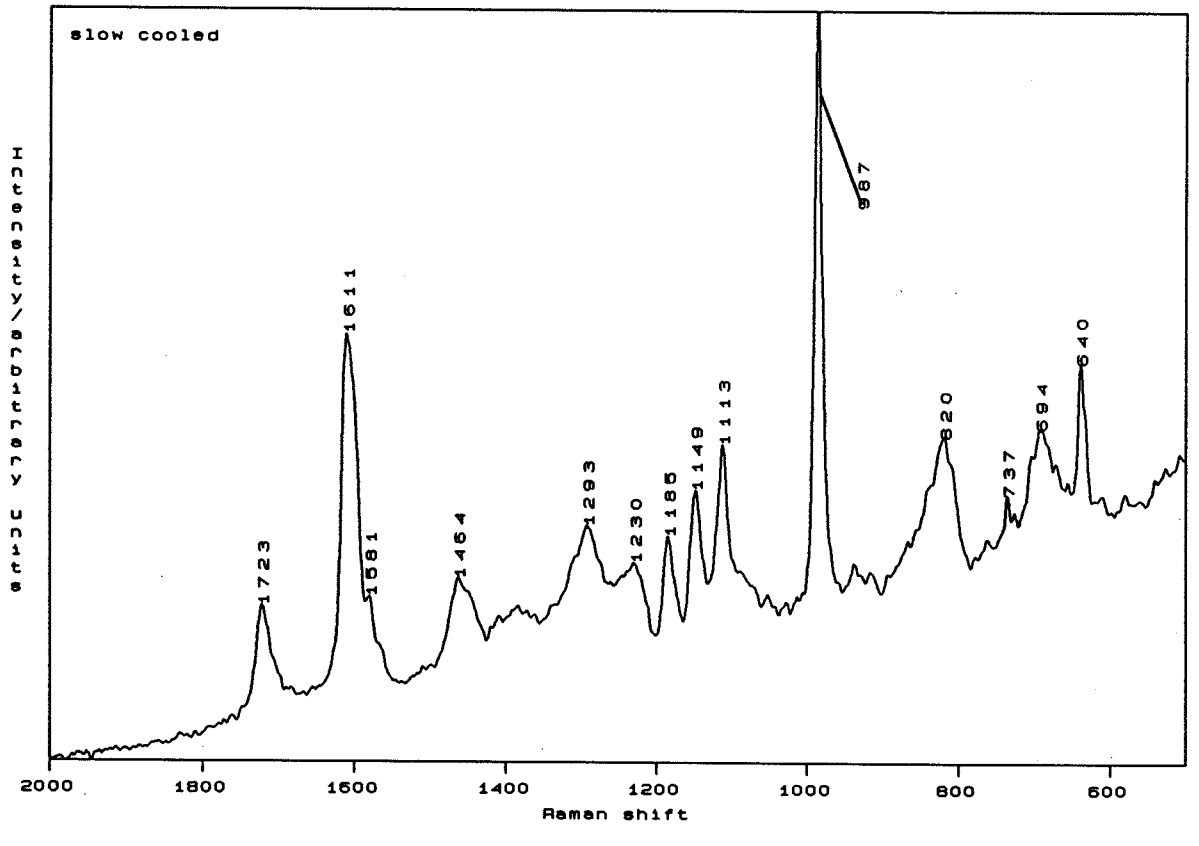

Figure 5.15 20%PBT/230°C/30 minutes

The Raman spectrum of the 20%PBT/80 epikote blend is essentially the spectrum of the epoxy resin (figure 5.15). The concentration of the polybutylene terephthalate is to low to have any effect on the curing characteristics of the epoxy resin. The carbonyl band of the polybutylene terephthalate at 1721cm^{-1} is present at a greatly reduced intensity and large FWHH value. Indicating the amorphous nature of the blend. DSC data confirms these findings. Whilst EM results indicate the formation of a polyester/epoxy crosslinked type network.

5.6 Conclusion

It has been shown from FT-Raman spectroscopy that annealing samples of pure polybutylene terephthalate just below the melt gives rise to a highly nucleated lamellar morphology [47-49] this point serves to increase the crystalline domains, as noted in figures 5.9 a, b, and c.

As the annealing temperature increases the FWHH tends to decrease to a point just below the melting point of the polymer (224 ° C), the reason for the decrease in the value is the restricted motion of the carbonyl groups around the benzene plane, in the more crystalline samples [40].

Above the melting point a gradual increase in the FWHH is observed, it is well known [18] that holding a polymer in the melt phase destroys the nuclei, thus decreasing the degree of crystallinity. Further, the longer the sample is held above the melting point, the greater the amorphous character (due to reasons mentioned above) once the sample is quenched.

It has been shown that bands in the methylene rocking region (1000-900cm^{-1}) and the methylene bending region (1495-1440cm^{-1}) are sensitive to annealing conditions. Raman bands at 808 and 883cm^{-1} associated with the *gauche-trans-gauche* conformation of the glycol residue are absent or of low intensity in the amorphous polymer. This is consistent with the move from a *gauche-trans-gauche* conformation in the crystalline regions to a predominantly *trans* conformation in

the amorphous zones [38].

Bands around 1279cm^{-1} assigned to ring-carbonyl stretch, O-C stretch and ring CH in-plane bend are also sensitive to crystalline character. Due to considerable band overlap it is impossible to assign with any certainty the vibrations, however as the amorphous content in the polymer increases then the band at 1298cm^{-1} appears to decrease, however bands assigned to these vibrations should not decrease in intensity due to an increase in amorphous character. What is being observed is band broadening resulting in severe band overlap.

In summary Raman spectroscopy can detect rotational isomerism in the glycol residue, due to changes in the degree of crystallization, also differences in the degree of planarity of the terephthalate residue, due to rotation of the carbonyl groups about the carbonyl-phenylene bond can be observed.

Looking at the Raman spectra of the cured and un-cured resin, several changes are apparent. Raman bands at 762, 807, 862, and 1158cm^{-1} which decrease in intensity as the cure proceeds have been assigned to the epoxy, as it is only these moieties which undergo reaction in the resin. Bands which remain invariant with respect to degree of cure namely those at, 640, 823, 1113, 1230, and 1608cm^{-1} have been assigned to the skeletal modes of the bisphenol-A residue.

Consider first the 50/50 blend system, from the Raman spectra the polybutylene terephthalate is miscible with both the uncured and cured epoxy resin. Irrespective of the cure conditions ie. wether the sample is cured at 217°C/30 minutes or 250°C/15 minutes, the polybutylene terephthalate remains amorphous. This fact is quantified by the FWHH of the carbonyl band which remains around 23cm^{-1} throughout the various heat treatments. DSC and electron microscopic (EM) studies conducted by CHOUDERY [46] indicate the amorphous nature of the samples. Raman results imply some form of network effect between the semicrystalline polymer and epoxy resin. These findings are collaborated by the DSC and EM results.

The 75/25 blend, follows the properties of the homopolymer. Up to 220°C annealing effects are observed, and with respect to the slow cooled samples a greater degree of crystallinity is evident, implying the lamellae ordering themselves slowly from the melt, as opposed to being "frozen in" in their melt state. The ability of polybutylene terephthalate to crystallize at temperatures below its melting point in the epoxy resin, and the appearance of the spectra, ie showing no trace of the epoxy resin suggest the polyester has phase separated. Results from DSC and more importantly EM show evidence of a phase separated system, and the existence of 2 different domains. This result is similar to that reported by CLARK et al [50].

Spectra of the 20/80 epoxy resin, indicate miscibility in the crosslinked blend. The spectra are essentially of the epoxy resin, although the crystalline sensitive -C=O band of the polybutylene terephthalate can be observed, broad, (FWHH = $25cm^{-1}$) and at a greatly reduced intensity, indicating the amorphous nature of the semicrystalline polymer. EM results provide visual evidence of a "networked" system.

It can be concluded that polybutylene terephthalate is miscible with the highly crosslinked, and semi-crosslinked epoxy resin, depending on the thermal history and composition of the blend.

References

1. H. Tadokoro, "Structure of crystalline polymers", Wiley Interscience, (1979)

2. C. Chaio, *Macromol.*, **23**, 1286 (1990)

3. A. Gupta, M. Cizmecioglu, D. Coulter, F.H. Liang, A. Yaurouain, F.D. Tsay, J. Moacanin, *J. Appl. Polym. Sci.*, **28**, 1011 (1983)

4. R.J. Morgan, *Adv. Polym. Sci.*, **72**, 1 (1985)

5. E. Canals, M. Mousseron, L. Souche, P. Peyron, *Compt. rend.*, **202**, 1989 (1936)

6. M. Mousseron, *Bull. Soc. Chim. Fr.*, 629 (1946)

7. O. Ballaus, J. Wagner, *Phys. Chem.*, **45B**, 272 (1940)

8. W.A. Patterson, *Anal. Chem.*, **26**, 823 (1954)

9. J. Bomstein, *Anal. Chem.*, **30**, 544 (1958)

10. R. Rambaud, M. Vessiere, *Bull. Soc. Chim. Fr.*, 1114 (1960)

11. C.S. Lu, J.L. Koenig, *Am. Chem. Soc. Div. Org. Coat. Plast. Chem. Pap.*, **32**, 112 (1972)

12. V. Janarthanan, G. Thyagarajan, *Proc. Ind Acad. Sci. (Chem. Sci.)*, **102**, (5) 721 (1990)

13. W. West, "Chemical applications of spectroscopy" in A. Weissberger, Technique of organic chemistry, **9**, Interscience, New York, (1956)

14. H. Dannenberg, *S.P.E. Trans.*, **78**, January (1963)

15. J.K. Agbenyega, G. Ellis, P.J. Hendra, W.F. Maddams, C. Passingham, H.A. Willis, J. Chalmers. *Spectrochimica Acta*, **46A**, 197 (1990)

16. J.R. Walton, K.P.J. Williams, *Vib. Spectrosc.*, **1**, 339 (1991)

17. P. Ingram, A. Peterlin, "Encyclopaedia of polymer science and technology", ed. H.F. Mark, N.G. Gaylord, N.M. Bikales, **9**, 204 (1968)

18. D.C. Bassett, "Principles of polymer morphology", Cambridge university press (1981)

19. C.W. Bunn, T.C. Alcock, *Trans. Far. Soc.* **41**, 317 (1945)

20. A. Keller, *J. Polm. Sci.* **39**, 151 (1959)

21. H.D. Keith, F.J. Padden, *J. Polym. Sci.* **39**, 101 (1959) and **39**, 123 (1959)

22. J.D. Hoffman, J.I. Lauritzen, *J. Chem. Phys.* **31**, 1680 (1959)

23. J.D. Hoffman, *J. Res. Nat. Bur. Std.*, **64**, 73 (1960)

24. F.C. Frank, M. Toshi, *Proc. Roy. Soc. London.* **263**, 323 (1961)
25. P.H. Geil, *Chem. Eng. News.* **16**, 72 (1965)
26. G.C. Oppenlander, *Science,* **159**, 1311 (1968)
27. A. Peterlin, *J. Polm. Sci.,* **9**, 61 (1965)
28. W.R. Krigbaum, *J. Polym. Sci.,* **15**, 251 (1966)
29. P.J. Flory, *J. Am. Chem. Soc.,* **84**, 2857 (1962)
30. A.Peterlin, *Macromol.,* **13**, 777 (1980)
31. L. Mandlekern, *Far. Disc. Chem. Soc.,* **68**, 310 (1979)
32. P.W. Atkins, "Physical Chemistry", 2nd. ed. Oxford university press (1982)
33. A. Noshay, I.M. Robeson, *J.Polym. Sci., Polym. Chem. Edn.* **12**, 689 (1974)
34. I.M. Ward, M.A. Wilding, *Polymer* **18**, 327 (1977)
35. I.M. Hall, M.G. Pass, *Polymer,* **17**, 3974 (1976)
36. M. Yokouchi, Y. Sakakibara, Y. Chatani, H. Tadokoro, T. Tanaka, K. Yoda, *Macromol.* **9**, 266 (1976)
37. Z. Meznik, *J. Polym. Sci., Polym. Phys. Ed.,* **13**, 473 (1975)
38. M.A. Wilding, PhD Thesis, Leeds University (1975)
39. C.A. Boye, T.R. Overton, *Bull. Am. Phys. Soc., Ser. 2,* **19**, 352 (1974)
40. A.J. Melveger, *J. Polym. Sci.,* Part A-2 **10**, 3322 (1972)
41. J. Purvis, D.I. Bower, *J. Polym. Sci., Polym. Phys. Edn.*, **14**, 1461 (1976).
42. T.R. Manley, D.A. Williams, *Polymer* **10**, 339 (1969)
43. F.R. Dollish, W.G. Fateley, F.F. Bentley, "Characteristic Raman frequencies of organic compounds", John Wiley & Sons, Inc. (1974)
44. J.H. Hibben, "The Raman effect and its chemical applications", Reinhold publishing corporation, New York (1939)
45. L.J. Bellamy, "The infra-red spectra of complex molecules", Methuen, London, (1958)
46. R. Choudery, ICI internal report
47. R.J. Cella, *J. Polym. Sci., Polym. Symp.* N°42 727 (1973)
48. R.M. Briber, E.L. Thomas, *Polymer* **26**, 8 (1985)

49. R.S. Stein, A. Misra, *J. Polym. Sci. Polym. Phys. ed.,* **18**, 327 (1980)
50. J.N. Clark, J.H. Daly, A. Garton, *J. Appl. Polym. Sci.,* **9**, 3381 (1984)

Chapter 6: Conclusions

Conclusions

Raman spectroscopy has proved to be of value to physicists and chemists over the last 20 years but its value has been minimal compared with more generally applicable methods such as infra-red, X-ray diffraction, Differential scanning calorimetry, or NMR. The reason, as is so often stated (see chapter 1) has always been the lack of applicability of the method. Many polymers fluoresce, others are coloured, when they are heat treated or degraded in service they further intensify their fluoresce. In addition they often darken, and so Raman spectra have been difficult and expensive to acquire. Now we have new-found freedom in the guise of FT-Raman spectroscopy, and hence the method has rapidly expanded in value. Recently, a book has been published by HENDRA, JONES, and WARNES, entitled *"Fourier transform Raman spectroscopy"*, which contains a vast range of applications based almost solely on the work from the Raman group at Southampton. A second book, entitled *"The Raman spectra of polymers"*, written by AGBENYEGA and HENDRA, as the tittle implies is devoted to the Raman spectra of polymers. It contains over 250 high quality polymer spectra, a theoretical account of the technique and validated experimental procedures with laboratory hints and tips to help both expert and in-experienced Raman users. This is followed by a current review of the method in the polymer field, with an extensive bibliography. Regular up-dates will be published containing new and replacement material, giving rapid access to recent research.

This thesis has demonstrated the potential of the FT-Raman technique applied to polymer analysis and more specifically, to surface coatings.

Chapter 3

FT-Raman and FTIR were used to follow the curing of an alkyd resin and its model compounds. FT-Raman was shown to provide detailed kinetic information from the C=C stretching region during the cure process. The C=C stretching band was found to decay over the period of the cure experiment. An initial

increase in unsaturation was observed, and is thought to be due to the normalisation of the band against the 1450cm^{-1} C-H band. Their was some broadening of the C=C band which is associated with the configurational changes expected during autoxidation. For comparison, the same resin with about 15% TiO_2 was investigated. The signal/noise ratio was much improved compared to the unpigmented system due to Raman scatter enhancement by the TiO_2. This improvement might well be unexpected but it is characteristic of FT-Raman measurements, turbid samples give better spectra than clear ones. The onset of curing in the pigmented samples was found to occur much earlier and reaches its limit much faster than in the unpigmented resin.
However from Raman measurements taken from the alkyd no information on *cis/trans* isomerism or conjugation could be deduced.

FT-Raman and FTIR spectroscopy has successfully shown how the cure of three model compounds, namely methyl oleate, methyl linoleate, and methyl linolenate proceed via three very different unsaturation/chain modification type mechanisms and rates. Changes appear in the C=C microstructures throughout the cure and are manifest in the peaks at; 1670, 1655, and 1640cm^{-1}, these changes have been assigned to *cis/trans* isomerism and to the migration of the double bonds during the hydroperoxide formation. Evidence of a previously unreported conjugated cyclic system in the cure of methyl linoleate is reported.

Further work

It was demonstrated in the thesis that the intensity of the Raman scatter is very sensitive to sample thickness, and as a consequence in-situ measurements on films of alkyd paint were not possible. Research into in-situ sampling is now under-way.

Alternative laser lines namely the 1.3μ of the Nd:YAG and the 784nm line of the tuneable Ti:sapphire laser are or will be soon available, these laser lines will provide interesting areas of research in the pigmented coatings area, as they may not promote the same degree of fluorescence in the samples as the conventional

514nm argon ion laser or the 1.064μ line of the Nd:YAG.

Environmentally a move is being made from the solvent based alkyd resin into the less harmful water based alkyds. A similar analysis into the curing mechanism of the water based system is envisaged.

NMR studies are now under-way to determine the nature of the conjugated cyclic structure suggested from the Raman data.

Chapter 5

This chapter describes the study of a series of main-chain thermotropic liquid crystalline polyesters, with flexible spacers of varying length and lateral substituents.

Studies were made using FTIR, FT-Raman spectroscopy , DSC, WAXS, and TOA. The Raman data obtained from the materials with chlorine substituents is completely novel, results have improved our understanding of the effects of lateral substituents in the mesogenic backbone.

The thermal properties of MC7TOB were characterized by DSC. It was shown how the properties of the polymer varied with the flexible spacer length (in MC4TOB), and the absence of lateral substituents (in the case of P7TOB and P4TOB).

Thermo-optical analysis and wide angle x-ray scattering showed the presence of a Smectic mesophase in the case of P7TOB and Nematic mesophase in P4TOB, and MC4TOB.

Initial conventional Raman data of these polymers (courtesy of Dr. G. Ellis) exhibited extremely high levels of fluorescence, and it was naturally thought that Raman data of any significant quality would be impossible to acquire. However when it had been demonstrated that the FT-Raman method could produce useful

data, a series of strong Raman lines were assigned, a reappraisal of the conventional technique was made, and from information obtained by the FT-device and exposure of the sample to the laser beam for many hours, some quite acceptable Raman spectra were recorded. Only a room temperature FT-Raman spectroscopic analysis was possible of MC7TOB and MC4TOB (the aim to determine any further information in to the conformation of the polymer). Transition temperatures in the polymers were to high to study the Raman spectra as a function of temperature, at present we are limited to temperatures below 150 °C, above this temperature the thermal background totally swamps the Raman signal.

Further work

The data from this preliminary study is set to provide many novel investigations into the Raman spectra of thermotropic liquid crystal polymers.

A series of experiments are planned to study the thermal behaviour of the polymers as they are heated through the phase transitions, whilst in the Raman hot cell, using the Ti:Sapphire laser temperatures in excess of 200 °C are possible[1].

Polarized vibrational spectroscopic studies of un-oriented and oriented fibres will be made in order to determine order parameters, and to obtain more detailed information as to the structure of the chains.

A vast range of thermotropic liquid crystalline polymers (of the mesogenic triad family) are yet to be synthesised. The aim will be to produce liquid crystal polymers with properties such as low transition temperatures, stable mesophases and chemical resistance.

Blends of LCP with themselves and semi-crystalline polymers such as

---

[1] M. Pellow Jarman, 1st year report, 1992.

polyethylene terephthalate and polybutylene terephthalate are planned. The study of the miscibility of such systems by FT-Raman spectroscopy is possible (see chapter 5).

Chapter 5

FT-Raman spectroscopy was shown to be a useful tool for the characterization of semi-crystalline blends. Information to support thermal data and morphological findings have been reported. The device was then used to study the miscibility of a polyester/crosslinked epoxy blend system. Raman data is shown concerning the effect of the epoxy resin on the crystallisable polymer.

FT-Raman is ideal for this analysis since very little sample preparation is required. The cured films can be simply mounted into the irregular solid sample holder, and viewed with no further sample preparation necessary. Data is presented on the feasibility of FT-Raman spectroscopy in determining the effect of temperature on the degree of crystallization of polybutylene terephthalate. A series of samples were annealed at different temperatures and times to study the effect. Below the melting point of the polymer, which is around 224 °C annealing effects are observed, but above this temperature no further increase in the degree of crystallization was noted. The longer the sample was annealed the greater the degree of crystallization however times of over 3 hours did not seem to increase the degree of crystallization. Results were confirmed by DSC.

A Raman analysis can be found of the epoxy crosslinker diamino diphenyl sulphone (DDS). Results are consistent with those found in the literature. A similar study was made of the cured and un-cured epoxy, strong Raman lines which are characteristic of epoxy resins were found at 640, 823, 1114, 1185, 1232, and 1608cm^{-1}.

A study of a range of blends (varying composition, and curing conditions) was successfully made using FT-Raman spectroscopy. Rapid identification was possible without the need of lengthy sample preparation. Certain bands related

to the polyester and the epoxy could be distinguished in the blends. This provided the method for determining the effect of the epoxy on the crystallization properties of the polyester. It was shown that in certain blends phase separation occurred as the blend cured; in the blends of the
75% PBT/20 % Epikote, phase separation was observed in the samples cured at temperatures below the melting point of the polybutylene terephthalate. Samples cured above the melting point were found to be miscible with the epoxy resin. Samples of the 50% PBT/50% Epikote blend tended to show only amorphous character in the polybutylene terephthalate segment.

Further work

Preliminary studies have been made of polyethylene terephthalate, and its 18% and 35% isophthalate copolymers. Blends containing these semi-crystalline polymers are planned. Studies in to the effect of the crosslinker concentration are planned, along with different epoxy resins.
Physical testing of the coatings is then planned, with an aim to relate physical properties to the degree of crystallization, and composition.

Jonathan Agbenyega

APPENDIX: Published work

Book

P.J. Hendra and J.K. Agbenyega, **The Raman Spectra of Polymers**
to be published by John Wileys and Sons 1992

Papers and Conferences

Agbenyega, J.K., Ellis, G., Hendra, P.J., Maddams, W.F., Passingham, C., and Willis, H.A. Applications of FT-Raman spectroscopy in the synthetic polymer field.
Spectrochimica acta, **46A**, No.2 197-217 (1990).

Agbenyega, J.K., Claybourn, M., Ellis, G. The application of FT-Raman spectroscopy to the study of paint systems.
presented and published at the XII International Conference on Raman Spectroscopy. Columbia, South Carolina. (1990)

Agbenyega, J,K., Claybourn, M., Ellis, G. A study of the autoxidation of some unsaturated fatty acid methyl esters using FT-Raman spectroscopy. Spectrochimica acta. **47A**, No.9/10 1991

Agbenyega, J.K., Claybourn, M., and Ellis, G. FT-Raman spectroscopy in the study of Paints.
American Chemical Society publications, "Advances in Chemistry Series 236: Structure Property Relations in Polymers". 1992

J.K. Agbenyega, J. del Pino and J.G. Fatou, Characterization and Thermal Study of Poly(n-methylene terephthaloyl -bis,bis-3-chloro, 4-oxybenzoate. In press

Polymer Processing, Structure and Properties, University of Leeds. 15-16 May 1991. Presented poster.

Macro Group UK Meeting, University of Lancaster, 26-28 March 1991. Presented poster.

Appendix 2. Vibrational Assignments.

Introduction

Historically spectroscopists tended to specify the wavelength of radiation, because this is the quantity most easily determined directly in the visible and infra-red regions, by using diffraction gratings of known ruling spacing. More recently it has become general practice to work in reciprocal wavelength units or wavenumber units, which specify the number of waves per metre or, more per cm. This is because in theoretical treatments frequencies are calculated, or in quantum-mechanical calculations energy levels, and the frequencies or differences between energy levels are proportional to the wavenumbers of the corresponding radiation.

The observed vibrational spectrum of any polymer consists of a large number of peaks and these peaks are said to be assigned, when its origin is understood. This assignment or understanding, may, in principle, be at one of several levels of accuracy or refinement. In practice the process of assignment may involve the implementation of several methods simultaneously. The levels at which the assignment may be known for a polymer are, in order of increasing detail.

(i) to a chemical species or molecular configuration.
(ii) to the crystalline or amorphous region
(iii) to a specific molecular conformation
(iv) to a symmetry species
(v) to a specific normal mode

Assignment to a particular chemical species or molecule

Consider a semicrystalline sample, if the crystallinity of the sample can be varied substantially, it should be possible to assign some peaks to the crystalline regions and some to the amorphous regions (note however that heating effects manifest themselves in changes to the molecular conformation in the non-crystalline regions, and spectral changes will generally accompany these in addition to any due to changes in crystallinity or crystalline perfection. (See appendix 3)

Examples of these kinds of assignment, which are at the first two levels of order, and of their usefulness in providing information about structure of polymers is examined in

chapters 3 and 5 of this thesis, along with the frequency approach.

Now let us consider in more detail the Group frequency approach. It is important to remember that every vibration of a molecule or crystal involves, the motion of every atom in the molecule or crystal, except when the amplitude of vibration of an atom or atoms is zero by symmetry.

It is sometimes possible to divide the vibrations of a molecule into two sets, those which involve mainly the coupled internal vibrations of particular groups of atoms and those which involve mainly vibrations of these atoms with respect to each other. An example of this is given in figure A2.1.

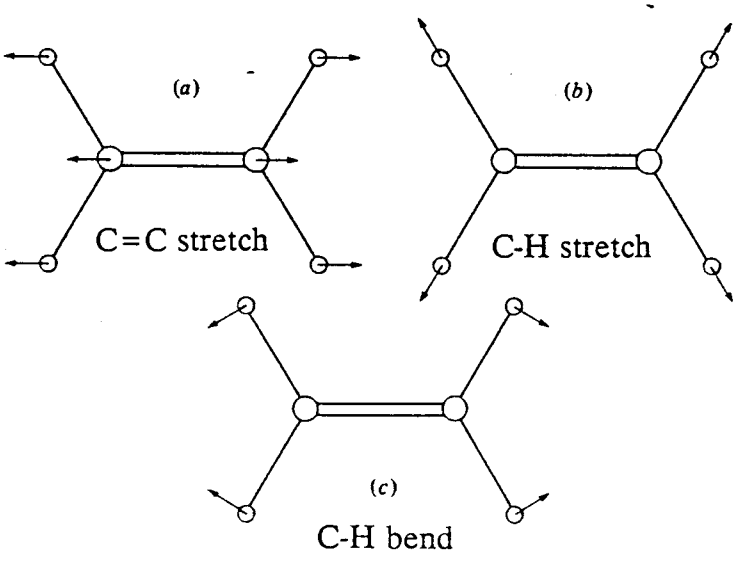

Figure A2 The symmetry modes of A_g species for the ethylene molecule

The actual vibrations which correspond to figures A2.1b and A2.1c involve, to a first

approximation , only internal vibrations of the $=CH_2$ groups whereas the actual vibration which corresponds to A2.1a is mainly a vibration of the two $=CH_2$ groups with respect to each other. It should be noted that the vibration which corresponds to figure A2.1b is only one of two possible modes in which each of the $=CH_2$ groups shows a symmetric stretch. The two modes have slightly different frequencies 3026 and 2989cm^{-1} respectively, because the vibration of the $=CH_2$ groups are coupled through the C=C bond. The difference of only 1% on their frequencies shows that the $=CH_2$ symmetric stretch gives rise to a good group frequency. The two vibrations which correspond to antisymmetric $=CH_2$ stretching have frequencies at 3106 and 3103cm^{-1} respectively with a difference of about 0.1% so that the antisymmetric $=CH_2$ stretching frequency is an excellent group frequency. The four vibrations which involve to a first approximation only the stretching of C-H bonds of $=CH_2$ groups have a total spread of frequencies from 2989 to 3106cm^{-1} or about 4%, so that the =C-H stretching frequency is also a relatively good group frequency, but not as good as either the symmetric or antisymmetric stretches of the $=CH_2$ groups as a whole. These ideas may be extended by considering the vibrations of a particular group of atoms common to several different molecules. If in each of two different molecules which include the same group of atoms, eg a $=CH_2$ group, there is a vibrational mode which involves to a good approximation only one of the internal modes of vibration of that group of atoms, the frequencies of the two modes will be very similar and the molecules are said to show this particular group frequency of the $=CH_2$ group.

The occurrence of group frequencies has been and still is of great importance in vibrational spectroscopy for several reasons. First they are useful in chemical analysis, if the vibrational spectrum of an unknown substance shows one or more modes with frequencies typical of a particular group of atoms, the presence of this group in the molecule is strongly suggested. In polymers this information may be extended to determining the presence or absence of a particular configurational of conformational isomer in the polymer or to a more quantitative assessment of the relative amount, and it may also be applied to obtaining information about the distribution of orientations of particular groups of atoms in an oriented polymer (See Chapter 6). Other methods of assignment exist at higher levels when simpler methods fail. Symmetry, selection rules

and polarization effects may be used in principle to produce assignments for the spectrum of a polymer consisting of a single chemical species with a single configuration and in regular conformational structures. The use of model compounds and isotope substitution is often used; the frequency of a vibrational mode depends on the masses of the atoms as well as the geometry of the molecule and the force constants. If the mass of one type of atom can be changed by substituting a different isotope from the normally predominant one, and the other factors which determine the frequency of the modes remain constant, then some simple predictions can be made about the change in frequency which will be observed. If the type of atom, for which for which the substitution is made does not move in a particular mode, the frequency of that mode will not change, however if the mode involves the movement of this type of atom the change of frequency may be quite large. Isotope substitution may thus be a useful aid in making vibrational assignments. For example, consider the totally symmetric "breathing mode" of the methane molecule, in which all four hydrogen atoms move radially in and out in phase with each other, in this mode the carbon atom does not move. The frequency of this mode is independent of the mass of the carbon atom it would not change if the mass of the carbon atom were changed by isotopic substitution, whereas if the masses of all the hydrogen atoms were changed from 1 to 2 atomic mass units by the substitution of deuterium the frequency would, in the case of the harmonic approximation, be reduced by a factor "root 2" = 1.414.

A more theoretical approach to detailed vibrational assignment and to the overall understanding of molecular dynamics involves the attempt to calculate vibrational mode frequencies.

The methods mentioned above will often allow modes to be correctly assigned. There are however often other modes which cannot be assigned in such a manor, because they are mixtures of simple symmetry or group modes of the same symmetry species. Further information on the nature of these modes can be obtained by calculating the normal mode frequencies. Such calculations can also show to what extent assignments made to symmetry or group modes are really approximations.

It is not the aim of this thesis to detail the theory of such calculations, a complete study of vibrational calculations can be found in reference 2.

The aim of this appendix has been to increase the awareness of the reader to other methods of band assignment should the usual method of *group vibrations* fail.

References

1. J.F. Nye, *"Physical Properties of Crystals"*, Oxford University Press, 1957

2. L.A. Woodward, *"Introduction to the Theory of molecules Vibrations and Vibrational Spectroscopy"*, Oxford University Press, 1972

3. H. Tadokoro, M. Kobayashi, *"Vibrational Analysis of Highly ordered Polymers"*, in *"Polymer Spectroscopy"*, ed. D.O. Hummel, VCH, 1974

Appendix 3: Polymer Crystallinity

Some polymers are capable of displaying a degree of crystalline ordering. The crystalline regions can be described, like any other crystal, in terms of a crystallographic unit cell. Polymers may adopt a wide variety of unit cells. However, because of the basic anisotropy of the polymer chains, and the difference between the cohesive forces along the chains and between neighbouring chains, no polymer forms a **cubic** unit cell.

In 1939 following the X-ray work which established the unit cell for polyethylene, BUNN [1] concluded that melt crystallized polymers contained small regions, typically 100Å-200Å in length, of three dimensional order, surrounded by amorphous material which had a melt-like structure [1]. In a paper published in 1945, BRYANT describes the *composite single phase model* for the structure of the melt crystallized material [2]. He argued that since a polyethylene chain was at least 1000 carbon atoms in length, extended crystalline regions up to 1300Å in length (depending upon the polymer branching) should be observed. Since experimental observations clearly indicated that the crystal regions rarely exceeded 300Å and were typically much smaller, he concluded that the polymer chains must meander between crystallites, from regions of disorder to those of well established three dimensional order. A diagram showing this model is shown in figure A3.1.

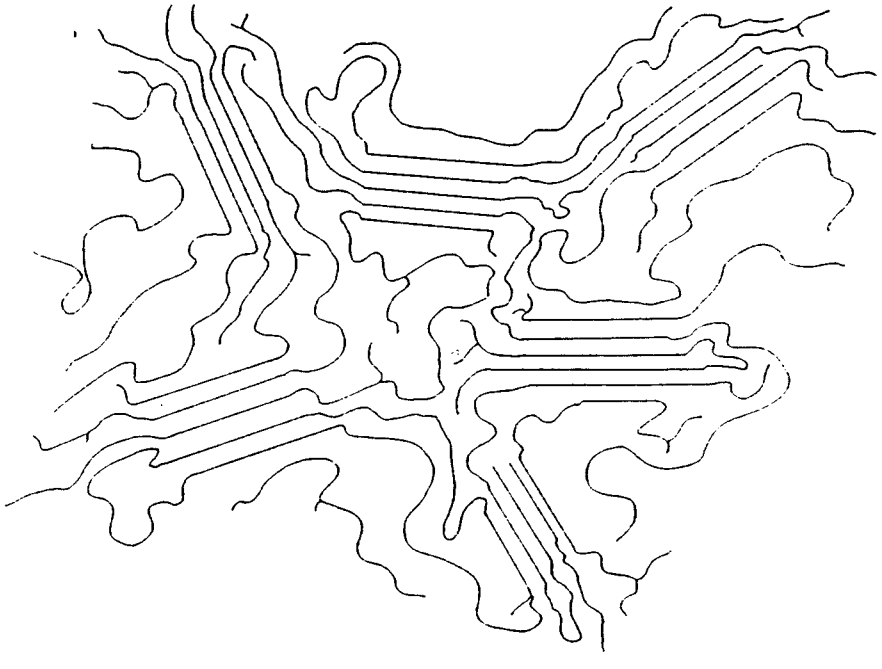

Figure A3.1 A diagrammatic representation of the *composite single phase model*

This model is also known as the *Fringed micelle* or *Fringed crystallite model.* It can be seen that the amorphous region is rich in chain ends, branches and defects in microstructure which would disrupt the order of the crystalline core.

In 1953, SCHLESINGER reported the formation of a single crystal of gutta percha [3] and in 1957, FISCHER, KELLER and TILL all reported that polyethylene could also be crystallized from solution [4-6]. Previously, although the formation of single polymer crystals had been observed during polymerization, it was thought that molecular entanglements would prevent crystals forming from solutions. A typical polyethylene crystal is shown in figure A3.2.

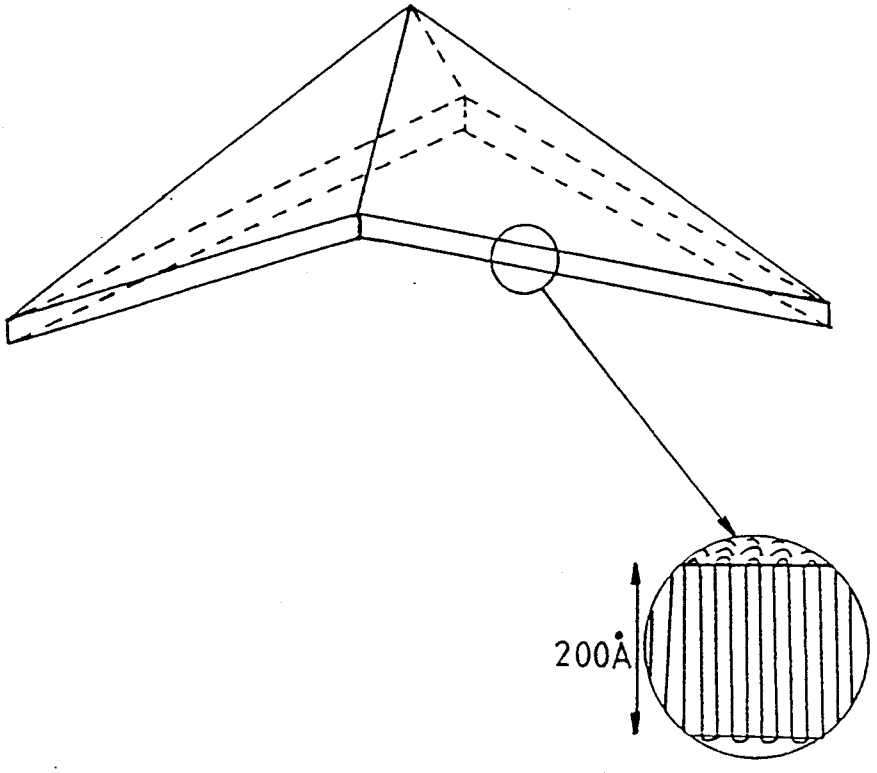

Figure A3.2 A diagram showing a single polyethylene crystal formed from solution. Solutions grown crystals are generally between 100 and 200Å thick. It was soon established that the polymer chains lay approximately perpendicular to the crystal faces and Keller, therefore proposed that the chains must be folded [5]. A number of models have been suggested to describe the detailed nature of the chain folding in these lamellar crystals. Figure A3.3 illustrates these different models.

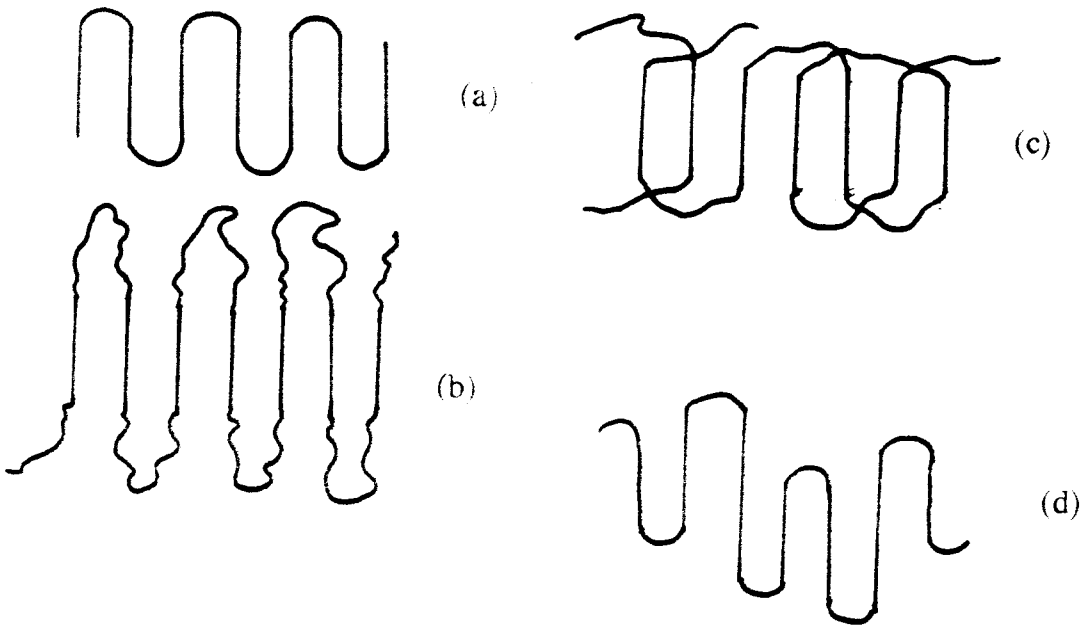

Figure A3.3 Schematic 2D diagrams of the proposed models for the fold surface in solution grown polymer lamellae: (a) regular adjacent re-entry with sharp folds, (b) adjacent re-entry with loops, (c) the "switchboard" model and (d) irregular fold length with adjacent re-entry.

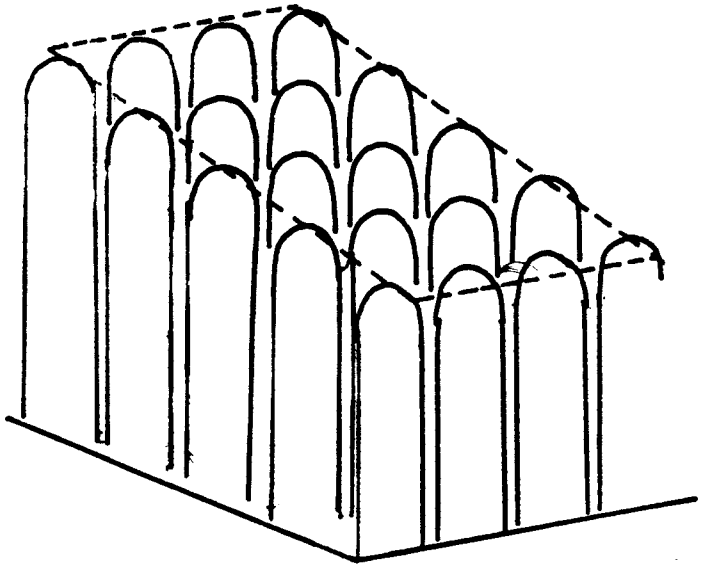

Figure A3.4 A model showing the adjacent re-entry of polyethylene chains which are staggered in the fold plane.

All these models incorporate the basic concept of a crystalline central core, it is the nature of the folding which is the subject of debate. X-ray and thermal measurements indicate that polyethylene crystals are less than 85% crystalline [7], hence implying that the disorder cannot be due solely to inter-crystalline defects. Infra-red measurements by KELLER and PRIEST suggest that approximately 90% of chain ends are excluded from the crystalline core [8]. KELLER has also shown that in polyethylene, chains appear to have a regular period, but that the fold surface is staggered to allow for the pyramidal form of the single crystals [9]. See figure A3.2. The folds are staggered both within a fold plane and between fold planes, but the fold period is always regular. Figure A3.4 shows the staggering of chains between fold planes. A totally random irregular fold period would result in a rough surface and can thus be disregarded because a rough surface has a high energy associated with it. Thus, the folding is thought to be regular and staggered to maintain a low energy smooth surface.

The current view is that the regularly folded chain model which exhibits adjacent re-entry is most likely for a single crystal and the disorder at the crystal surface is explained by the presence of protruding chain ends or cilia which lie on the crystal surface. HOFFMAN has suggested that lower molecular weight fractions may also be adsorbed on to the surface [10].

An alternative explanation is the *"switchboard model"* proposed by FLORY in 1962 [11]. This is shown in figure A3.3, it incorporates loose and irregular folds. For this model, there must be a relatively thick, non-crystalline layer on each side of the crystal. It is now thought that this model is not appropriate for solution grown crystals as it does not appear to explain the characteristic pyramidal shape. The many similarities between solution and melt grown crystals led to the suggestion that the melt crystallized material must be lamellar and also contain folded chains. In addition, calculations based on geometrical considerations indicated that chain folding must occur in at least half of the chains. However, they also showed that a simple two phase model was unrealistic. For linear molecules, the density of the boundary region between crystalline and completely amorphous regions would have to be higher than in the crystal. It is now

accepted that melt crystallized polymers must contain three phases, a pure crystalline core, a completely amorphous region and an interfacial region which still retains some conformational order and some chain folding.

HOFFMAN and LAURITZEN developed a model for chain folded crystal growth in solution and from the melt based on kinetic considerations [10]. FLORY made several calculations based on the relaxation time of long chain molecules and concluded that, especially at high supercooling when crystallization occurs very rapidly, the polymer chains would not have time to undergo a complete rearrangement to form a regular chain. He proposed that many molecules contribute to a lamellar crystal, and that although regular adjacent re-entry may occur, it is rare. Figure A3.5 shows illustrates the model described by Flory.

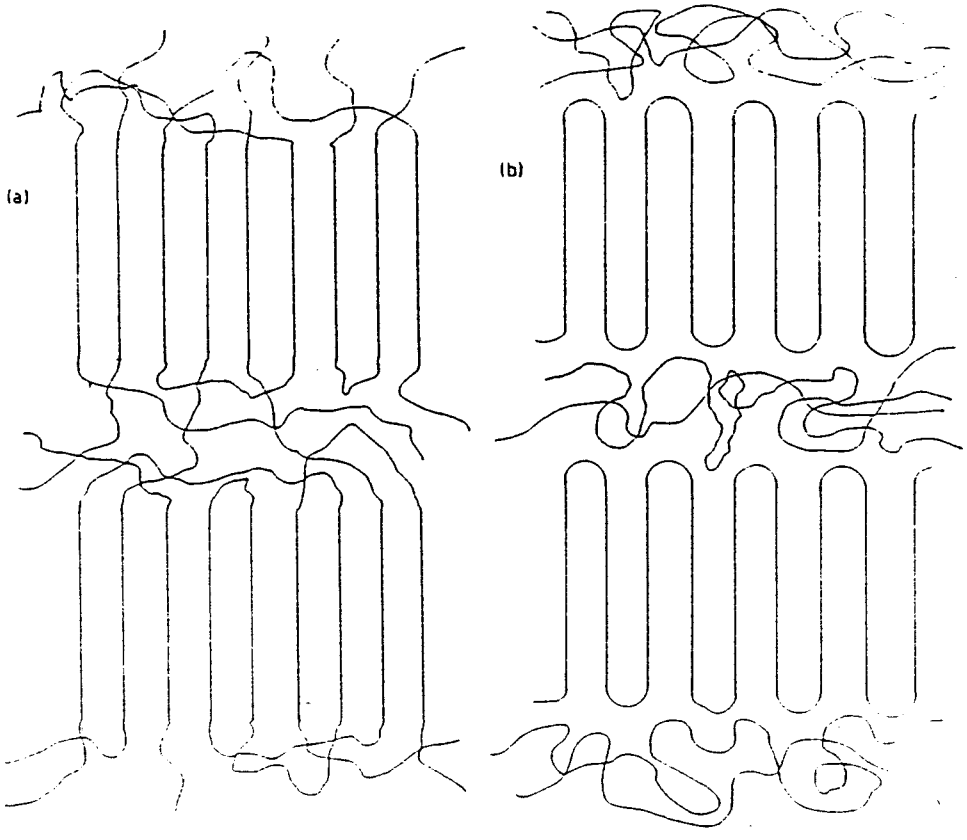

Figure A3.5 Diagrammatic representation of (a) the model described by Flory for the structure of melt crystallized polymers and (b) the model proposed by Hoffman and Lauritzen.

It is an extension of the switchboard model developed for solution grown crystals.

HOFFMAN and LAURITZEN maintained, however, that regular folding with adjacent re-entry always occurs even at very high supercooling, when crystallization is most rapid [10].

In melt crystallized polymer samples, lamellae aggregate into larger structures which are known as spherulites. there has been some debate as to whether they are formed by rearrangement of previously crystallized material or, as is now most widely believed, as products of primary crystallization. The structure of a typical spherulite is shown in figure A3.6. Crystallization may be nucleated at a point or along a line. The nucleus may be a foreign particle, such as a speck of dust (heterogeneous nucleation) or may occur spontaneously in the melt (homogeneous nucleation). Crystallization spreads by the growth of individual lamellae. These lamellae form long "ribbons" which spiral out from the nucleation centre. Spherulites can grow to as large as several millimetres in diameter. They form a characteristic *"Maltese Cross"* pattern when viewed through crossed polarizers under an optical microscope.

It must be noted that the crystalline habit described above is that usually adopted by polymers when crystallized from the melt under static conditions. If the polymer is crystallized under stress, different crystalline habits can occur [12-14].

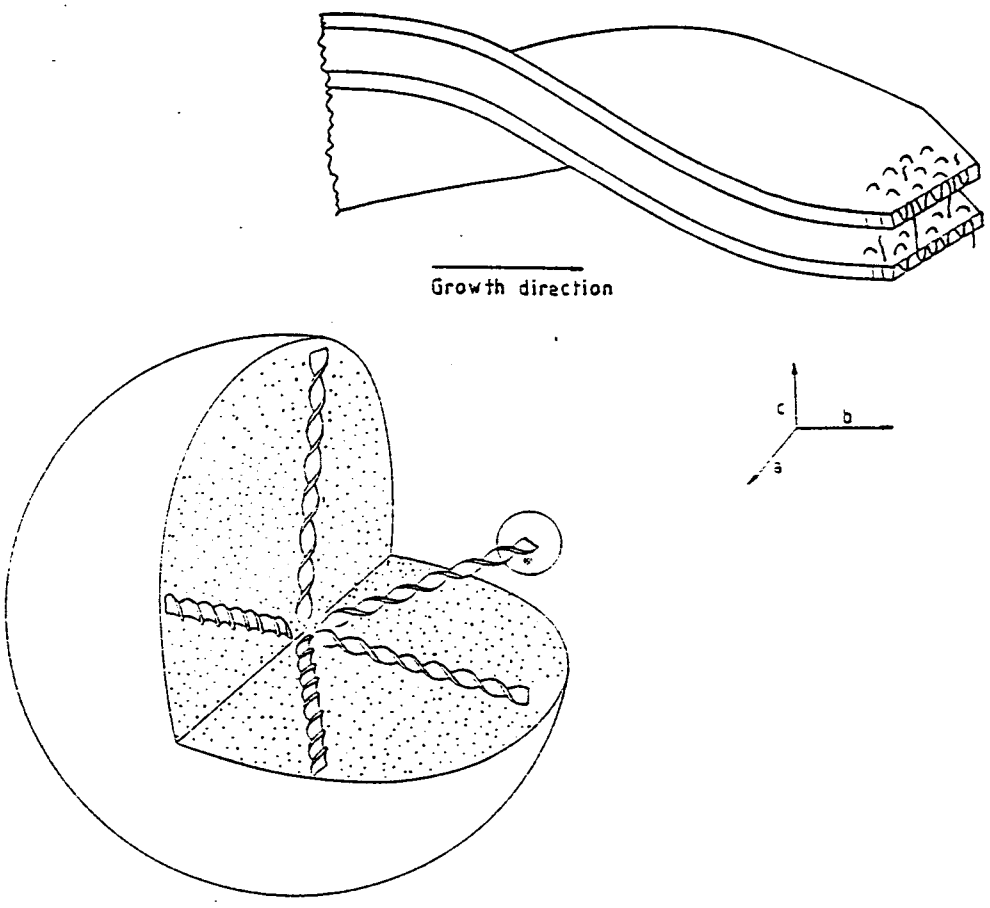

A3.6 A diagram showing the structure of a spherulite

Supplementary Discussion and Conclusion

The following section provides supporting material, for Chapter 5, and should be read in conjunction with this Chapter and in particular section 5.4.1.

As already mentioned Spherulites are morphological features of bulk-crystallized polymers. They consist of a very large number of lamellar crystallites, radiating in all directions from one point, with well-defined boundaries. Differences in spherulitic texture (viewed under crossed polaroids in a polarizing microscope) depend on the chemical structure, molecular weight, and crystallization conditions. Structures may vary from well-developed spherulites to rods and sheetlike aggregates as well as to random collections of lamellae. For example, it is known that in low molecular weight polyethylene under isothermal conditions of crystallization, thin rods or axialites are formed, whereas with higher molecular weights, sheet-like structures develop. The higher molecular weight fractions, however, form spherulites at lower crystallization temperatures; their structure deteriorate as the molecular weight increases and are random lamellar at the highest molecular weights [15]. Extending this theory to the work reported here, it can be envisaged that depending on the molecular weight of the polybutylene terephthalate, changes in the miscibility of the polymer with the epoxy can be expected.

Spherulitic growth is typical of a nucleation-controlled process. This conclusion has been deduced from the characteristic large negative temperature coefficient of the growth rate in the vicinity of the melting temperature. Homogeneous nucleation takes place when spherulite development starts as a result of random fluctuations in the pure melt [16]. In general, conditions appropriate to homogeneous nucleation are difficult to attain.

Nucleation of polymers to give spherulites has been described frequently as a heterogeneous process, which takes place at a non-constant rate and is initiated over particles of insoluble impurities. Evidence that nucleation is heterogeneous in many systems has been obtained by the observation of the appearance of successive meltings and crystallizations. Nucleation starts on insoluble heterogenieties, which, because of the high viscosity of the melt, cannot move. This occurs in the samples annealed at temperatures below the actual melting point of the polybutylene terephthalate, seen in

section 5.4.1 and figure 5.9. Also remnants of polymer crystalline order are not destroyed when the melting temperature is not high enough or when the time at which the melting temperature is maintained is short and thus spherulites start where remnants of old spherulites remain. When the temperature of the sample is held above the melting point of the polymer before crystallization the number of spherulites per unit volume is reduced. Evidence for this is shown in figure 5.9 and the increase in the value of the full width at half height for the carbonyl stretching band. It should also be noted that if the melting temperature is high and the residence time is long, the polymer may degrade, frequently with a reduction of molecular weight. This fact favours the appearance of bigger spherulites with growth rates that are higher than the corresponding value for intact material. Many polymers have been analyzed with regard to spherulite growth, and results of such studies can be followed-up in reference [17].

Empirical studies have been made in Chapter 5 to determine the feasibility of the Raman technique to study blend systems. In order to reach more exacting conclusions validation of results obtained from the Raman experiment need to be made, using techniques such as polarized light microscopy, differential scanning calorimetry and electron microscopic analysis. Readers are directed to ICI Paints in Slough and DR R.CHOUDERY who in the near future will be publishing results of the Raman analysis in conjunction with the techniques mentioned above.

References

1. C.W. Bunn, *Trans. Far. Soc.,* **35**, 482 (1939)

2. W.M.D. Bryant, *J. Polym. Sci.,* **2**, 547 (1947)

3. W. Schlesinger, H.M. Leeper, *J. Polym. Sci.,* **11**, 203 (1953)

4. E.W. Fischer, *Z. Naturforsch,* **12a**, 753 (1957)

5. A. Keller, *Philos. Mag.,* [8] **2**, 1171 (1957)

6. P.H. Till Jr., *J. Polym. Sci.,* **24**, 301 (1957)

7. P.H. Geil, Chapter 5: *"Polymer Morphology"* in *"Introduction to Polymer Science and Technology"*, eds. H.S.Kaufman, J.J. Flacetta, Wiley Interscience, J. Wiley & Sons, New York (1977)

8. A. Keller, D.J. Priest, *J.Macromol. Sci. (Phys.)*, **B2**, 479 (1968)

9. D.C. Bassett, F.C. Frank, A. Keller, *Phil. Mag.,* **8**, 1739 (1963)

10. J.D. Hoffman, G.T. Davis and J.I. Lauritzen, Chapter 7: *"The Rate of Crystallization of Linear Polymers wiht Chain Folding"* in *"Treatise on Soid State Chemistry, Crystalline and Non-crystalline Solids"*, **3**, ed. N.B. Hannay, Plenum, New York, (1976)

11. P.J. Flory, *J. Chem. Soc.,* **84**, 2857 (1962)

12 A.J. Pennings *J. Polym. Sci. Symp.,* **59**, 55 (1977)

13. B. Wunlerlich, L. Nelillo, *Makromol. Chem.,* **118**, 250 (1968)

14. D.C. Bassett, *Polymer,* **17**, 460 (1976)

15. L. Mandelkern, M. Glotin, R. Benson, *Macromol.,* **14**, 22 (1981)

16. P.J. Flory, A.D. McIntyre, *J. Polymer Sci.,* **18**, 592 (1955)

17. P.J. Hendra, J.K. Agbenyega, *"The Raman Spectra of Polymers"*, John Wiley and Sons, (1993)